YAMAGUCHI UNIVERSITY

The Graduate School of Sciences and Technology for Innovation

Enhancing the Mechanical Properties of Polypropylene-Based Green Composites through Surface Modification and Utilization of Regenerated Cellulose Fibers

(表面改質と再生セルロース繊維の利用によるポリプロピレン系グリーン複合材料の機械的特性の向上)

Wycliffe Odhiambo Ondiek

September 2025

Declaration

I, Wycliffe Odhiambo Ondiek, of the Department of Mechanical Engineering, Yamaguchi University, hereby declare that this thesis is my own original work. All figures, tables, equations, artworks, and illustrations are original, except where the work of others has been explicitly acknowledged, quoted, or referenced. I understand that failure to provide proper attribution constitutes plagiarism, which is a serious academic offence and will be subject to disciplinary action.

I give my consent for a copy of this report to be shared with future students as an exemplar.

I give my consent for this report to be made available to members of Yamaguchi University and the general public for purposes of teaching, learning, and research.

Wycliffe Odhiambo Ondiek
August 11, 2025

Abstract

The rising awareness of environmental degradation caused by synthetic and fossil fuel-derived materials has significantly increased the demand for sustainable manufacturing practices in the 21st century. In the composites industry, renewable lignocellulosic fibers are currently being incorporated with biodegradable resins to produce fully biodegradable materials, commonly referred to as green composites. The fabrication of fully green composites is an ultimate objective in sustainable materials development. However, challenges related to the processing and mechanical performance of composites comprising fully biodegradable reinforcements and matrices remain significant. Consequently, alternative strategies, such as combining natural biodegradable fibers or artificial cellulose fibers with recyclable thermoplastic polymers to form semi-biodegradable composites, present a practical and effective interim solution. These composites are still classified as green due to the recyclability of the thermoplastic matrices, which help reduce the overall environmental impact.

As research in this field advances, numerous strategies have been explored to enhance the mechanical performance of polymer composites, including fiber-matrix ratio optimization, the incorporation of micro- and nanofillers, and advanced molding techniques. However, certain areas remain under-explored—particularly the potential of post-fabrication processes such as surface treatment, coating, and lamination to improve composite performance, as well as the role of fiber pre-treatment with resin in enhancing fiber hydrophobicity prior to integration with hydrophobic polymer matrices. To address these gaps, this study developed polypropylene (PP)-based composites reinforced with wood fibers (WF), Cordenka fibers, and ramie fibers. The mechanical and morphological properties of these composites were systematically examined, with particular focus on the effects of surface modification methods such as PP and polyethylene terephthalate (PET) film lamination, and surface coating using cellulose nanofibers dispersed in acrylic resin. Additionally, the impact of different fiber types on the PP matrix was evaluated, and the performance of Cordenka regenerated cellulose fibers was compared with that of ramie fibers.

Neat polypropylene (PP) and wood fiber-reinforced polypropylene composite (WP) specimens were prepared in dumbbell and strip shapes via injection molding. The WP composites were produced with fiber contents of 15 wt%, 25 wt%, and 50 wt%, and their surfaces were subjected to various treatments, including lamination with 0.1 mm thick PP and polyethylene terephthalate (PET) films applied in different configurations: one-side half coverage (1S-H), one-side full coverage (1S-F), and two-side full coverage (2S-F). Additional surface treatments included ultraviolet (UV) irradiation, plasma irradiation, and immersion coating in an acrylic resin containing homogeneously nanodispersed TEMPO-oxidized cellulose nanofibers (CNF) of two lengths—short (0.2–0.3 μm) and long (0.7 μm)—each applied at concentrations of 0%, 1%, and 4%. In parallel, continuous Cordenka/PP and ramie/PP composite strands were fabricated using the Multi-Pin Assisted Resin Infiltration (M-PaRI) process, sectioned into 15 mm lengths,

and further compounded with additional PP resin through injection molding to produce dumbbell and strip specimens with fiber contents of 15 wt% and 20 wt%. All specimens were subjected to mechanical testing in accordance with ASTM and JIS standards, and the results were analyzed to assess the effects of fiber type, fiber content, and surface modification on the mechanical performance of the composites.

For the neat PP and WP specimens, the results demonstrated that 0.1 mm PET film was more effective than 0.1 mm PP film as a laminating material, with the highest tensile strength improvement of 12.3% observed in the 2S-F PET film configuration on the 25 wt% WP specimen, relative to its unlaminated counterpart. Furthermore, the effectiveness of PET film lamination was found to correlate with the percentage of surface coverage—the greater the coverage, the more pronounced the enhancement in tensile strength. In contrast, PP film lamination generally led to a reduction in tensile strength for both neat PP and 25 wt% WP specimens, likely due to the inherently low strength of PP film. However, in the 2S-F configuration, PP film achieved a notable 5% increase in the tensile strength of the 25 wt% WP specimen, which was attributed not to the strength of the film itself, but rather to its ability to smoothen the specimen's rough surface and seal fracture initiation sites.

Plasma treatment combined with surface coating with acrylic resin containing CNF enhanced the tensile strength of neat PP, 25 wt% WP, and 50 wt% WP specimens by average values of 6.2%, 3.8%, and 3.2%, respectively, although this treatment resulted in reduced fracture strain. Similarly, UV irradiation followed by surface coating led to tensile strength improvements of 4.8%, 3.4%, and 0.3% for neat PP, 25 wt% WP, and 50 wt% WP specimens, respectively, compared to untreated controls. Neat PP specimens demonstrated superior ductility compared to WP specimens, elongating significantly after initial failure without fracturing, regardless of the surface functionalization method. In contrast, all WP composite specimens displayed brittle fracture behavior, as evident from their low fracture strains. Surface roughness measurements and Scanning Electron Microscopy (SEM) observations confirmed that both film lamination and surface coating with acrylic resin and CNF improved surface properties by covering surface voids, enhancing surface homogeneity, and effectively sealing fracture origins, thereby contributing to the mitigation of premature failure.

For the Cordenka/PP and ramie/PP composite specimens, the results revealed that the 20 wt% Cordenka/PP composite achieved the highest tensile strength of 68.7 MPa, representing a 2.04-fold increase over neat PP and a 1.66-fold improvement compared to the 20 wt% ramie/PP composite. Remarkably, this tensile strength surpassed even that of the 50 wt% WP composites. The superior performance of the Cordenka/PP composites was attributed to the regeneration treatment of Cordenka fibers, which significantly enhanced their mechanical properties and improved interfacial adhesion with the hydrophobic polypropylene matrix. Impact testing further showed that Cordenka/PP composites absorbed two to 2.5 times more impact energy than ramie/PP composites, regardless of the presence of notches. Fiber length analysis confirmed that Cordenka fibers retained lengths beyond the critical threshold necessary for effective stress transfer, thus serving as more efficient reinforcements compared to ramie fibers, which fell below this critical length. As a result, the Cordenka/PP composites demonstrated markedly improved mechanical performance. Although scanning electron microscopy (SEM) revealed fewer fiber pullouts in ramie/PP composites—suggesting better interfacial bonding—this did not translate into superior mechanical properties, indicating that fiber length and regeneration played a more decisive role in reinforcement effectiveness.

These findings underscore the potential of post-fabrication processes such as film

lamination and surface coating to enhance the mechanical performance of green composites. Additionally, they demonstrate the viability of Cordenka, ramie, and wood fibers as sustainable alternatives to conventional synthetic, non-biodegradable reinforcements in polypropylene-based composites. The study also emphasizes the critical role of pre-fabrication techniques—including industrial fiber regeneration and the Multi-Pin Assisted Resin Infiltration (M-PaRI) process—in improving the mechanical properties of natural fiber-reinforced composites. Collectively, these results highlight promising pathways for advancing the application of green composites in high-performance sectors and provide a solid foundation for future research in these relatively underexplored domains.

Keywords: green composites, injection molding, surface modification, film lamination

Dedication

This work is dedicated to my beloved wife, Ms. Faith Moraa, and my dear son, Mr. Edson Handel, for their unwavering support throughout my studies.

Acknowledgements

My deepest gratitude goes to the Almighty God and my Savior, Jesus Christ, for His divine protection and guidance throughout my studies. I am truly appreciative of my parents, Mr. Joseph Odhong' and Ms. Gladys Migwasi, as well as my siblings, Mr. Alfrick Ondiek and Ms. Renish Ondiek, for their prayers and unwavering encouragement during my study period. I am also grateful to my supervisors, Prof. Koichi Goda and Prof. Arnaud Macadre, for their invaluable guidance and support throughout my research. I would like to extend my heartfelt thanks to Ms. Asano Tomoko, the international students' advisor, for her immense and consistent support during my studies. I am grateful to the Ministry of Education, Culture, Sports, Science and Technology (MEXT), Japan, and Egerton University (EU), Kenya, for their financial support during my research. I greatly appreciate Mr. Hesborn Ayub Rasugu for acting as my guarantor during the academic leave of absence I secured from work. I also appreciate the entire Hofu SDA Church family for their prayers and encouragement during my research period. Lastly, I would like to thank all my fellow mechanical engineering graduate students and all my well-wishers for their continued support.

Contents

List of Figures

List of Tables

Abbreviations and Symbols

AF	Aramid Fiber
AKD	Alkyl Ketene Dimer
aCNF	Alkaline Treated Cellulose Nanofibrils
APP	Ammonium Polyphosphate
APTES	(3-Aminopropyl)triethoxysilane
ASTM	American Society for Testing and Materials
av-RR	Average Heat Release Rate
CAGR	Cumulative Annual Growth Rate
CF	Carbon Fiber
CFRPs	Carbon Fiber Reinforced Plastics
CM	Compression Molding
CMC	Cellulose Microcrystals
CMF	Cellulose Microfiner
CNF	Cellulose Nanofiber
CNC	Cellulose Nanocrystal
CNW	Cellulose Nanowhisker
CT	Computed Tomography
DSC	Differential Scanning Calorimetry
EP	Epoxy
FRPs	Fiber Reinforced Plastics
FTIR	Fourier Transform Infrared Spectroscopy
GC	Green Composite
GF	Glass Fiber
GFRPs	Glass Fiber Reinforced Plastics
HDPE	High-Density Polyethylene
IM	Injection Molding
JIS	Japanese Industrial Standards
KP	Cordenka-Polypropylene Composite

LDH	Layered Double Hydroxide
LOI	Limiting Oxygen Index
LSR	Lamination Strength Ratio
MAPE	Maleic Anhydride Polyethylene
MAPP	Maleic Anhydride Grafted Polypropylene
MCC	Microcrystalline Cellulose
MFA	Microfibrillar Angle
MFC	Microfibrillated Cellulose
MMT	Montmorillonite
MPaRI	Multi-Pin Assisted Resin Impregnation
MSR	Model Strength Ratio
MTM	Mold Thermoset Matrix
MPOE	Maleic Anhydride Poly(oxyethylene)
NCC	Nanocrystalline Cellulose
npPP	N_2 (Nitrogen) Plasma Modified Polypropylene
OCC	Old Corrugated Cardboard
OMMT	Organically Modified Montmorillonite
PE	Polyethylene
PET	Polyethylene Terephthalate
PHA	Polyhydroxyalkanoates
PCL	Polycaprolactone
PLA	Polylactic Acid
PMMA	Polymethyl Methacrylate
POM	Polarized Optical Microscopy
PP	Polypropylene
PP-g-MA	Polypropylene Grafted with Maleic Anhydride
PVA	Polyvinyl Alcohol
PVC	Polyvinyl Chloride
pHRR	Peak Heat Release Rate
r-PP	Recycled Polypropylene
rCF	Recycled Carbon Fiber
RWF	Recycled Wood Fiber
RubWPC	Rubber Wood Plastic Composite
SDCNF	Spray Drilled Cellulose Nanofibrils
SEBS-g-MA	Styrene-Ethylene-Butylene-Styrene Grafted with Maleic Anhydride

SEM	Scanning Electron Microscopy
Si-CNF	Silane Surface Modified Cellulose Nanofibrils
TEMPO	2,2,6,6-Tetramethylpiperidine-1-oxyl
TGA	Thermogravimetric Analysis
THR	Total Heat Release
TMB	Thermomechanical Bleaching
TSP	Total Suspended Particulates
U-CNF	Unmodified Cellulose Nanofibrils
U-CNF-PP	Composites of Unmodified CNF with Polypropylene
VR-PA	Vapor-Reduced Polyamide
v-PP	Virgin Polypropylene
WF	Wood Fiber
WBG	Wood-Based Grade
WP	Wood Fiber-Polypropylene Composite
WPC	Wood Plastic Composite
XPS	X-ray Photoelectron Spectroscopy

The following symbols are used in this document:

T_m	Melting point [°C]
M_W	Molecular weight [$kg\ mol^{-1}$]
$L \times W \times t$	Dimensions (length, width, thickness) [mm]
Sa	Surface roughness [μm]
σ_{nc}	Tensile strength of non-coated specimen [MPa]
σ_c	Tensile strength of coated specimen [MPa]
A_{nc}	Cross-sectional area before coating [mm^2]
A_c	Cross-sectional area after coating [mm^2]
A_f	Cross-sectional area of acrylic resin film [mm^2]
d_f	Fiber diameter or width [μm]
σ_f^*	Fiber strength [MPa]
τ_{my}	Shear yield stress of matrix resin [MPa]

Chapter 1

Introduction

1.1 Background

In recent years, global environmental challenges have become increasingly severe, leading to a growing outcry for the regulation of human activities to mitigate environmental degradation and promote sustainable practices. In the manufacturing sector for instance, composite materials made entirely from synthetic fibers such as glass, carbon, and aramid; and resins such as epoxy, polyester, vinyl ester, polypropylene, and nylon, have been widely used, significantly enhancing the convenience of daily life. These fiber-reinforced plastic (FRP) materials are widely applied in industries such as automotive, aerospace, marine, and construction, and are renowned for their lightweight properties and superior mechanical characteristics.

Among the FRPs, glass fiber reinforced plastics (GFRPs) and carbon fiber reinforced plastics (CFRPs) which utilize glass and carbon fibers, respectively, as reinforcing materials are prevalent. GFRPs and CFRPs have excellent specific strength and rigidity, hence their application in a wide range of disciplines such as sporting goods, industrial equipment, military, marine, automobile and aircraft industries [2, 3, 4]. However, notwithstanding the excellent mechanical properties exhibited by FRPs, their continued use has precipitated environmental deterioration through extensive consumption and disposal, contributing significantly to global warming [5, 6, 7, 8, 9, 10, 11, 12, 13]. Considering that FRPs mainly consist of glass fibers as the primary reinforcement material, they require substantial energy during manufacturing. Additionally, these composites are difficult to incinerate and are often disposed of in landfills, raising concerns about the depletion of landfill capacity [14, 15, 16].

Figure 1.1 summarizes the key environmental challenges and material limitations driving the transition from conventional fiber-reinforced plastics to more sustainable alternatives, and highlights the resulting research directions aimed at advancing green composite technologies. Addressing these challenges requires extensive research into new materials and the implementation of technological methods that promote environmental protection, resource conservation, and energy efficiency [17, 18, 19, 20]. Consequently, substantial efforts are currently underway to develop advanced recycling technologies and innovative materials that incorporate naturally biodegradable alternatives [21, 22]. One promising sustainable solution is the development of green composites (GCs), which combine natural fibers with biodegradable or recyclable resins [23, 24, 25].

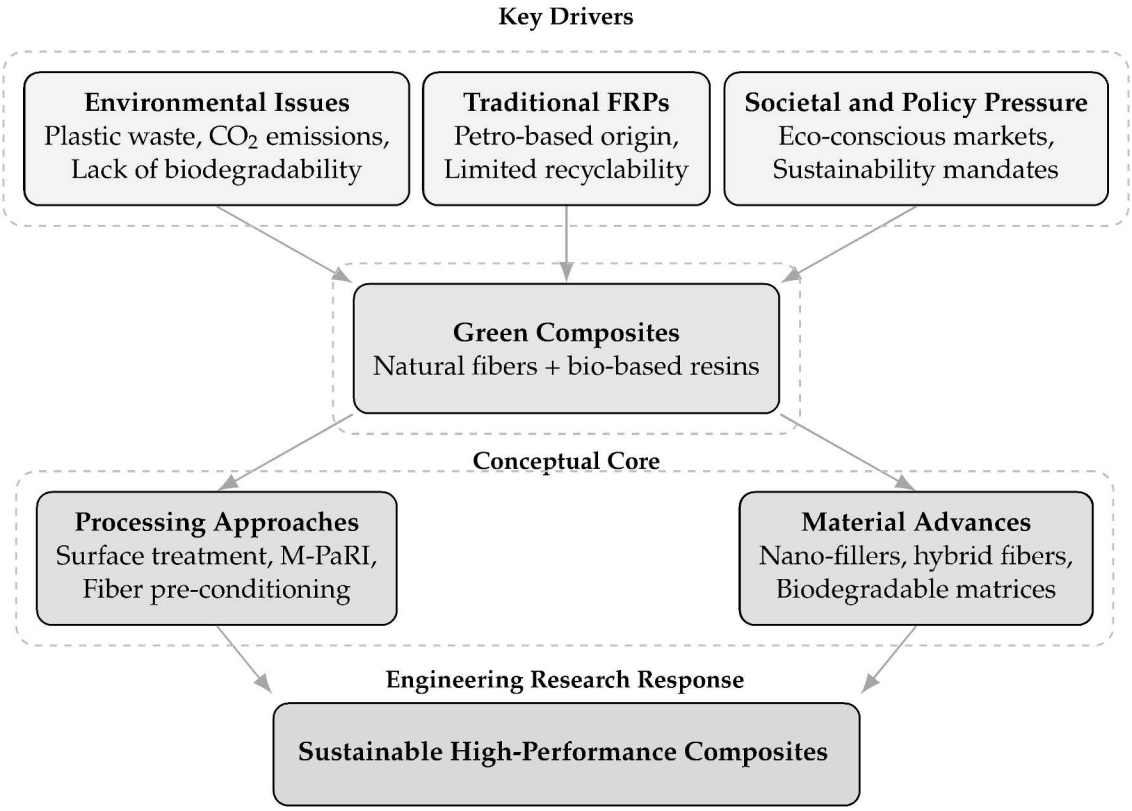

Figure 1.1: Schematic representation of key drivers, green composite concept, and research responses toward sustainable composite materials.

1.2 Green Composites

Natural fibers, such as hemp, flax, bamboo, and wood, form the cornerstone of green composites (GCs). Compared to traditional composites, GCs offer significant environmental benefits, including lightweight properties, recyclability, biodegradability, and affordability [26, 27, 28]. Green composites are well known for their ability to decompose into water and carbon dioxide through the activity of microorganisms and enzymes present in natural environments [29, 30]. Therefore, these materials not only consist of natural fibers, commonly used as reinforcement, but also incorporate artificial biodegradable fibers, further enhancing their sustainability and reducing their environmental impact. Since regenerated cellulose fibers such as rayon, cupro, and lyocell, and biomass-derived fibers such as polylactic acid (PLA) fibers exhibit biodegradability, composite materials that use these fibers as reinforcing materials also fall under the category of GCs. Furthermore, in a broader sense, the term 'green' can also include recyclable materials, allowing composites with thermoplastic resins to be considered GCs.

An overview of the classification of green composites based on fiber and matrix types is illustrated in Figure 1.2.

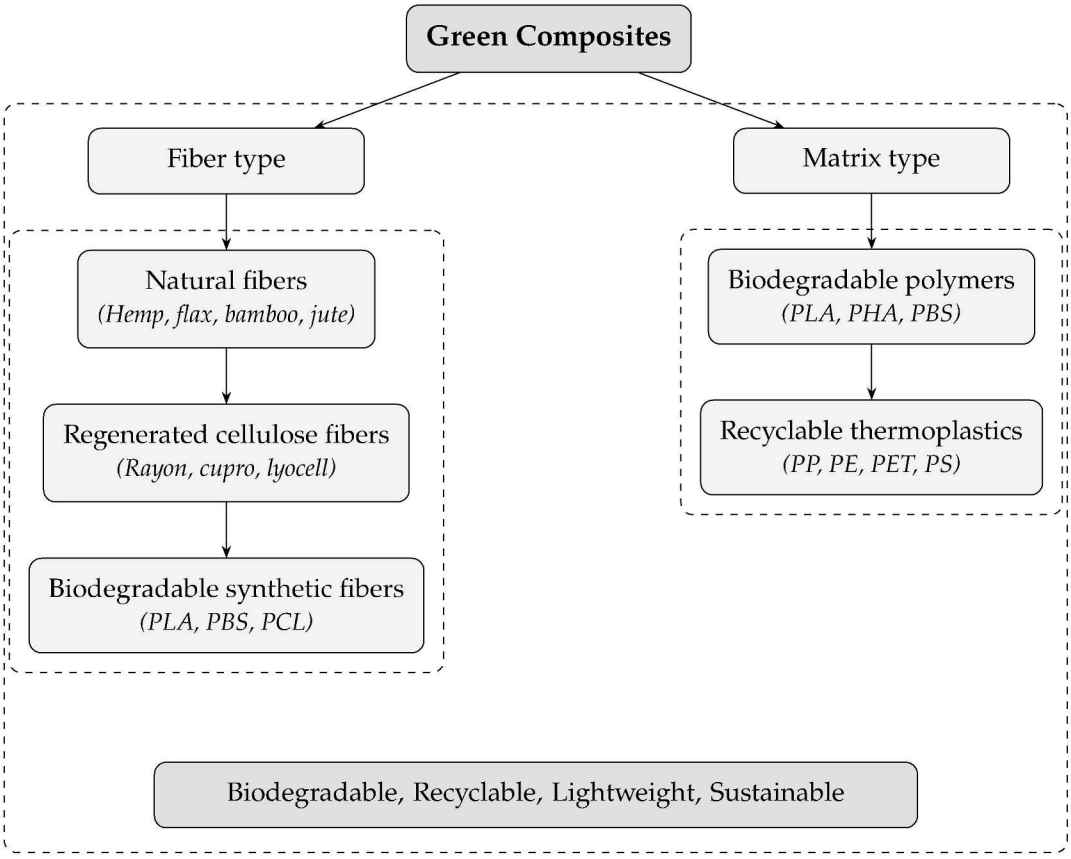

Figure 1.2: Classification of green composites based on fiber and matrix types, highlighting examples and sustainability features.

1.2.1 Thermoplastic Resin Systems

Polypropylene (PP), polyethylene (PE), polystyrene (PS), and polyvinyl chloride (PVC) are commonly referred to as the 'big four' general-purpose thermoplastic resins. These materials are characterized by their widespread availability, low cost, and high production volumes, which make them integral to the manufacture of affordable GCs. The mechanical properties of these resins are summarized in Table 1.1 [31, 32, 33].

Table 1.1: Typical mechanical properties of common thermoplastic resins

Mechanical Property	**PP**	**PE**	**PVC**	**PS**
Specific Gravity	0.90–0.91	0.94–0.97	1.30–1.58	1.04–1.09
Young's Modulus [MPa]	1098–1548	412–1235	2401–4116	2746–4120
Fracture Strain [%]	200–700	20–1300	40–80	1–6
Tensile Strength [MPa]	29.4–38.3	20.6–38.3	41.2–52.0	34.3–82.4
Compressive Strength [MPa]	38.3–55.0	18.6–24.5	54.9–89.2	79.4–109.8
Bending Strength [MPa]	41.2–55.0	33.3–48.1	68.7–109.8	54.9–96.1
Izod Impact Strength [J/m]	11–117	27–1068	21–1068	13–21

The table clearly shows that PP has the lowest specific gravity among the four major resins, ranging from 0.90 to 0.91, making it the lightest thermoplastic resin of the four. Additionally, PP exhibits excellent processability, toughness and high flexural strength, alongside impact resistance and rigidity, particularly when considering its strength-to-weight ratio. Its high surface hardness provides excellent scratch resistance and contributes to its glossy finish. PP also possesses a high melting point of 160–170 °C and manifests outstanding resistance to chemicals, oils, and stress cracking. Composed solely of carbon and hydrogen, the incineration of PP produces minimal harmful gases, such as chlorine, which implies a lower environmental impact.

1.2.2 Biodegradable Fiber Types

Wood-Derived Fibers

Suitable reinforcements for green composites include wood fibers derived from waste wood and thinned wood raw materials [34], whilst industrial waste plastics are appropriate for use as base materials. Wood fiber, otherwise called wood flour owing to its finely divided particles approximating those of cereal flours in size, appearance, and texture, has a high modulus of rigidity and low thermal expansion [35]. On the other hand, discarded industrial thermoplastic resins and pure resins are highly recyclable, durable, water resistant, and moldable [36]. By combining these two elements, the resulting WPC exhibits excellent synergistic properties that compensate for the weaknesses of both wood and plastic [37].

The demand for WPCs as an alternative to plastic technology has been increasing exponentially since their utility was recognized. In 2019, the global market size of WPCs was $4.77 billion, and it was envisaged to reach $8.76 billion by 2022 and $9.03 billion by 2027. The cumulative annual growth rate during this forecast period was 8.57% [38]. This trend is illustrated in Figure 1.3. As of 2022, the projected global market volume was 8 million tons [39, 40]. Based on this promising trend, and with the increasing discovery of WPC strength enhancement techniques to guarantee their suitability for broader applications, it can only be anticipated that this demand will continue to rise.

To support this growing demand, research has increasingly focused on improving the mechanical properties of WPCs. Significant enhancements have been achieved through the optimization of raw material ratios and the addition of modifiers such as coupling agents and compatibilizers, which are carefully selected based on the material type and usage conditions. More recently, preliminary findings suggest that the incorporation of nanomaterials can further enhance WPC compactness by filling gaps between fibers, thus improving their mechanical performance. Although nanomaterials such as carbon nanotubes, nano-titanium dioxide, nano-silicon dioxide, and nano-calcium acid have been investigated, future efforts are expected to explore green alternatives like cellulose nanofibers. This represents a timely research direction and a paradigm shift that may contribute to reducing plastic waste while promoting the broader adoption of WPCs in engineering applications [35].

Cellulose Nanofibers

Cellulose nanofibers (CNFs) are ultrathin fibers derived from the microfibrils of woody or herbaceous plants, processed to nanoscale dimensions via mechanical and/or chemical methods [41]. Specifically, TEMPO-mediated oxidation introduces carboxyl groups

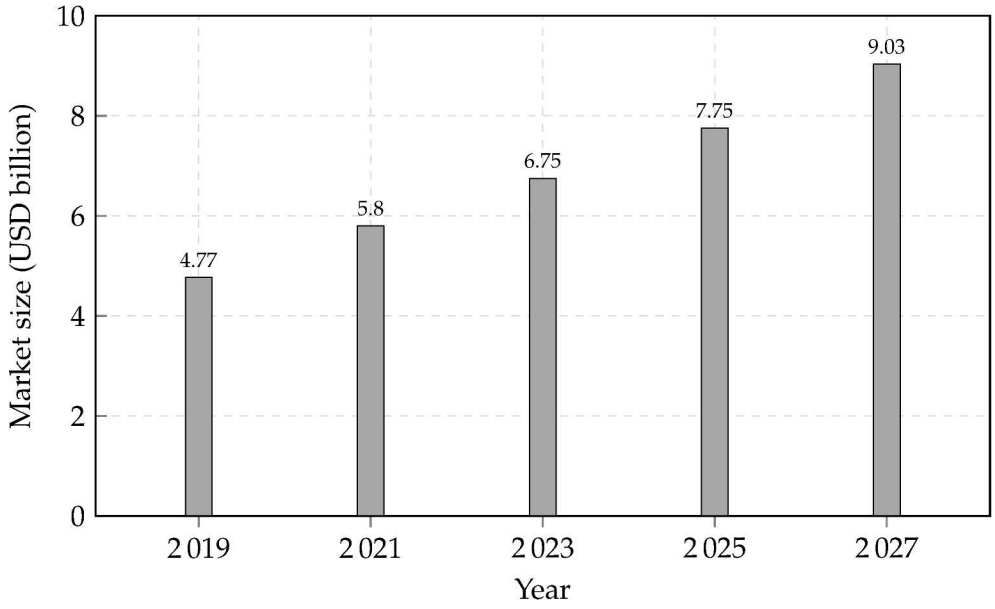

Figure 1.3: Historical and projected global WPC market size (2019–2027), based on data from Fortune Business Insights and others (CAGR $\approx 8.6\%$).

on the fiber surface, inducing electrostatic repulsion that facilitates efficient individualization of nanofibers [42]. Compared to traditional reinforcements such as carbon and glass fibers, CNFs offer a sustainable alternative sourced from abundant, renewable biomass. Their density (1.6 g/cm^3) combined with exceptional tensile strength (2.0–3.0 GPa) positions CNFs as lightweight yet high-performance reinforcement candidates [43, 44, 45, 46, 47].

CNFs possess outstanding properties including high specific surface area, elastic modulus comparable to aramid fibers, low thermal expansion akin to glass, and excellent gas barrier performance [48, 49]. These attributes have catalyzed their incorporation in diverse sectors such as flexible electronics, automotive components, biomedical devices, packaging, and construction materials [50, 51, 52, 53, 54]. As depicted in Figure 1.4, the intrinsic properties and broad application spectrum of CNFs underpin their growing significance in advanced composite materials development.

Many researchers have developed composite materials by combining CNF with various resins [55, 56, 57, 58, 59, 60, 61, 62, 53]. As from 2014, Butterfly (Tamas Co., Ltd., Tokyo, Japan), which had been focusing on CNF started developing CNF-equipped rackets in collaboration with Daio Paper Co., Ltd., Tokyo, Japan, a major paper manufacturer in Japan. The two companies were able to prove that the power of hitting balls can be increased by incorporating CNF on table tennis rackets. The CNF enhanced table tennis rackets [63, 64], popularly known as Revordia CNF, are currently being manufactured and sold globally. The milestones achieved so far have spurred an interest to further explore the feasibility of CNF, particularly its potential to enhance mechanical properties of green composites. Therefore, this study examined the effect of modifying the surface of WPCs through plasma treatment, UV irradiation, coating with PEGylated CNF nanodispersed in acrylic paint, and film lamination, on their mechanical properties.

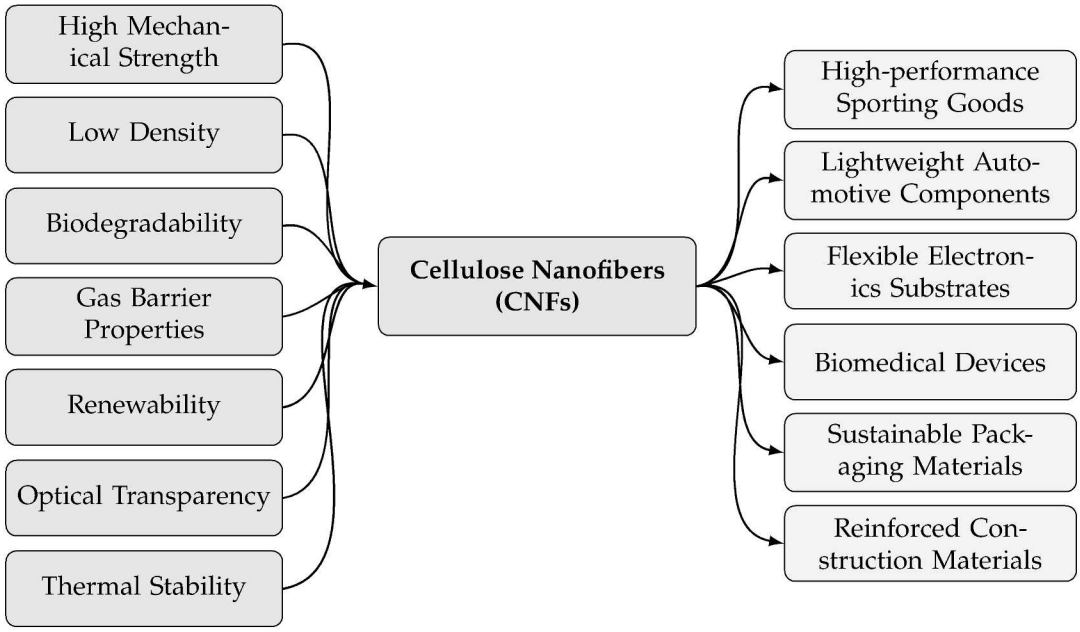

Figure 1.4: Schematic overview of key material properties (left) and principal application areas (right) of cellulose nanofibers (CNFs).

Regenerated Natural Fibers

The extraction of CNF represents one method for processing natural fibers. In addition to this method, natural fibers also have a well-established history in the textile industry, where they undergo a process known as 'regeneration', applicable to both woody and herbaceous fibers. Regenerated fibers are produced by extracting cellulose, the primary structural component of plants, dissolving it through chemical processes, and reconstituting it into fibers [65]. Rayon, for instance, is a regenerated fiber used in applications like car tires. It is produced by dissolving cellulose in an alkaline solution, such as sodium hydroxide or carbon disulfide, to form viscose, which is then wet-spun in an acidic bath. Unlike petroleum-based synthetic fibers like polyester, rayon is still biodegradable after processing. In Obernburg, Germany, industrial rayon is manufactured under the brand name Cordenka. It is widely recognized for its excellent mechanical properties, including strong adhesion to rubber and plastics, high resistance to heat, aging, and chemicals, a high elastic modulus, low thermal shrinkage, and exceptional dimensional stability [66, 67, 68, 69]. Its applications extend from tires to mechanical rubber products.

Until now, there has not been as much focus on regenerated fibers as there is on green composites. If regenerated fiber-reinforced composites can demonstrate mechanical properties comparable to CNF-based composites, they could be effectively utilized in modern material production and structural applications, particularly due to their biodegradability, similar to natural fiber composites. Therefore, this study focused on evaluating the mechanical properties of green composites (GCs) reinforced with Cordenka, a regenerated cellulose fiber, in a polypropylene (PP) matrix. The performance of these composites was compared with that of Ramie fiber-reinforced PP composites and wood fiber-reinforced PP composites. Although Cordenka is not classified as a natural fiber, it contains cellulose, which categorizes it as a regenerated cellulose fiber. Traditionally, and continuing to this day, Cordenka fibers have been widely used in tire cord applications. However, recent studies have explored the properties of composites made

from Cordenka fibers and matrices such as polylactic acid (PLA), polypropylene (PP), and epoxy resin (EP). These studies have further compared the performance of these composites with green composites reinforced with cellulose-based natural fibers, such as flax and jute [70, 71].

1.3 Composite Processing Techniques

Composite fabrication encompasses pre-processing, processing, and post-processing techniques aimed at enhancing fiber-matrix compatibility and optimizing the final material's properties. Pre-processing methods include chemical treatments such as alkali treatment and silane coupling, which improve fiber surface roughness and introduce functional groups to enhance adhesion with hydrophobic polymer matrices [72, 73, 74, 75]. The addition of compatibilizers, such as maleic anhydride-grafted polypropylene (MAPP), further strengthens the interfacial bond. During processing, advanced techniques like Multi-Pin Assisted Resin Impregnation (M-PaRI) ensure thorough resin penetration and uniform fiber dispersion [76]. Precise control of injection molding parameters minimizes defects such as voids and thermal degradation [77]. Post-processing techniques, including plasma irradiation, acrylic resin and cellulose nanofiber (CNF) coating, and lamination, improve surface properties such as gloss, wettability, weather resistance, heat resistance, corrosion resistance, electrical conductivity (if required), and scratch resistance [78, 79, 80, 81, 82]. These integrated approaches are crucial for producing high-performance composites suitable for demanding industrial applications.

1.4 Review of Existing Research

Recent research has increasingly focused on improving the mechanical performance of wood-plastic composites (WPCs) by addressing inherent limitations of lignocellulosic fiber reinforcements. Compared to traditional synthetic fibers such as glass, lignocellulosic fibers offer environmental and economic advantages while still providing competitive mechanical properties [83]. Accordingly, a wide range of studies have explored innovative approaches to enhance WPC performance through material design, formulation strategies, and integration of functional additives. In particular, the literature highlights various experimental modifications—such as the inclusion of flame retardants, coupling agents, and regenerated fibers—that have been successfully implemented to improve composite strength, stiffness, and durability [35, 84, 85, 86]. These efforts are often tailored to address specific application demands, ranging from structural reinforcement to fire resistance and environmental durability. The following subsections provide a comprehensive overview of selected studies that exemplify current advancements and methodologies employed to enhance the structural and functional properties of WPCs.

1.4.1 Review of Material, Interfacial, and Functional Modification Strategies in Wood-Plastic Composites

Farsi et al.[87] investigated the effects of various chemical surface treatments of wood flour—namely alkaline, silane, acrylic acid, and benzoyl chloride—on the mechanical performance of wood–plastic composites. These treatments were combined with 3 wt% maleic anhydride grafted polypropylene (PP-g-MA) in a polypropylene-based matrix to

enhance interfacial compatibility and overall composite behavior. The materials were compounded via melt mixing and shaped by injection molding, after which tensile, flexural, and impact properties were evaluated. The results indicated that alkaline-treated wood flour, when used alongside the PP-g-MA compatibilizer, led to the most notable gains in both tensile and flexural strength, highlighting the improved adhesion at the filler–matrix interface. However, chemically treated composites exhibited slightly diminished impact resistance compared to unmodified ones. Notably, the combined use of surface modification and compatibilizer produced a synergistic improvement in mechanical properties, suggesting that dual modification strategies are particularly effective in reinforcing WPCs through enhanced interfacial bonding.

Kallakas et al. [88] investigated the effect of various chemical treatments applied to birch wood flour (WF) on the mechanical and thermal behavior of polypropylene-based wood–plastic composites (WPCs). In their study, WF was subjected to six distinct modification techniques: alkaline treatment, polyvinyl alcohol (PVA) coating, silanization using 3-aminopropyltriethoxysilane (APTES), acetylation, cyanoethylation, and esterification. These treatments aimed to improve its compatibility with the hydrophobic polymer matrix. The modified WPCs were fabricated using twin-screw extrusion followed by injection molding, and were assessed through flexural and impact tests, thermal analysis, and SEM imaging. Results indicated that all modification methods enhanced interfacial adhesion to varying degrees, resulting in better flexural strength and increased crystallinity, although impact resistance declined across the board, indicating a shift toward brittleness. Furthermore, chemical treatment generally led to a reduction in melting temperature, with performance outcomes differing depending on the specific modification route used. This work affirms that targeted chemical treatments can significantly tailor WPC properties by strengthening fiber–matrix interaction.

Migneault et al. [89] explored how the surface chemical composition of lignocellulosic fibers influences the mechanical performance of wood–plastic composites (WPCs). Using six different fiber types, the researchers characterized the fiber surfaces via X-ray photoelectron spectroscopy (XPS) and Fourier-transform infrared spectroscopy (FTIR), then compounded them at 40 wt% with high-density polyethylene and maleated polyethylene (MAPE) as a compatibilizer. Mechanical tests and microscopic examination of the fiber–matrix interface revealed that fiber surfaces rich in oxidized carbon species—typically associated with carbohydrates—contributed positively to composite strength, whereas high levels of unoxidized carbon—attributed to lignin and extractives—were detrimental. FTIR analysis further supported these findings, showing that increased lignin-related peak intensity correlated with lower mechanical strength. The study suggested that esterification between MAPE and carbohydrate hydroxyl groups plays a key role in enhancing interfacial adhesion. Nevertheless, factors such as fiber geometry and mechanical interlocking were also acknowledged as influencing the final properties of the composites. This work highlighted the pivotal role of fiber surface chemistry in determining WPC performance.

Widiastuti et al. examined the influence of polymer matrix type, wood species, and fabrication method on the mechanical and physical performance of wood plastic composites (WPCs) developed using wood waste and recycled polypropylene [90]. Their study compared composites fabricated from virgin and recycled polypropylene (v-PP and r-PP) matrices combined with teakwood or ironwood flour, using both compression moulding (CM) and injection moulding (IM) techniques. Results from tensile testing revealed that specimens produced via injection moulding exhibited notably higher tensile strength and lower water absorption than their compression-moulded counterparts. Among IM sam-

ples, composites reinforced with teakwood showed better mechanical performance than those incorporating ironwood. Additionally, virgin polypropylene matrices generally outperformed recycled ones in tensile strength, especially under CM processing. Water immersion tests in both freshwater and seawater further demonstrated that moisture uptake was significantly affected by both the type of polymer and the processing route. These findings highlight the critical roles of material selection and processing method in optimizing the structural integrity and durability of sustainable WPCs.

Friedrich et al. [91] tried UV irradiation and ozonation on PP, polyethylene (PE), and polyethylene terephthalate (PET). In their study, they conducted low-pressure oxygen plasma treatment and corona treatment to compare their influence on adhesion properties and surface energy of the polymer surfaces. Their results showed that low pressure plasma at the rate of 17 J mol^{-1} was most efficient in increasing the surface energy to 65 mN m^{-1}, a value higher than the 45 mN m^{-1} exhibited by corona treatment. Yáñez et al. [92] also performed surface modification on WPCs made from different polymers using an atmospheric pressure plasma jet, and studied the effect of varying the platform speed and nozzle distance on the composites' surface characteristics. They ascertained that plasma treatment removed a large portion of the WF and exposed the resin to the surface, changing their surface chemistry and topography by forming new polar carbon moieties. As a result, adhesion properties were enhanced. Additionally, they established that surface-nozzle distance of 1 cm and platform speed of 0.5–2 m min^{-1} were the optimal conditions for achieving best adhesion results. Composites with inorganic fillers and low wood content yielded less surface modification after plasma treatment. In a separate study, Scarselli et al. observed a considerable increase in the lap shear strength of polyether ether ketone and polyphenylene sulfide based composite joints after UV irradiation and atmospheric plasma treatment [93]. According to their findings, plasma treatment worked more effectively than UV treatment. They attributed this to the capability of plasma treatment to activate the material surface, consequently increasing their free surface energies, a phenomenon not achievable with UV irradiation.

Hünnekens et al.[94] investigated the effect of atmospheric-pressure plasma treatment on the surface morphology and chemistry of wood–plastic composites (WPCs). Their findings revealed that extending the exposure time from 10s to 60 s led to substantial surface degradation and exposure of embedded wood particles. As a result, rather than improving the adhesion and wettability of the hydrophobic matrix, the treatment became ineffective due to hydrophobic recovery—a phenomenon similarly documented by Mortazavi et al.and Bormashenko et al.[95, 96]. These observations highlight the need for empirical determination of optimal plasma exposure conditions to avoid surface damage and to ensure that the intended surface modification benefits are realized.

Luo et al. proposed a crystallization-based strategy to enhance the toughness of polypropylene composites filled with wood flour, addressing a common limitation of such materials [97]. Their approach involved incorporating self-assembling β-nucleating agents into the PP matrix, specifically comparing the performance of an aryl amide compound (TMB5) and a rare-earth-based complex (WBG II) at various concentrations. Both agents proved highly efficient in promoting β-phase crystallization, with the β-phase fraction (kβ) reaching as high as 0.8 at a minimal loading of 0.05 wt%. This modification refined the crystalline structure by reducing spherulite size and elevating crystallization temperature, thereby accelerating solidification. The altered crystalline morphology led to marked gains in toughness; with 0.3 wt% of either additive, the notched impact strength rose by about 28% and the elongation at break improved by roughly 40%. While the WBG-modified composites exhibited a slightly higher β-content,

TMB yielded a finer crystalline network, contributing to superior tensile strength and stiffness. This study underscores the potential of nucleation-induced crystallinity control as an effective means to simultaneously enhance both the ductility and structural integrity of wood-filled thermoplastic composites.

1.4.2 Review of Cellulose-Based Fiber Reinforcement in Polypropylene Composites

Fujishita et al. [98] conducted a comprehensive investigation into the influence of fiber dispersion and agglomeration on the nonlinear mechanical performance of polypropylene (PP) composites reinforced with cellulose nanofibers (CNF). To overcome limitations associated with conventional composite fabrication—typically involving powdered CNF and solid maleic anhydride-modified PP (MAPP)—they introduced a novel aqueous-phase processing route utilizing water-dispersed CNF in combination with water-dispersible MAPP. This method significantly improved fiber distribution within the matrix. High-resolution X-ray computed tomography (CT) was employed to assess the internal morphology and characterize agglomeration behavior, while tensile tests were used to evaluate mechanical response. The enhanced dispersion achieved through the new method translated into superior mechanical performance. Furthermore, the authors implemented a multiscale modeling strategy, grounded in homogenization theory, to simulate fiber agglomeration through a two-step homogenization process that incorporated CT-derived dispersion metrics. The simulations aligned well with experimental observations, confirming the robustness of the model. By introducing quantitative descriptors—namely aggregation domain size (k) and aggregation density (x)—they effectively linked microstructural parameters to macroscopic behavior, offering practical guidelines for optimizing fiber dispersion in CNF-reinforced thermoplastic composites.

Hwang et al. [99] investigated the influence of spray-dried cellulose nanofibrils (SDCNFs), produced from bleached and unbleached Kraft pulp as well as old corrugated cardboard (OCC), on the mechanical performance of polypropylene (PP) composites. CNFs were prepared via mechanical disk refining to 90% and 100% fines content, then spray-dried using a pilot-scale rotary disk atomizer, which yielded spherical microparticles with particle size dependent on fibrillation level. The SDCNFs were compounded into a PP matrix using a masterbatch technique to ensure uniform dispersion, with maleic anhydride-grafted PP serving as a compatibilizer. Mechanical testing revealed that larger SDCNF particles enhanced tensile and flexural strength and modulus, whereas smaller particles improved impact resistance. Incorporation of 10 wt% SDCNFs resulted in increases of up to 29% in tensile strength, 66% in tensile modulus, 15% in flexural strength, 27% in flexural modulus, and 11% in impact strength compared to neat PP, demonstrating the significant role of particle morphology and dispersion in determining composite performance.

Al-Haik et al. [100] investigated the influence of nanocrystalline cellulose (NCC) on the mechanical and thermal performance of polypropylene (PP) nanocomposites, aiming to identify an optimal NCC loading for property enhancement. NCC was incorporated into the PP matrix at varying concentrations via injection molding. The resulting composites were characterized through mechanical tests—including three-point bending and nanoindentation—and thermal analyses such as DSC and TGA, along with morphological and chemical examinations using SEM and FTIR. Results showed that the inclusion of NCC improved strength, modulus, and hardness by 6.5%, 19%, and 150%, respectively. While DSC confirmed that NCC had minimal influence on the melting temperature, TGA

revealed improved thermal stability in all NCC-reinforced samples except at 5 wt% loading. This enhancement was attributed to the formation of tortuous heat-transfer paths by the rod-like NCC particles, as evidenced in SEM and supported by FTIR analysis. The study demonstrated that NCC addition not only enhances the mechanical properties of PP but can also contribute to improved thermal resistance when appropriately loaded.

Jung et al. [55] investigated methods to enhance the dispersion of CNF within a PP matrix and improve interfacial adhesion through alkaline and plasma treatments. They synthesized nanocomposites by introducing alkaline-treated CNF (aCNF) into PP that had undergone nitrogen (N_2) and oxygen (O_2) plasma treatments. Their findings demonstrated that nanocomposites made from N_2 plasma-modified PP (npPP) in combination with aCNF achieved the highest tensile strength and oxygen barrier properties. Specifically, the yield strength and modulus of elasticity of the npPP/aCNF nanocomposite increased by 32.8% and 26.3%, respectively, compared to pure PP. Additionally, the oxygen permeability was significantly reduced to 94.31 cc·mm/m^2·day·atm, marking a substantial improvement over unmodified PP.

Yang et al. [56] developed PP composites incorporating CNF, microfibrillated cellulose (MFC), and microcrystalline cellulose (MCC). They studied how these fillers affected the tensile and flexural properties at various loading levels. Their findings indicated that composites with cellulose nanofibers maintained strong tensile strength up to 10% filler loading, whereas those with MCC showed a consistent decrease in tensile strength. Moreover, the tensile modulus increased with higher filler content across all cellulose types. CNF and MCC-filled composites exhibited plastic deformation and greater elongation at break compared to MFC-filled ones, which displayed brittle behavior under tension. Their study concluded that CNF fillers offer superior mechanical performance compared to MCC and MFC counterparts.

Kahavita et al. [57] conducted an analysis on how modifying CNF surfaces affects the processing, mechanical properties, water absorption, and morphological properties of CNF/PP nanocomposites. The Composites were fabricated with up to 5 wt% loading of unmodified (U-CNF) and silane (Si-69) surface modified CNF (Si-CNF). The study revealed that Si-CNF-PP composites had significantly improved mechanical properties over U-CNF-PP composites, which was attributed to enhanced interfacial bonding facilitated by silane modification. In particular, the 3.5 wt% Si-CNF composite exhibited the highest tensile strength and hardness, along with superior morphological characteristics. Moreover, these composites showed moderate enhancements in impact resistance and water absorption. It was also observed that Si-CNF provided better stability in the PP matrix compared to U-CNF. Thus, 3.5 wt% Si-CNF was identified as the optimal reinforcement level for achieving peak mechanical performance.

Wang et al. [48] explored the development of lightweight polypropylene (PP) nanocomposite foams reinforced with cellulose nanofibers (CNFs) using core-back foam injection molding. Both unmodified and chemically modified CNFs, with degrees of substitution (DS) of 0.2 and 0.4, were melt-compounded into isotactic PP to assess their effect on foam structure and mechanical performance. The incorporation of CNFs significantly enhanced the foamability of PP, leading to a 100- to 1000-fold increase in cell density compared to neat PP foams. Mechanical testing showed that the addition of CNFs improved tensile modulus and yield strength in both solid and low-expansion (2-fold) foams, with superior reinforcement observed in systems containing surface-modified CNFs. Notably, in high-expansion (10-fold) foams, PP/CNF composites with DS 0.4 demonstrated substantial improvements in compressive properties, with elastic modulus and collapse stress increasing by 486% and 468%, respectively. These findings underscore the dual role

of CNFs in promoting microcellular foam formation and significantly reinforcing the mechanical integrity of PP foams, highlighting their value in fabricating high-performance, lightweight bio-based polymer composites.

1.4.3 Review of Compatibilizers, Coupling Agents, and Flame Retardants in Wood-Plastic Composites

Pokhrel et al. explored the viability of using wood pellets as an alternative lignocellulosic filler in polypropylene-based wood plastic composites, aiming to reduce transportation costs associated with raw material supply [101]. Their study compared WPCs fabricated from conventional wood flour and ground wood pellets derived from four hardwood and softwood species, with and without the incorporation of maleic anhydride polypropylene (MAPP) as a coupling agent. Microscopic analysis revealed a more uniform dispersion of particles in the polymer matrix when wood pellets were used, although tensile strength, modulus, and impact resistance were slightly lower compared to the composites reinforced with wood flour. Flexural performance showed mixed results: pellet-based composites exhibited higher strength in the absence of MAPP, but slightly lower values when MAPP was included. Nonetheless, most mechanical property differences remained within a 0.5–10% range, and statistical evaluation confirmed that the differences were not significant. These results suggest that wood pellets can be a practical substitute for wood flour in WPC manufacturing, offering comparable mechanical performance with the added advantage of reduced transportation expenses.

Zhu et al. developed a fully bio-based intumescent flame retardant, termed VR-PA, to improve the fire safety of wood flour/polypropylene (WFPP) composites [102]. VR-PA was synthesized through a Schiff base reaction between vanillin and l-arginine, followed by the introduction of phytic acid via electrostatic interaction. When incorporated into WFPP at 20 wt%, this novel flame retardant significantly enhanced the composite's fire performance, raising the limiting oxygen index (LOI) to 28.2% and reducing both the peak heat release rate and total heat release by 35.4% and 20.6%, respectively. A 15 wt% loading also yielded a pronounced 42.1% reduction in total smoke production. These improvements are attributed to VR-PA's dual action: in the gas phase, it captures free radicals during combustion, and in the condensed phase, it promotes the formation of a robust, expanded char layer. The findings demonstrate that VR-PA offers an environmentally friendly strategy for enhancing the flame retardancy and smoke suppression of WFPP composites without compromising sustainability.

Gairola et al. investigated the use of boron-based cross-linking to enhance the flame retardancy of natural fiber-reinforced polypropylene composites [103]. In this study, jute-sisal fabrics were modified using borax and subsequently integrated into a PP matrix to fabricate fire-retardant biocomposites. The borax pretreatment significantly elevated flame resistance, reflected in a 25.28% rise in limiting oxygen index (LOI), a 60.16% reduction in peak heat release rate (pHRR), and a 3.59% drop in average heat release rate (av-HRR) relative to untreated counterparts. When used as reinforcement in PP, the borax-treated fibers yielded composites with markedly improved thermal and flammability properties, including a 22.01% gain in LOI, and reductions of 22.29% and 22.23% in pHRR and av-HRR, respectively. Additional enhancements were observed in dimensional thermal stability, evidenced by favorable shifts in heat deflection temperature and thermal expansion coefficients. Post-combustion residue analysis revealed that the treated fibers formed a compact char structure, which likely acted as an effective thermal barrier, limiting heat transfer and delaying material degradation during combustion.

Yang et al. investigated the combined use of ammonium polyphosphate (APP) and self-assembled montmorillonite/layered double hydroxide (MMT/LDH) nanosheets as a flame-retardant system for wood plastic composites (WPCs) [104]. Recognizing the limitations associated with high APP loading—namely, increased smoke emission and compromised mechanical strength—they introduced a two-dimensional hybrid additive to counteract these drawbacks. The incorporation of MMT/LDH nanosheets, known for their catalytic charring and smoke-suppressing capabilities, enhanced the dispersion and synergistic action of APP. This approach significantly reduced peak heat release rate (pHRR), total heat release (THR), and total smoke production (TSP) by 35.6%, 21.0%, and 13.8%, respectively, compared to neat WPCs. Importantly, the modified composites also exhibited a modest improvement in mechanical properties, underscoring the potential of this phosphorus–nitrogen–inorganic hybrid system for producing safer, structurally reliable flame-retardant WPCs.

Zárate-Pérez et al. examined how different coupling agents influence the mechanical and thermal performance of polypropylene composites reinforced with wood flour, aiming to overcome the inherent incompatibility between hydrophilic fibers and the hydrophobic polymer matrix [105]. Their investigation compared graft and masterbatch-type compatibilizers within a melt intercalation processing route. The study found that grafted agents promoted more effective molecular interaction with the matrix, resulting in improved elastic modulus—rising by approximately 82% compared to neat PP—though tensile strength gains were limited due to inadequate interfacial adhesion. Despite the mechanical limitations, wood flour enhanced the crystallinity of the composites, acting as a nucleating agent and thereby influencing thermal behavior. The processing route also played a significant role: melt blending encouraged molecular alignment, whereas injection molding appeared to erase the material's previous thermal history. Morphological analysis revealed that weak fiber-matrix adhesion hindered stress transfer, contributing to reduced ductility, with failure occurring soon after yielding at strains of just 2–4%. Overall, the findings emphasized that while stiffness and thermal properties can be enhanced through appropriate compatibilization and processing, tensile strength remains constrained by interfacial bonding limitations.

Zhang [106] conducted a study on the impact of a novel coupling agent called alkyl ketene dimer (AKD) on the strength of polypropylene composites reinforced with wood fibers. They compared these results to composites treated with the more commonly used maleic anhydride grafted polypropylene (MAPP). The findings revealed that at 70 wt% WF, the samples treated with 5% AKD showed slightly higher tensile strength, impact strength, and tensile modulus compared to those treated with 5% MAPP. This superior performance of the AKD-treated composites was attributed to better compatibility between the wood fibers and the polymer matrix. Ndiaye et al. [107] also compared maleated anhydride polypropylene and oxidized polypropylene as coupling agents in WP composites. X-ray diffraction results indicated improved compatibility between polypropylene and wood with coupling agent addition. Maleated anhydride polypropylene showed superior interfacial bonding compared to polypropylene oxide and neat polypropylene. Mechanical testing revealed enhanced tensile and flexural properties in samples treated with coupling agents compared to untreated ones.

Elamin et al. [108] examined the effectiveness of Maleic anhydride grafted polyethylene octene elastomer (MPOE), octadecyl organically modified montmorillonite (OMMT), and their combinations as compatibilizers in composites made from Cunninghamia lanceolata waste and low-density polyethylene. Physical and mechanical properties of the composites were then determined using SEM, FTIR, and mechanical testing. Results re-

vealed a notablet 41.46% increase in tensile strength with the combined use of MPOE and OMMT, while the inclusion MPOE alone improved impact strength by 26.89%. This dual hybrid compatibilization approach proved to be more efficient in enhancing interaction and mechanical properties of the composite.

Zhou et al. [109] also reported positive results achieved through the use of multiple coupling agents for compatibilization. Specifically, they employed a combination of maleic anhydride polyethylene (MAPE) with bis(triethoxysilylpropyl)tetrasulfide, as well as a blend of MAPE with vinyltrimethoxysilane in rubber-wood-plastic composites (RubWPC). Their findings indicated that composites treated with these hybrid coupling agents displayed a higher storage modulus compared to both untreated samples and those treated with a single coupling agent. This improvement was attributed to the superior quality of interfacial bonding. Moreover, the observed shift in relaxation peak and glass transition temperature (Tg) towards higher values in the treated composites further confirmed the enhancement of fiber-matrix interfacial interaction and adhesion. Khamtree et al. [110], however, experimented with three distinct fiber varieties—coir fiber, rubberwood flour (RWF), and palm fiber—embedded within a polypropylene matrix. Their findings demonstrated that the incorporation of MAPP notably influenced the physical and mechanical properties of these WPCs, leading to improved interfacial adhesion between fibers and matrix, as well as enhanced crystallization characteristics.

Ghorbani et al. [111] investigated the impact of silane compounds on the properties of poplar wood polymer composites. Samples were impregnated with 3-trimethoxysilyl propyl methacrylate, styrene, methyl methacrylate, and their mixtures using vacuum-pressure method. Observations from scanning electron microscopy and Fourier transform infrared analysis revealed tight polymer contact with wood cell walls, especially with styrene/methyl methacrylate and 3-trimethoxysilyl propyl methacrylate combinations. Styrene impregnation increased composite density compared to methyl methacrylate, particularly with 3-trimethoxysilyl propyl methacrylate. Improved mechanical strength was noted, with the greatest strength observed in samples treated with 3-trimethoxysilyl propyl methacrylate/styrene/methyl methacrylate, while the highest hardness was achieved through cross-link formation between the modified wood cell wall and polymer. These findings provide empirical support for the hypothesis positing that the synergistic combination of coupling agents yields more significant improvements in WPC properties compared to their isolated application.

Yeh et al. [112] investigated the effectiveness of coupling agents, namely polypropylene grafted with maleic anhydride (PP-g-MA) and styrene ethylene-co-butylene styrene block copolymer grafted with maleic anhydride (SEBS-g-MA), in polypropylene-based wood–plastic composites (WPCs) containing 50 wt% wood flour. The study revealed that incorporating up to 5 wt% PP-g-MA resulted in a doubling of tensile strength and more than doubling of reversed-notch Izod impact strength, while maintaining the tensile modulus. On the other hand, SEBS-g-MA showed a greater enhancement in impact strength compared to tensile strength, albeit with a reduction in tensile modulus. Moreover, when 2 wt% PP-g-MA and 1 wt% SEBS-g-MA were combined, there was a significant enhancement in impact strength, without any significant reduction in tensile strength or modulus, in contrast to the effects observed with PP-g-MA alone. In a similar study, Elrasas et al. [113] used maleic anhydride (PE-g-MA) coupling agent instead, and examined how the physical and mechanical properties of wood-recycled High Density Polyethylene (HDPE) composites were affected by varying the PE-g-MA ratios. Their SEM analysis showed improved homogeneity due to the use of PE-g-MA, and FT-IR results revealed the presence of new chemical bonds between the wood fibers and polyethylene chains. TGA results

also portrayed enhanced thermal stability. Both mechanical and physical properties of the WPC improved with increase in PE-g-MA content, peaking at 2% weight, before declining. Farsi et al. [114] also employed PE-g-MA as a compatibilizer in HDPE/WF nanocomposites and observed a significant improvement in their tensile strength, tensile modulus, toughness, and physical properties by incorporating PE-g-MA up to 3%.

In a work published by Bhandari et al. [115], the impact of incorporating 5 wt% MAPP compatibilizer on the mechanical and morphological characteristics of cost-effective WP composites were investigated. These composites, containing both untreated and treated Sorea robusta WF, were manufactured using various WP weight ratios via melt mixing and compression molding techniques. Their SEM analysis indicated enhanced interfacial adhesion in MAPP-coupled composites, with no observable pulled-out fibers, along with reduced water absorption. In particular, MAPP-compatibilized composites containing 40 wt% WF exhibited water absorption levels similar to those of 20 wt% composites lacking MAPP. These findings also underscored the efficacy of MAPP in augmenting filler-matrix interaction and enhancing the overall performance of WPCs.

Similar studies on various coupling agents exist in literature, most of which concur that the use of compatibilizers in low concentrations, typically below 5% leads to a significant boost in mechanical properties of natural fiber reinforced polymer composites [116, 117, 118, 119, 120, 121, 122, 123, 124, 125, 126, 127, 128, 129, 130]. Among the coupling agents investigated, Maleic Anhydride Polypropylene (MAPP) stands out as particularly effective for enhancing the performance of PP bio-composites. Studies have consistently shown that MAPP contributes to minimizing phase separation and fosters strong adhesion between the PP matrix and bio-based fibers, leading to improved interfacial bonding and efficient stress transfer within the resulting biocomposites. This enhanced interfacial interaction is crucial for achieving optimal mechanical performance and long-term durability in PP-based biocomposite materials. [131, 132, 117, 133].

1.4.4 Review of Cordenka Fiber-Reinforced Thermoplastics and Thermosets

Bax et al. [70] compared Cordenka/PLA injection molded materials with Flax/PLA counterparts, reporting that the former exhibited superior tensile and impact strength. Ganster et al. [71] compared Cordenka/PP injection molded materials with glass fiber/PP counterparts, noting that Cordenka/PP materials showed higher tensile strength and significantly improved impact strength in unnotched specimens. Such improvements are attributed to the high toughness of Cordenka fibers. Ganster et al. [71] compared Cordenka/PP injection molded materials with glass fiber/PP counterparts, noting that Cordenka/PP materials showed higher tensile strength and significantly improved impact strength in unnotched specimens. Such improvements are attributed to the high toughness of Cordenka fibers.

Kovalovs et al. [134] analyzed the impact response of hybrid biocomposites made from polypropylene homopolymer (HP400R) reinforced with Cordenka fibers and softwood microfibers (Weho 500). Their findings demonstrated that combining these fillers improved the impact properties, with the incorporation of Cordenka fibers increasing the absorbed energy by 372% compared to unreinforced polypropylene and by 243% compared to polypropylene with 30 wt% Weho fibers. Similarly, Meredith et al. [135] created laminates by combining Biotex flax, Lineo flax, Lineo flax preg, and Cordenka rayon with MTM49, MTM28, and Araldite LY5150 high-strength epoxy resins, and conducted various tests to determine their mechanical properties. Their results showed that Cordenka MTM49 and Biotex MTM49 composites exhibited the highest compressive strengths of

299.6 MPa and 223.5 MPa, respectively. Additionally, Cordenka composites registered a higher tensile strength of 92.6 MPa compared to the flax materials, which ranged from 63 to 77.6 MPa.

Malaba et al. [136] examined the mechanical properties of unidirectional Cordenka fiber-reinforced Furan resin biocomposites with varying high fiber weight fractions. They found that increasing the fiber weight fraction from 51 wt% to 64 wt% enhanced the tensile strength of the biocomposite. However, further increasing the fiber content to 75 wt% led to a reduction in tensile strength. Scanning electron microscopy (SEM) analysis of the tensile fracture surfaces revealed a decline in fiber–matrix adhesion as fiber content increased. This deterioration was primarily attributed to diminished fiber wetting, which weakened the fiber–matrix interfacial bonding and hindered effective stress transfer at the interface.

Japins et al. [137] evaluated the tensile and flexural properties of PP composites reinforced with Cordenka regenerated cellulose fibers and HM400X cellulose microfibers (CMFs). The study reported increases in tensile strength by 34% and flexural strength by 21% for composites reinforced with Cordenka and CMFs, respectively, at a fiber volume fraction of 27%. Moreover, composites reinforced with Cordenka fibers exhibited superior mechanical performance, with tensile strength 45% higher and flexural strength 28% higher than those reinforced with HM400X microfibers. These findings indicate that the regeneration process employed for Cordenka fibers significantly enhanced the interfacial adhesion between the fibers and the polypropylene matrix, thereby contributing to the improved mechanical performance of the composites. Similarly, Wunderlich et al. [138] reported that composite materials incorporating Cordenka fibers exhibit superior impact strength and tensile strength compared to those utilizing flax fibers. These enhanced mechanical properties position Cordenka-based composites favorably for potential applications in the automotive and electronics industries.

1.5 Research Gap and Motivation

From the reviewed literature, it is evident that significant efforts have been dedicated to enhancing the mechanical performance of wood–plastic composites (WPCs), focusing on reinforcement types, fiber–matrix ratios, processing techniques, compatibilizers, and functional additives. Nonetheless, critical knowledge gaps persist. Notably, while cellulose nanofibers (CNFs) have been extensively incorporated into polymer matrices—primarily as fillers or components in hybrid composites with the aid of compatibilizing agents—their utilization as surface coatings on preformed WPCs remains unexplored. Similarly, the effects of surface modification techniques such as plasma treatment and ultraviolet (UV) irradiation on the mechanical and morphological characteristics of WPCs have not been sufficiently investigated. Furthermore, the application of thin-film plastic laminates to WPC surfaces as a means to improve mechanical properties has yet to be addressed in the literature. In the context of regenerated cellulose fibers, although Cordenka fibers have been employed as reinforcements in polymer composites, strategies to optimize their interfacial adhesion with polypropylene (PP), particularly via multi-pin-assisted resin impregnation (M-PaRI), have not been reported. Addressing these gaps will provide valuable insights into surface engineering and fiber pre-treatment methods aimed at advancing the performance of WPCs and natural fiber–polymer composites.

1.6 Aim of the Study

This study aims to investigate the influence of surface modification techniques including plasma treatment, ultraviolet irradiation, thin-film lamination, and cellulose nanofiber-based coatings on the mechanical and morphological properties of wood fiber reinforced polypropylene composites. Additionally, a comparative analysis is conducted between polypropylene composites reinforced with regenerated cellulose fiber known as Cordenka and those reinforced with natural cellulose fiber such as ramie to clarify performance differences under consistent processing conditions. Both fiber types underwent melt-press-assisted resin impregnation with polypropylene resin before composite fabrication via injection molding. This approach facilitates a direct comparison of the mechanical behavior and microstructural characteristics of regenerated and natural cellulose fiber composites within the same polypropylene matrix and processing framework.

1.7 Research Objectives

1.7.1 General Objective

To investigate the mechanical and morphological properties of polypropylene composites reinforced with wood, regenerated cellulose (Cordenka), and natural cellulose (ramie) fibers, focusing on the effects of fiber type, fiber pre-impregnation, and post-fabrication surface modification treatments on composite performance.

1.7.2 Specific Objectives

The specific objectives are to:

- Fabricate polypropylene composites reinforced with wood, Cordenka, and ramie fibers, employing melt-press-assisted resin impregnation for fiber pre-processing where applicable.
- Apply surface functionalization techniques, including plasma treatment, ultraviolet irradiation, thin-film lamination, and cellulose nanofiber-based coatings, to the fabricated composites.
- Conduct mechanical testing to evaluate tensile strength, modulus, and impact resistance of the composites.
- Perform morphological characterization to assess fiber-matrix adhesion and composite microstructure.
- Analyze and interpret the mechanical and morphological data to elucidate the influence of fiber type and surface treatment on the overall composite performance.

1.8 Significance of the Study

In an era of increasing global emphasis on sustainability, industries face mounting pressure to adopt eco-friendly practices and materials. This study is both timely and essential, as it addresses two critical priorities: advancing sustainable manufacturing practices and improving the performance of composite materials. By exploring surface treatments for

composite materials and the use of regenerated cellulose fibers, such as Cordenka, as alternatives to conventional synthetic fibers, this research contributes to reducing reliance on non-renewable resources while promoting greener manufacturing solutions. The outcomes of this study have far-reaching implications. In the industrial sector, it could lead to the development of stronger, more durable, and environmentally sustainable products, ranging from pressure vessels to bridge components and wind turbine blades. From an economic perspective, the adoption of renewable materials and improved production processes could reduce costs associated with waste management and carbon taxes. On a societal level, this research supports global efforts to combat climate change by aligning with sustainable development goals, including zero carbon emissions and resource efficiency. By addressing these critical challenges, this study is poised to make a meaningful groundbreaking contribution to advancing material science and engineering while fostering sustainable development in industries worldwide.

1.9 Scope and Limitations

This study is limited to the development of polypropylene composites reinforced with Cordenka, ramie, and wood fibers, and to the evaluation of the effects of fiber type, fiber pre-treatments, and surface modification techniques on the mechanical and morphological properties of the composites. Aspects beyond these parameters are not considered in this research.

1.10 Organization of the Thesis

This thesis is organized into six chapters. Chapter 1 introduces the study by providing the background, defining the research context, reviewing relevant literature on green composites and surface modification techniques, and outlining the research objectives, scope, and rationale. Chapter 2 investigates the influence of thin-film surface lamination on the mechanical properties of wood-plastic composites, including detailed descriptions of materials, methods, results, and their interpretation. Chapter 3 examines the effects of plasma and ultraviolet (UV) irradiation, as well as surface coatings with acrylic resin and cellulose nanofibers, on composite performance, presenting comprehensive experimental procedures and analyses. Chapter 4 compares the mechanical and morphological behavior of Cordenka and ramie fiber-reinforced polypropylene composites, focusing on differences in their mechanical and morphological behavior. Chapter 5 synthesizes the key findings of the study, draws overall conclusions, and proposes directions for future research aimed at enhancing the performance of fiber-reinforced polymer composites.

The organization of the thesis is summarized in the chapter roadmap diagram shown in Figure 1.5.

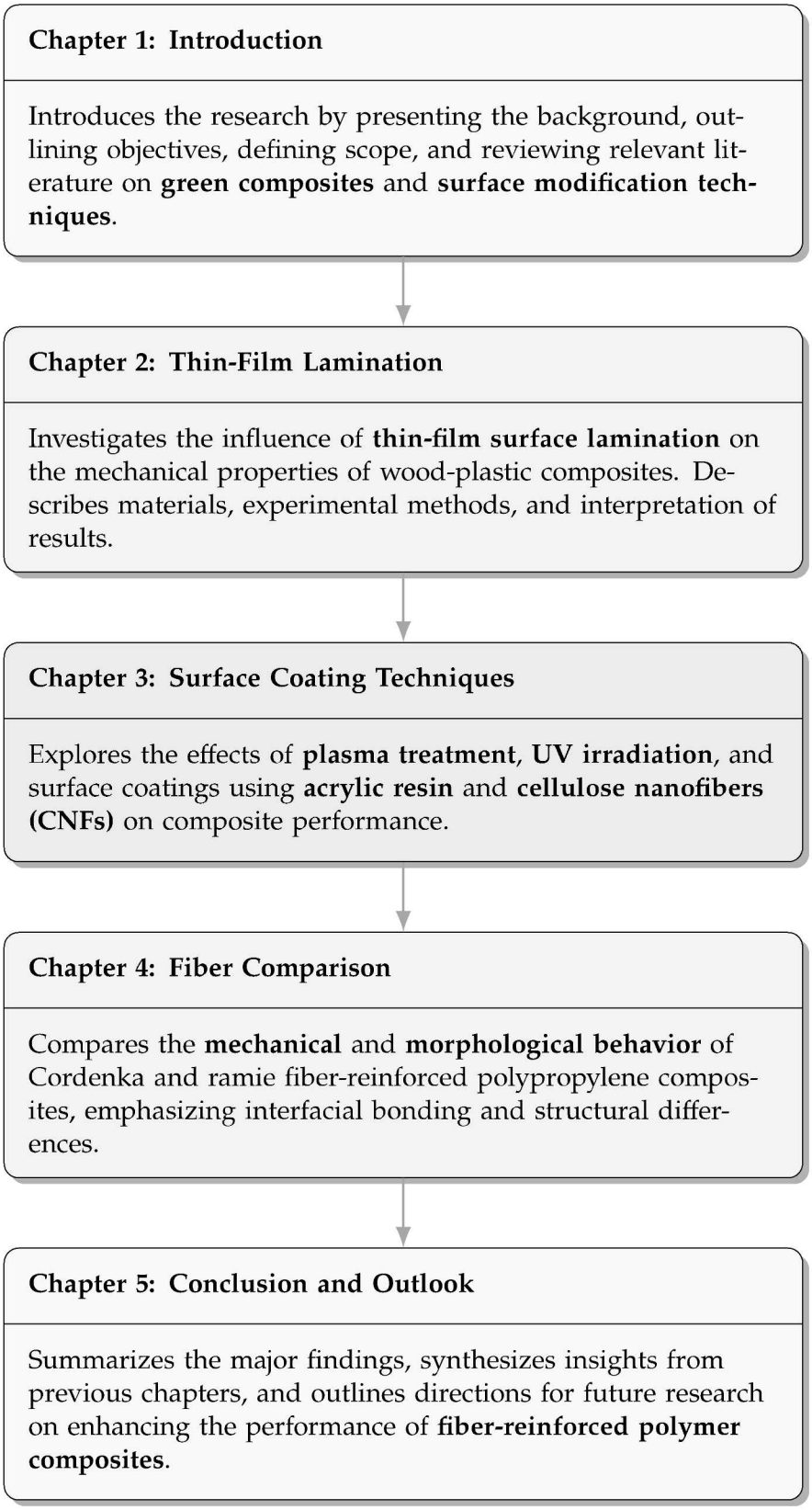

Figure 1.5: Visual roadmap of the thesis structure.

Chapter 2

Influence of Film Lamination on the Mechanical Properties of Wood-Plastic Composites

2.1 Introduction

As highlighted in Chapter 1, the effect of film lamination on the tensile properties of wood-plastic composites (WPCs) has not been extensively studied. This chapter investigates the influence of laminating WPC surfaces with polymer films, specifically PP and PET, on their mechanical properties. PP and PET were selected due to their contrasting tensile strengths: PP has lower tensile strength than WPC, while PET has higher tensile strength. This contrast is crucial for assessing whether the lamination process itself, regardless of the inherent tensile strength of the films, can enhance the mechanical properties of WPCs. The results show that PET film exhibited significant lamination effectiveness, as indicated by higher strength values than those predicted by the rule of mixtures. In contrast, PP film generally reduced the tensile strength of the substrates but demonstrated lamination effectiveness when applied to double-sided laminated WP substrates. These findings suggest that PET film is more effective for enhancing the mechanical properties of WPCs through lamination.

2.2 Materials and Methods

2.2.1 Raw Materials

Wood fiber masterbatch (Celbrid N, comprising 68.1 wt% wood fiber (WF), 29.2 wt% polypropylene (PP), and 2.7 wt% maleic anhydride-grafted polypropylene (MAPP); Toclas Corporation, Hamamatsu, Shizuoka, Japan) was used as the reinforcement material. Pelletized PP (J108M; Prime Polymer Co., Ltd., Tokyo, Japan) served as the matrix resin. MAPP (Kayabrid 006PP; Kayaku Akzo Co., Ltd., Tokyo, Japan), added at 2 wt% of the base material, was used as a compatibilizer to enhance interfacial adhesion. For surface lamination of the specimens, 0.1 mm PP film (735H10; King Jim Co., Ltd., Tokyo, Japan) and 0.1 mm PET film (HBF-321BN; Iris Ohyama Inc., Sendai, Japan) were applied using a plastic adhesive (Cemedine PPX CA-522; Cemedine Co., Ltd., Tokyo, Japan).

(a) **(b)** **(c)**

Figure 2.1: Raw materials: **(a)** PP pellets (J-108M, Prime Polymer Co., Ltd.); **(b)** WP masterbatch (Celbrid-N, Toclas Co., Ltd.); and **(c)** MAPP compatibilizer (Kayabrid 006PP, Kayaku Akzo Co., Ltd.).

2.2.2 Preparation of Neat PP and WP Specimens

WP specimens containing 25 wt% WF were prepared by melt compounding PP pellets, WF masterbatch (Celbrid N), and maleic anhydride-grafted polypropylene (MAPP; Kayabrid 006PP) in a kneading machine (DS0.5-3MHB-E, Satake Chemical Machinery Industry Co., Ltd., Tokyo, Japan) at 210°C for 10 minutes to ensure homogeneous dispersion of the constituents. The formulation was calculated based on the known composition of the masterbatch—comprising 68.1 wt% WF, 29.2 wt% PP, and 2.7 wt% MAPP [139] —so that the resulting composite contained exactly 25 wt% WF in the PP matrix, taking into account the PP and MAPP contributed by the masterbatch. The compounded material was then cooled and pelletized into granules approximately 2 mm in length using a pulverizing machine (U-280, ZI-420 type, Horai Co., Ltd., Higashi-Osaka City, Japan).

Prior to injection molding, silicone spray (Kure Industry Co., Ltd., Meguro-ku, Tokyo, Japan) was applied to the mold surface of the injection molding machine (Babyplast 6/10P, Rambaldi + Co. I. T. Srl, Molteno (LC), Italy.) to reduce friction and facilitate easy removal of the molded specimens. The granules were then injection molded into dumbbell-shaped specimens. After molding, the specimens were allowed to cool at room temperature for 24 hours. Subsequently, silicone remover (Musashi Holt Corporation, Chiyoda-ku, Tokyo, Japan) was used to clean the specimen surfaces and eliminate any residual silicone spray prior to further processing such as surface lamination. Neat PP specimens were prepared following the same procedure, using only PP pellets (PP J108M; Prime Polymer Co., Ltd., Chuo-ku, Tokyo, Japan), and processed under identical injection molding and cooling conditions. The dumbbell-shaped specimens were prepared in accordance with JIS K7139-A32 specifications. A schematic diagram showing the dimensions of the A32-type specimen is presented in Figure 2.3 [139].

2.2.3 Preparation of PP and PET Film Specimens

PP and PET films, each with a thickness of 0.1 mm, were manually cut into rectangular strips measuring 75 mm in length and 5 mm in width using a sharp hand-held cutting blade. To facilitate secure gripping during tensile testing and to reduce the likelihood of slippage or edge failure, rigid plastic plates (gripping plastics) were prepared from a 2 mm thick plastic sheet and cut into 10 mm $\times$ 5 mm pieces. These gripping plastics

(a) Kneader (DS0.5-3MHB-E, Satake Chemical Machinery Industry Co., Ltd.).

(b) Pulverizing machine (U-280, ZI-420 type, Horai Co., Ltd.).

(c) Injection molding machine (Babyplast 6/10P, Rambaldi + Co. I.T. Srl).

Figure 2.2: Main processing equipment used during specimen preparation.

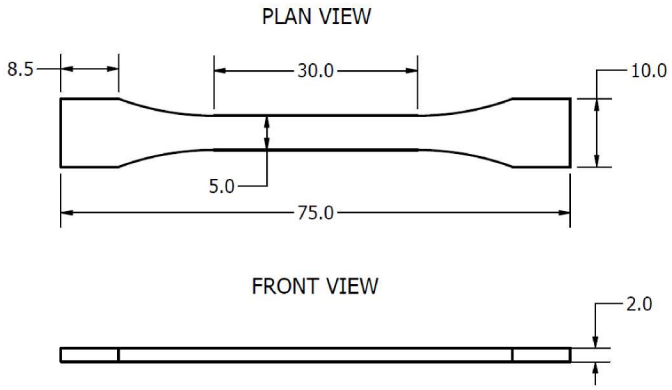

Figure 2.3: Plan and front views of the dumbbell-shaped tensile test specimen prepared in accordance with JIS K7139-A32 standards. All dimensions are in millimeters.

were bonded to both the top and bottom surfaces at each end of the film strips. To ensure effective adhesion, a primer (Cemedine PPX Primer; Cemedine Co., Ltd.) was first applied to the bonding regions of the film strips. Within 30 seconds of applying the primer, a cyanoacrylate-based adhesive designed for polyolefins (Cemedine PPX CA-522) was applied, and the gripping plastics were immediately positioned. Gentle finger pressure was used to maintain full surface contact and proper alignment. The bonded specimens were then left at room temperature for 24 hours to allow complete curing. A dimensioned schematic of the prepared film specimen is shown in Fig. 2.4.

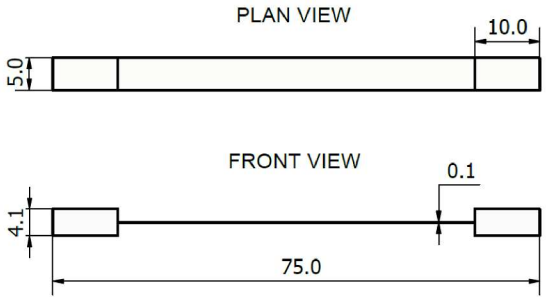

Figure 2.4: Plan and front views of a tensile test film specimen. The film is 0.1 mm thick and 5 mm wide, with plastic gripping plates (2 mm thick) bonded on both top and bottom faces at each end.

2.2.4 Film Lamination of Tensile Specimens

To prepare the laminated dumbbell specimens, the same PP and PET films described in the previous section—each with a thickness of 0.1 mm—were cut into narrow strips 5 mm in width, corresponding to the gauge section of the tensile specimens. Likewise, the same primer used for attaching the gripping plastics in the film specimens was applied to the surface of both neat PP and 25 wt% WP specimens at room temperature. Within 30 seconds of primer application, the previously introduced cyanoacrylate-based adhesive was applied to the primed surface. The film strips were then carefully positioned and laminated onto the adhesive-coated surfaces by pressing manually with finger pressure to ensure intimate contact.

Lamination was performed in four distinct configurations: no lamination (0S), full-surface lamination on one side (1S-F), full-surface lamination on both sides (2S-F), and partial lamination on one side extending from one end to the specimen midspan (1S-H). In all laminated configurations, the film extended continuously across the full specimen length, including the gripping sections—except in (1S-H), where it covered only half the length. A schematic illustration of the lamination configurations is shown in Figure 2.5. All laminated specimens were left to cure under ambient conditions for 24 hours to ensure complete bonding. No external pressure or thermal treatment was applied during the curing period. Representative images of the film and tensile specimens are provided in Figures 2.6 and 2.7, respectively. For clarity and conciseness, representative specimens are presented: PET film specimens for the film sample category and PP film-laminated specimens for the dumbbell tensile specimens. Among the various lamination configurations, only those laminated in the 1S-F configuration are shown, as their external appearance is consistent with all other types.

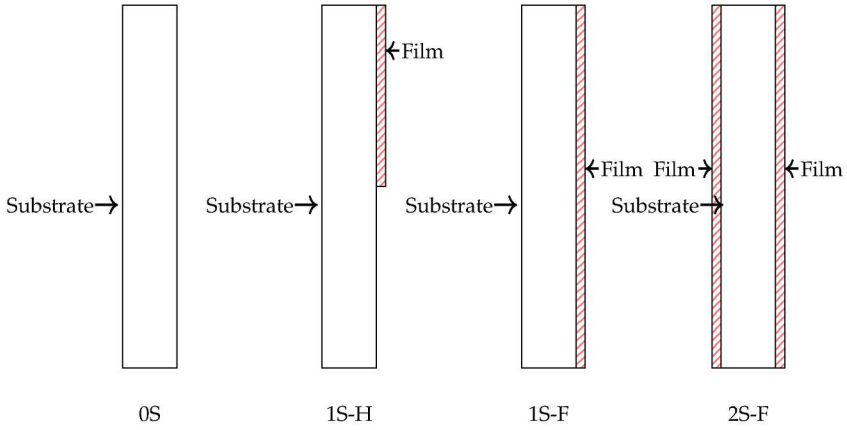

Figure 2.5: Schematic diagram showing the four lamination configurations: unlaminated (0S), one-side half lamination (1S-H), one-side full lamination (1S-F), and two-side full lamination (2S-F). Hatched areas indicate the applied laminating film on the substrate surfaces.

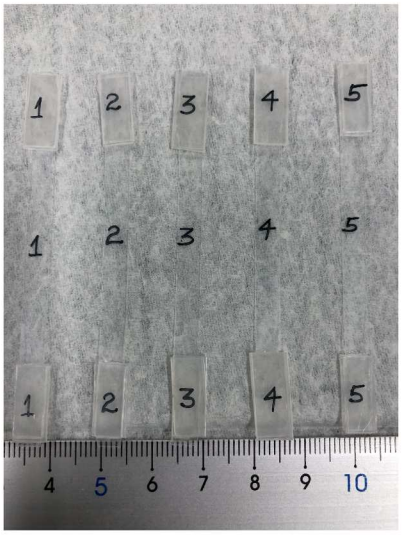

Figure 2.6: Representative images of the 0.1-mm PET film tensile test specimens.

2.2.5 Fourier Transform Infrared Spectroscopy (FTIR)

Fourier Transform Infrared Spectroscopy (FTIR) was performed to verify the chemical composition of the PP and PET films. Spectral data were obtained using a Fourier Transform Infrared Spectrometer (FT/IR-6300, JASCO, Tokyo, Japan). A photograph of the FTIR spectrometer used in this analysis is presented in Figure 2.8. The measurements were carried out in the range of 650–4000 cm^{-1} with a resolution of 0.96 cm^{-1}, and the spectra were recorded in absorbance mode. Each scan produced 3475 data points, and the characteristic absorption peaks were compared with reference spectra to confirm the identity of the materials.

2.2.6 Surface Roughness Measurements

Surface roughness was measured using a surface roughness and contour measuring machine (SURFCOM NEX 031/041 DX2/SD2, Tokyo Seimitsu, Japan). The measuring

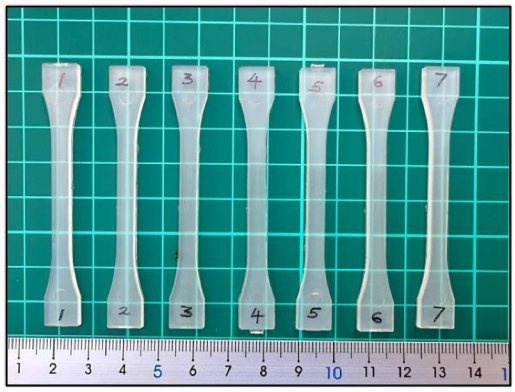

(a) Unlaminated neat PP specimens

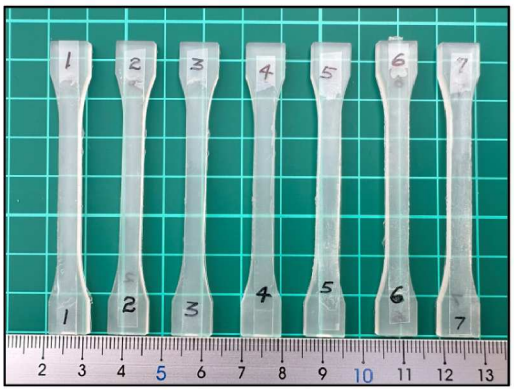

(b) Film-laminated neat PP specimens

(c) Unlaminated 25 wt% WP specimens

(d) Film-laminated 25 wt% WP specimens

Figure 2.7: Representative images of unlaminated and film-laminated tensile specimens. The 1S-F configuration shown in **(b)** and **(d)** is representative of other laminated specimen configurations. Lamination was performed using 0.1 mm thick PP or PET films bonded to the specimen surfaces with a plastic-compatible adhesive.

Figure 2.8: Fourier Transform Infrared Spectrometer (FT/IR-6300, JASCO, Tokyo, Japan) used for spectral analysis of PP and PET films.

instrument used for surface roughness analysis is shown in Figure 2.9. For the unlam-

inated neat PP and WP specimens, measurements were taken in both the longitudinal and transverse directions to comprehensively assess surface topography. The analysis focused specifically on the bonding surfaces, where adhesive would typically be applied. conversely, for the 0.1 mm-thick PP and PET laminating films, measurements were conducted in randomly selected directions. This approach was appropriate given that the films were manufactured via biaxial processing, resulting in isotropic surface characteristics that obviate the need for directional constraints.

Surface roughness measurements were not performed directly on the laminated specimens. Instead, the surface profiles of the laminating films were considered representative of the surface condition of the laminated composites. For each surface, measurements were taken at three randomly selected locations, and the average surface roughness (R_a) was calculated. Scans were performed over a length of 4.0 mm at a speed of 0.150 mm/s. A least-squares line was used for form removal, and a Gaussian filter with a cutoff wavelength (λ_c) of 0.8 mm was applied during data processing.

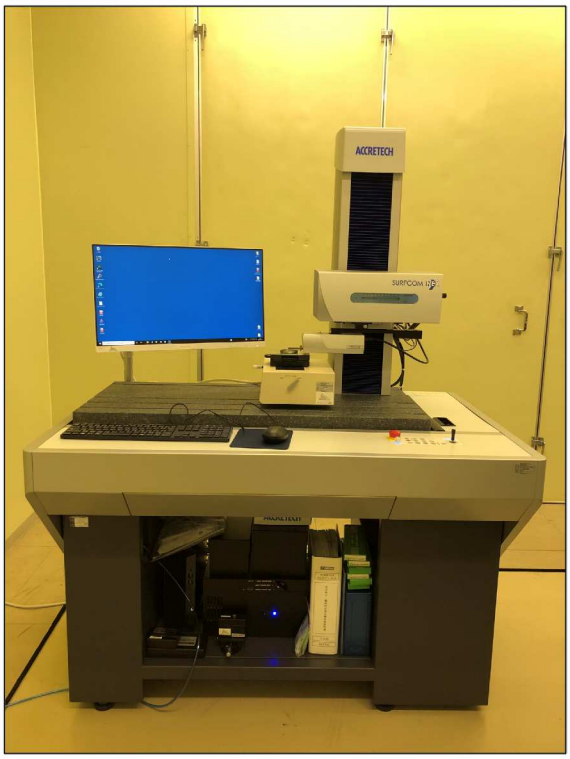

Figure 2.9: Surface roughness and contour measuring machine (SURFCOM NEX 031/041 DX2/SD2, Tokyo Seimitsu, Japan) used to evaluate the surface topography of PP, PET, and composite specimens.

2.2.7 Scanning Electron Microscopy (SEM)

The surface morphologies of both unlaminated and laminated 25 wt% WP specimens were examined using a field emission scanning electron microscope (FE-SEM; JSM-7000F, Japan Electron Optics Laboratory Co., Ltd., Akishima, Tokyo, Japan). The SEM apparatus used for these observations is shown in Figure 2.10. In addition, fractured surfaces obtained after tensile testing were observed to evaluate interfacial characteristics and fracture mechanisms. Prior to imaging, all samples were sputter-coated with a thin layer of platinum to enhance surface conductivity and minimize charging effects. SEM

observations were carried out at an accelerating voltage of 15.0 kV. Magnification levels were varied depending on the morphological features of interest to enable both general surface assessment and detailed interfacial analysis.

Figure 2.10: Field emission scanning electron microscope (FE-SEM; JSM-7000F, Japan Electron Optics Laboratory Co., Ltd., Akishima, Tokyo, Japan) used for surface and fracture morphology analysis of composite specimens.

2.2.8 Mechanical Testing

Tensile tests were performed on both laminated and unlaminated injection-molded specimens, as well as on the laminating films (PP and PET), to evaluate their mechanical properties. All tests were conducted using an LSC-1/30D universal testing machine (JT Tosi) equipped with a 1 kN load cell, operated at room temperature (25 °C) and a constant crosshead speed of 10 mm/min. The universal testing machine used for tensile testing is shown in Figure 2.11.

For each material and test condition, 5 specimens were evaluated, and the recorded load–displacement data were processed and transformed into corresponding engineering stress–strain curves, using established analytical formulations as described in standard references [140, 141].

$$\sigma_t = \frac{P}{A} \tag{2.1}$$

$$\varepsilon_t = \frac{\Delta L}{L_0} \tag{2.2}$$

where σ_t is the engineering tensile stress (MPa), P is the applied load (N), A is the original cross-sectional area of the specimen (mm^2), ε_t is the engineering tensile strain (dimensionless), ΔL is the elongation (mm), and L_0 is the original gauge length (mm).

Figure 2.11: Universal testing machine (LSC-1/30D, JT Tosi, Japan) used for evaluating the tensile properties of molded specimens and laminating films.

2.3 Results & Discussion

2.3.1 Surface Roughness of Unlaminated Specimens and Laminating Films

Table 2.1 presents the average surface roughness (R_a) values for the unlaminated neat PP and 25 wt% WP specimens, while Table 2.2 presents the surface roughness values for the 0.1 mm thick PP and PET laminating films. For all materials, the coefficient of variation (CV)—expressed as a percentage of the mean—is shown in parentheses to indicate measurement variability. Representative surface roughness profiles for the specimens and films are illustrated in Figures 2.12 and 2.13, respectively.

Table 2.1: Surface roughness R_a of unlaminated specimens measured in transverse and longitudinal directions

Material	**Transverse R_a [μm]**	**Longitudinal R_a [μm]**
Neat PP-0S	1.56 (12.00)	0.12 (10.58)
25 wt% WP-0S	0.86 (6.14)	0.31 (2.53)

Note: Values in parentheses indicate the coefficient of variation (CV%) based on replicate measurements, calculated as CV = $\frac{\sigma}{\mu} \times 100$, where σ is the standard deviation and μ is the mean.

Table 2.2: Surface roughness R_a of laminating films

Film	**R_a [μm]**
PP film	0.10 (2.44)
PET film	0.03 (1.40)

Note: Values in parentheses indicate the coefficient of variation (CV%) based on replicate measurements, calculated as CV = $\frac{\sigma}{\mu} \times 100$, where σ is the standard deviation and μ is the mean.

As shown in Table 2.1 and Figure 2.12, the surface roughness (R_a) in the transverse direction was substantially higher than in the longitudinal direction for both unlaminated

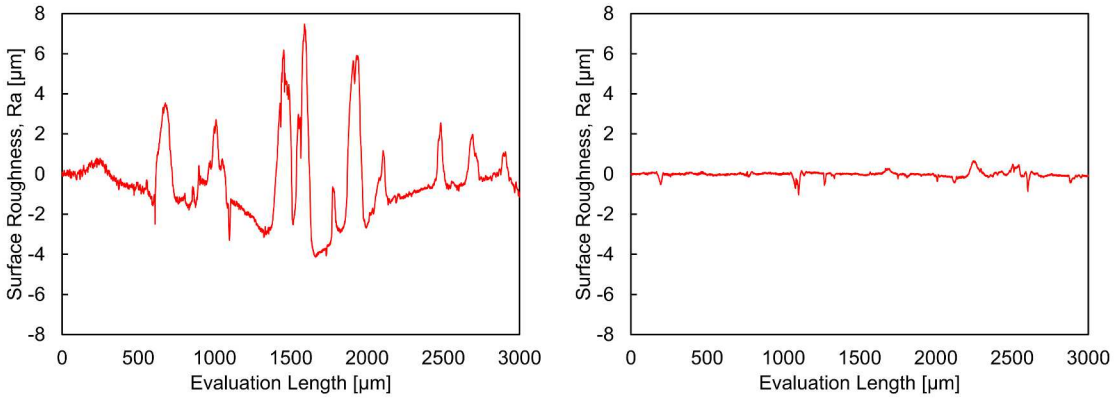

(a) Neat PP (transverse)

(b) Neat PP (longitudinal)

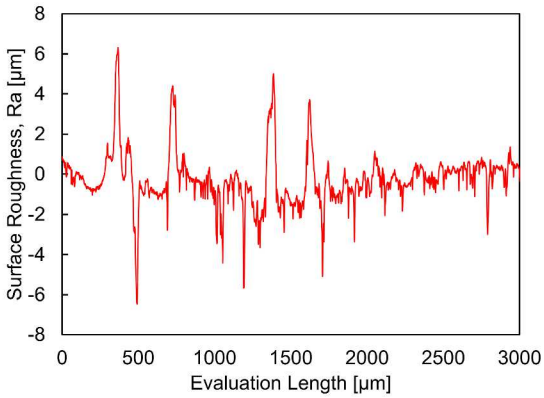

(c) 25 wt% WP (transverse)

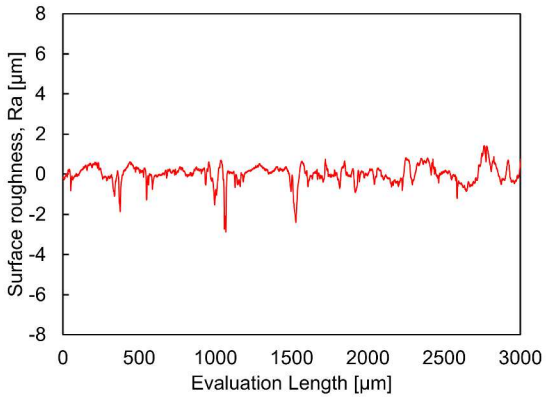

(d) 25 wt% WP (longitudinal)

Figure 2.12: Surface roughness profiles of unlaminated neat PP and 25 wt% WP specimens, plotted for both transverse and longitudinal directions.

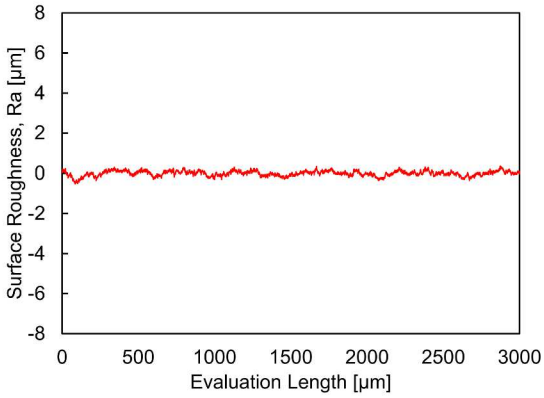

(a) 0.1 mm PP film

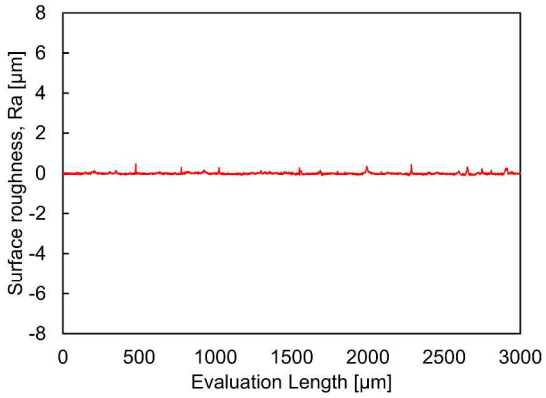

(b) 0.1 mm PET film

Figure 2.13: Representative surface roughness profiles of 0.1 mm PP and PET laminating films. Measurements were conducted without a specific orientation relative to the film's production direction.

neat PP and 25 wt% WP specimens. Specifically, the transverse roughness was approximately 13 times greater for neat PP and 2.8 times greater for 25 wt% WP compared to their respective longitudinal values. In the longitudinal direction, neat PP exhibited lower roughness than 25 wt% WP, whereas in the transverse direction, the opposite trend was observed. This pronounced increase in transverse roughness is likely due to scratches and flaws on the mold die surface, which were replicated on the specimen surface during fabrication. Notably, neat PP specimens appeared more sensitive to these surface imperfections.

For the 0.1 mm PP and PET films (see Table 2.2 and Figure 2.13), surface roughness values differed significantly from those of the neat PP and 25 wt% WP specimens. The films exhibited low and uniform surface roughness, with average R_a values of 0.10 and 0.03 μm for the PP and PET films, respectively. In contrast, the neat PP and 25 wt% WP specimens showed higher roughness values of 1.56 and 0.86 μm, respectively, in the longitudinal direction—the direction with maximum surface roughness. The low roughness and small coefficients of variation observed in the films confirm their homogeneous surface texture, which contributed to the smoothing and homogenization of the composite surface upon lamination. These results demonstrate that both PP and PET films are effective laminating materials for reducing surface roughness and masking surface defects in neat PP and WP specimens.

A comparison of the two laminating films (PP and PET) based on Table 2.2 and Figure 2.13 shows that the 0.1 mm PET film exhibits a smoother surface than the 0.1 mm PP film. The PET film recorded a lower average R_a value of 0.03 μm, compared to 0.10 μm for the PP film. In addition, the surface profile of the PET film (Figure 2.13**b**) appears finer and more uniform than that of the PP film (Figure 2.13**a**), indicating a higher degree of surface homogeneity. Although both films effectively reduced the surface roughness of the neat PP and WP specimens when applied as laminating layers, the PET film proved more effective in achieving a smoother and more uniform laminated surface. This superior performance can be attributed to the intrinsic smoothness and finer microtexture of the PET film, which likely enhanced its ability to conform to and mask surface irregularities in the substrate during lamination.

2.3.2 SEM Surface Morphology of WP Specimens

Figure 2.14 presents scanning electron micrographs of 25 wt% WP specimens, comparing surface morphologies of unlaminated samples with those laminated using a 0.1 mm PET film. Each image includes a scale bar to provide accurate dimensional context. The unlaminated surfaces (Figures 2.14**a** and **b**) exhibit a visibly rough morphology. At increased magnification (Figure 2.14**b**), distinct surface irregularities become apparent, including a prominent void partially bridged by embedded wood fibers within the PP matrix. This feature suggests limited fiber–matrix interfacial bonding; however, the void remains only partially filled, likely due to inadequate wetting or insufficient fiber dispersion during processing. In contrast, the laminated specimens (Figures 2.14**c** and **d**) display a markedly smoother and more continuous surface profile. Even under higher magnification (Figure 2.14**d**), the surface maintains a uniform texture with minimal observable defects.

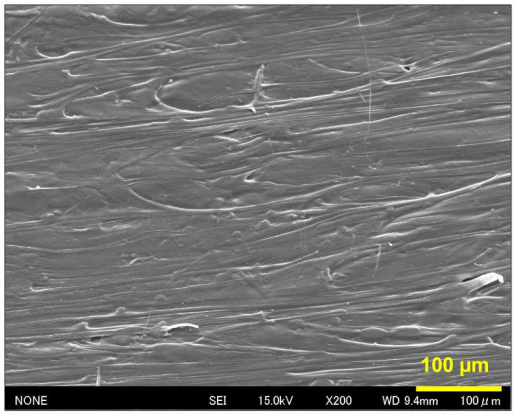

(a) Unlaminated WP specimen surface

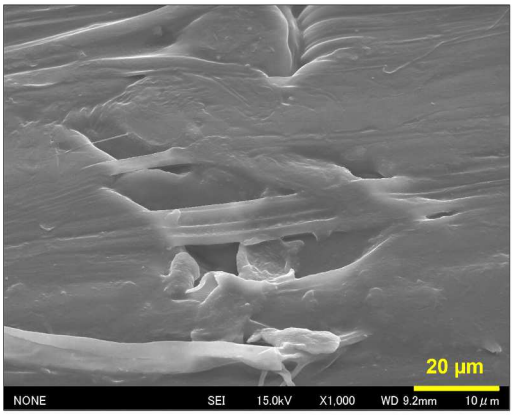

(b) Unlaminated WP specimen surface

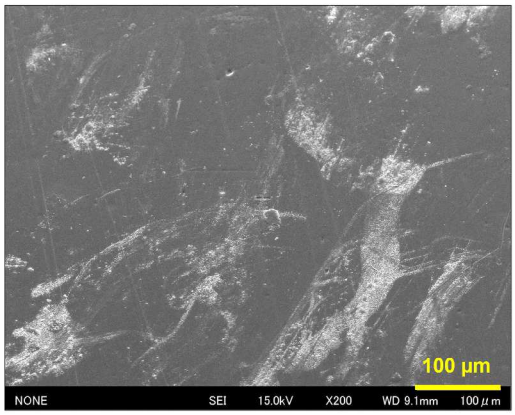

(c) Laminated WP specimen surface

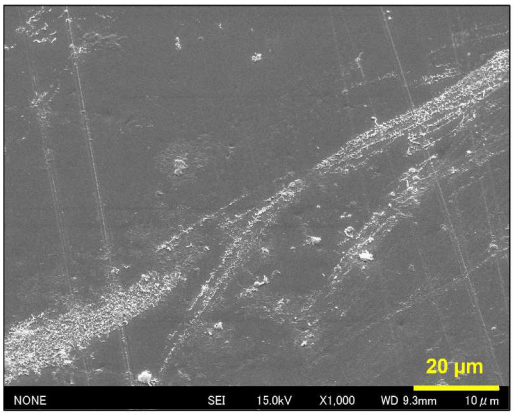

(d) Laminated WP specimen surface

Figure 2.14: Scanning electron micrographs showing the surface morphology of 25 wt% WP specimens. Panels **(a)** and **(b)** show the unlaminated surface at two different magnifications. Panels **(c)** and **(d)** show the surface of WP specimen laminated with a 0.1 mm PET film, also at two different magnifications.

These findings affirm the effectiveness of PET film lamination in mitigating surface irregularities, sealing surface voids, and significantly enhancing the overall surface homogeneity of WP specimens. This observed improvement in surface morphology aligns with reports on WPCs treated with nanodispersed cellulose nanofiber (CNF)-reinforced acrylic resin coatings [139], where both plain and TEMPO-oxidized CNFs also contributed to improved surface homogeneity. However, the degree of surface refinement achieved through PET film lamination in the present study appears to surpass that obtained with these CNF-based treatments. This suggests that the continuous physical barrier provided by film lamination offers a more comprehensive and robust approach for optimizing surface characteristics in WP specimens compared to dispersed nanofiller coatings.

2.3.3 FTIR Analysis of PP and PET Films

The FTIR spectra of the PP and PET films are shown in Figure 2.15 **(a)** and **(b)**, respectively. For the PP film, prominent absorption peaks were observed between 2600-3000 cm^{-1} and 1300-1500 cm^{-1}, which are characteristic of C–H stretching and bending vibrations. In the PET spectrum, strong absorption bands were present in the range of 700-1800 cm^{-1},

indicating ester carbonyl stretching and aromatic ring vibrations, typical of PET. In both cases, the experimental spectra (ATR-corrected) closely matched reference spectra from the FTIR database, confirming that the tested materials are consistent with polypropylene and polyethylene terephthalate films, as stated by the manufacturer.

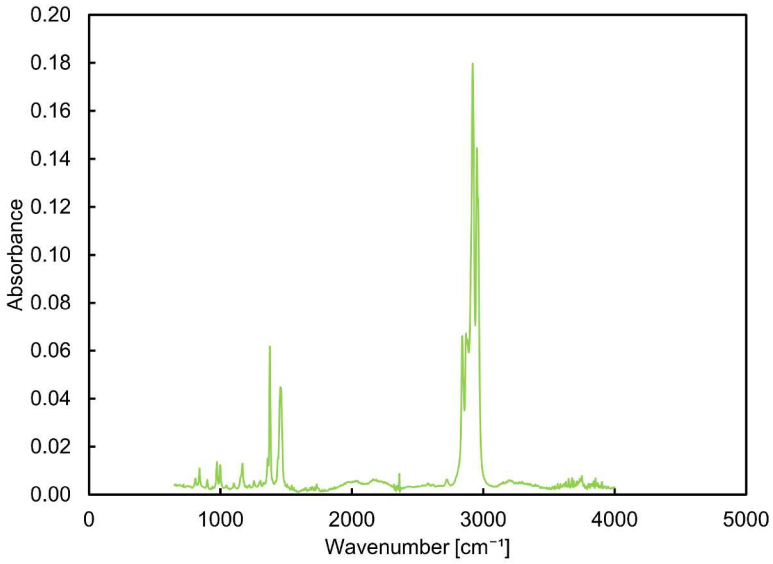

(a) FTIR spectrum of PP film

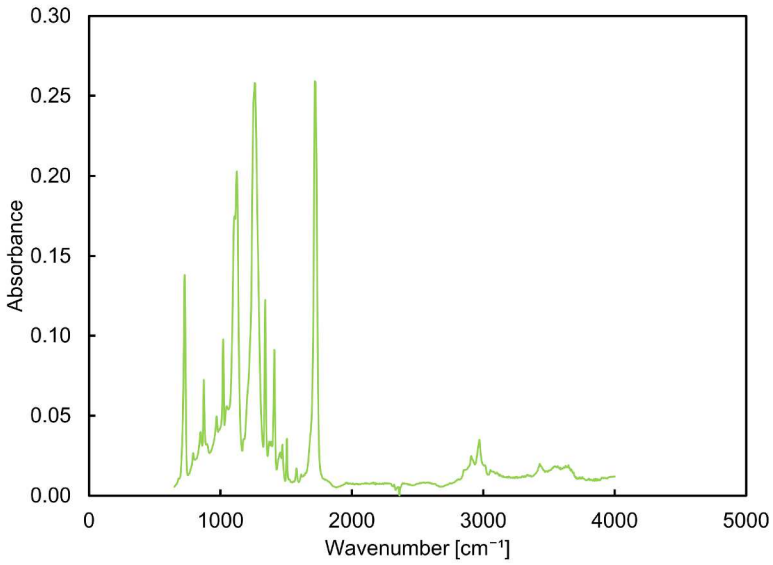

(b) FTIR spectrum of PET film

Figure 2.15: FTIR spectra of 0.1 mm thick polymer films. Both spectra exhibit characteristic absorption bands corresponding to specific functional groups present in polypropylene (PP) and polyethylene terephthalate (PET), respectively. These features confirm the chemical composition and structural identity of each film.

2.3.4 Effect of Lamination on the Tensile Properties of PP and WP Specimens

Table 2.3 details the tensile properties of 0.1 mm PP and PET films, while Table 2.4 presents those of neat PP and 25 wt% WP specimens under their various lamination configurations (0S, 1S-H, 1S-F, and 2S-F), with coefficients of variation shown in parentheses beside the respective values. Figure 2.16 illustrates representative tensile stress–strain curves for the films, and Figure 2.17 depicts the stress–strain behavior of neat PP and WP specimens under these different lamination conditions. Additionally, a **Lamination Strength Ratio (LSR)** column is provided in Table 2.4. This ratio, calculated as σ_L/σ_0, represents the tensile strength of each laminated specimen (σ_L) relative to its unlaminated reference (σ_0). LSR values greater than one indicate enhanced tensile strength due to lamination.

Table 2.3: Tensile properties of PP and PET films

Film Type	Tensile Strength [MPa]	Fracture Strain [%]
PP film	29.5 (2.31)	NF (>100)
PET film	113.2 (2.80)	88.1 (1.47)

Note: Values in parentheses represent coefficients of variation (CV%) based on replicate tests, calculated as $\mathrm{CV} = \frac{\sigma}{\mu} \times 100$, where σ is the standard deviation and μ is the mean. "NF" denotes no fracture observed up to 100% strain.

Table 2.4: Tensile properties of unlaminated and laminated neat PP and 25 wt% WP specimens

Specimen	Laminating Film	Lamination Type	Tensile Strength [MPa]	LSR[a] (σ_L/σ_0)	Fracture Strain [%]
Neat PP	—	0S[b]	37.3 [1.42]	1.00	NF[c]
	PP	1S-F	35.8 [2.15]	0.96	NF
	PP	2S-F	34.9 [1.70]	0.94	18.61 [4.70]
	PET	1S-H	38.0 [0.30]	1.02	14.35 [6.05]
	PET	1S-F	38.4 [1.40]	1.03	NF
	PET	2S-F	41.9 [1.60]	1.12	NF
25 wt% WP	—	0S[b]	39.3 [0.71]	1.00	9.75 [1.85]
	PP	1S-F	39.3 [0.46]	1.00	10.60 [3.27]
	PP	2S-F	41.3 [1.86]	1.05	10.35 [6.13]
	PET	1S-H	40.7 [2.27]	1.04	7.74 [7.83]
	PET	1S-F	41.6 [1.40]	1.06	10.14 [4.52]
	PET	2S-F	47.6 [1.18]	1.21	13.19 [8.99]

[a] Lamination Strength Ratio (LSR) is defined as σ_L/σ_0, where σ_L is the tensile strength of the laminated specimen, and σ_0 is that of the unlaminated reference specimen.
[b] 0S indicates the unlaminated control specimen used as a reference.
[c] NF: No fracture observed up to 200% strain.
Values in parentheses represent coefficients of variation (CV%) based on replicate tests, calculated as $\mathrm{CV} = \frac{\sigma}{\mu} \times 100$, where σ is the standard deviation and μ is the mean.

As shown in Figure 2.16, the tensile properties of the 0.1 mm PET and PP films reveal a marked contrast, underscoring their differing suitability for use as surface laminates in composite structures. The PET film exhibits a tensile strength of

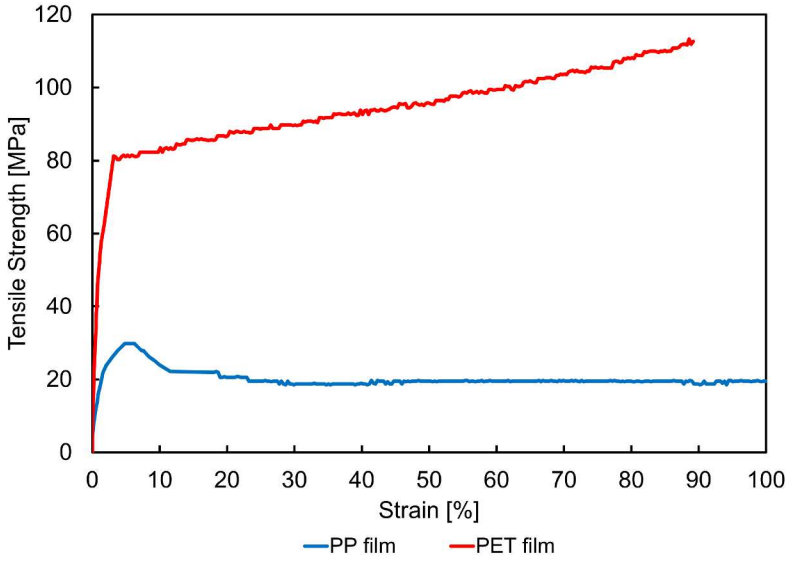

Figure 2.16: Tensile stress-strain curves of 0.1 mm PP and PET films.

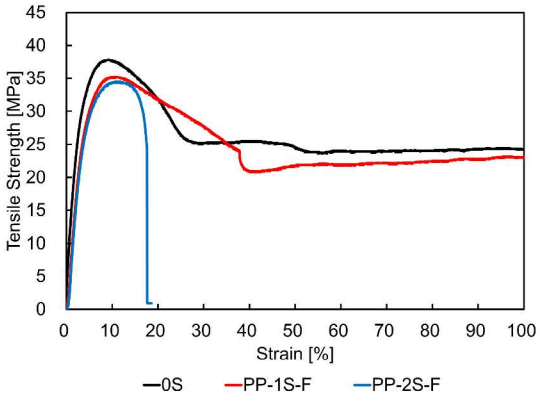

(a) Neat PP laminated with PP films

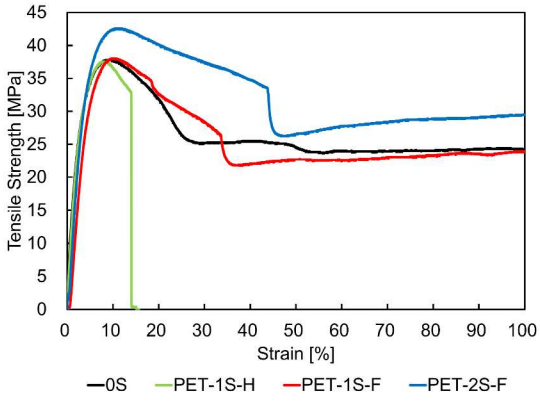

(b) Neat PP laminated with PET films

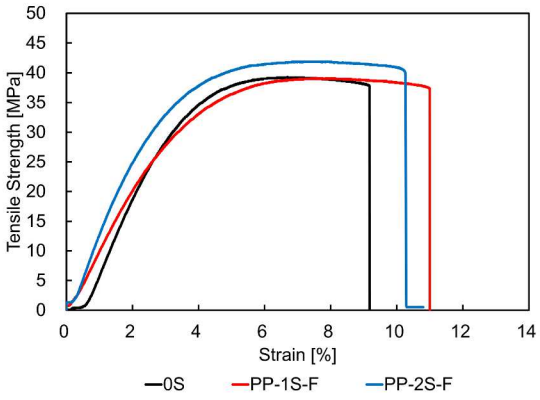

(c) 25 wt% WP laminated with PP films

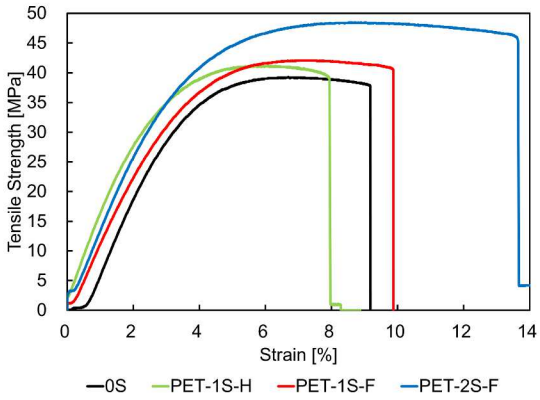

(d) 25 wt% WP laminated with PET films

Figure 2.17: Representative stress-strain curves of neat PP and 25 wt% WP specimens laminated with 0.1 mm PP or PET films across different lamination configurations (**0S, 1S-H, 1S-F, 2S-F**). Panels **(a)** and **(b)** display results for neat PP, while panels **(c)** and **(d)** show results for 25 wt% WP specimens, laminated with PP and PET films, respectively.

113.2 MPa—approximately 3.8 times greater than the 29.5 MPa recorded for the PP film—attributable to the inherently higher stiffness and molecular orientation of PET. While both films display large fracture strains, the PP film is more ductile, with strains exceeding 100% of the original gauge length, compared to an average of 88.1% for PET. These results demonstrate that PET offers superior strength, whereas PP contributes more to flexibility.Moreover, the PET film undergoes significant strain hardening after yielding, with its maximum strength approximately 42% higher than the yield point. In contrast, the PP film appears to exhibit strain softening, characterized by a reduction in stress after peak strength, followed by stable plastic deformation. These contrasting behaviors are critical in evaluating their performance as laminating materials. The strain hardening of PET enhances its load-bearing capability and resistance to plastic deformation under tensile loading, making it more effective in reinforcing the structural integrity of laminated composites. Conversely, the higher ductility of PP may offer advantages in applications requiring flexibility but contributes less to overall stiffness and strength. Accordingly, PET is the more suitable choice for applications where mechanical reinforcement of the substrate is a primary requirement.

Turning to the stress–strain curves of the dumbbell specimens shown in Figure 2.17, it is observed that lamination with the 0.1 mm PP film led to a reduction in tensile strength for the neat PP specimens, as indicated by LSR values below unity. Specifically, the 1S-F configuration exhibited a 4.0% decrease in tensile strength, while the 2S-F configuration showed a more pronounced 6.4% reduction compared to the unlaminated PP specimen. This decline is primarily attributed to the lower tensile strength of the laminated PP film relative to the bulk PP substrate, which introduced a mechanically weaker surface layer and consequently diminished the overall load-bearing capacity of the specimens. This interpretation is further reinforced by the observed trend in which tensile strength decreases progressively with increasing laminated surface area, as seen in the transition from the 0S to the 1S-F and 2S-F configurations. Thus, although PP film lamination may offer certain surface-related advantages—such as homogenization, void sealing, and improved surface smoothness—the overriding influence of its low intrinsic strength ultimately led to a net reduction in tensile performance.

Another reason for the observed decline in strength may be the high sensitivity of polypropylene to stress concentrations, which are often introduced by notches or microcracks that can form on the film surface due to firm adhesive bonding during lamination. Given that PP–PP adhesion is relatively strong compared to bonding with dissimilar materials, any initial crack in the adhesive layer can easily propagate through the film and into the underlying substrate. Because the adhesive bond between the film and the specimen is strong, delamination does not occur, allowing the crack to transfer directly to the specimen surface. This mechanism likely contributes to the observed reduction in tensile strength. This behavior is particularly evident in the 2S-F configuration, which unexpectedly exhibits a markedly low fracture strain. It is inferred that double-sided lamination imposes significant constraints on the specimen during tensile loading. In the absence of debonding, as previously discussed, cracks originating from the film or adhesive interface are rapidly transferred to the substrate, resulting in premature rupture and fracture. This explains the anomalous fracture behavior observed in the 2S-F configuration.

In contrast, the other configurations—namely 0S and 1S-F—exhibited normal ductile behavior, with fracture strains exceeding 200% of the original gauge length. Such extensive elongation is consistent with the well-known ductility of polypropylene and aligns with expectations for unreinforced or single-laminated PP specimens. The 1S-F config-

uration, in particular, retains an unlaminated surface, which allows greater deformation freedom on one side. This reduces the constraining effect associated with film bonding, thereby mitigating premature crack transfer and enabling fracture strain behavior comparable to that of the unlaminated specimen.

The lamination of neat PP specimens with the 0.1 mm PET film, however, resulted in improved tensile strength, as reflected by LSR values exceeding one. The tensile strength increased progressively with greater surface coverage—by 1.9% for the 1S-H configuration, 2.9% for 1S-F, and 12.3% for 2S-F—relative to the unlaminated specimen. This positive correlation is primarily attributed to the superior intrinsic strength and stiffness of PET, which imparts a reinforcing effect akin to that of a composite layer when firmly bonded to the PP substrate. Further evidence is provided by surface roughness measurements and SEM observations (Figures 2.13 and 2.14), which indicate that PET lamination effectively sealed surface voids and irregularities, producing a more uniform and defect-free surface. This morphological improvement likely reduced stress concentrations and delayed the onset of crack initiation under tensile loading. The most significant enhancement was observed in the 2S-F configuration, which benefited from full surface coverage on both sides—minimizing the number of flaw sites and maximizing structural reinforcement, thereby yielding the highest tensile strength improvement among the tested configurations. Additionally, although the adhesive bond between the PET film laminate and the PP substrate is relatively weaker than that observed with PP film lamination, the reinforcement provided by the PET film's superior intrinsic strength appears to outweigh the drawbacks associated with the weaker interfacial bonding. This indicates that the mechanical advantage conferred by the PET layer is primarily governed by its own strength and stiffness, rather than by adhesive performance alone.

With respect to fracture strain, all PET-laminated PP specimen configurations—except for 1S-H—exhibited pronounced ductility, with elongation exceeding 200% prior to failure. This behavior is consistent with the inherent ductility of polypropylene, as previously discussed. In contrast, the 1S-H configuration showed a markedly reduced fracture strain. This anomaly is attributed to stress concentration localized at the specimen midspan, where the PET film coverage terminates. The abrupt interface between the laminated and unlaminated regions likely acted as a stress riser, initiating crack formation at the substrate surface. The crack then propagated rapidly through the specimen, leading to premature rupture. This explanation is supported by the observation that, in all tested specimens within the 1S-H configuration, fracture consistently occurred at the midspan—precisely at the transition point between the bonded and unbonded regions.

For the WP25 specimens, lamination with the PP film exhibited a distinct behavior compared to the neat PP specimens. Under the 1S-F configuration, tensile strength remained essentially unchanged, as reflected by LSR value of 1.00. However, the 2S-F configuration showed a significant increase of 5.0% in tensile strength relative to the unlaminated composite. This contrasts with the trend observed in neat PP specimens, where lamination with the same PP film consistently reduced tensile strength across all configurations. This difference suggests that, despite the intrinsically low tensile strength of the PP film, its lamination on the rougher surface of the WP composite produced a net positive effect. The presence of wood fibers inherently increases surface roughness and introduces interfacial voids or micro-defects during molding. When laminated with PP film, these surface irregularities were effectively smoothed and sealed, resulting in enhanced surface homogeneity. This likely reduced stress concentration sites and delayed crack initiation under tensile loading.

Moreover, although the lamination introduces a relatively weaker surface layer and

restricts local deformation due to the strong but brittle adhesive bond, these drawbacks appear to be outweighed in the case of WP specimens by the reduction in surface flaws and improved load distribution at the interface. Especially in the 2S-F configuration, where both surfaces are covered, the cumulative effect of void sealing and stress mitigation becomes more pronounced, resulting in a net gain in tensile performance. These results underscore that surface modification through PP film lamination can be more beneficial for composite materials—where stress concentration is a greater concern—than for homogeneous polymers.

For the WP25 specimens laminated with PET film, tensile strength improvements of approximately 4%, 6%, and 21% were observed for the 1S-H, 1S-F, and 2S-F configurations, respectively, relative to the unlaminated baseline. These results demonstrate that lamination in all configurations led to measurable enhancements in tensile strength, with the 2S-F configuration yielding the most pronounced improvement—21%, the highest observed in this study. The mechanism underlying this enhancement is consistent with that described for PET-laminated neat PP specimens. Specifically, the improvement arises from a combination of the reinforcing contribution of the PET film—whose inherent tensile strength exceeds that of the substrate—and the beneficial surface homogenization effect. The PET film effectively masks surface voids and irregularities, promoting more uniform stress distribution during loading. The superior performance of the 2S-F configuration underscores the importance of bilateral surface modification: lamination on both sides more effectively seals surface defects, mitigates premature failure by suppressing crack initiation sites, and thus yields a substantial gain in mechanical performance. This interpretation is further supported by the fractographic analysis presented in the subsequent section.

Regarding the fracture strains of the WP25 specimens, film lamination generally led to increased ductility across all configurations, as evidenced by higher fracture strains compared to the unlaminated specimen (Table 2.4, Figure 2.17). This enhancement is attributed to the synergistic interaction between the ductile laminating films and the brittle WP substrate, whereby the films absorbed part of the applied strain and redistributed stress more uniformly, effectively delaying fracture initiation. An exception was observed in the 1S-H configuration, which exhibited a noticeably reduced fracture strain. As discussed earlier in the case of neat PP specimens laminated with PET film, this reduction is likely due to asymmetric surface coverage—specifically, the film terminating near the specimen's mid-span—creating a localized stress concentration that served as a crack initiation site. The consistent mid-span fracture location observed in this configuration supports this interpretation.

In summary, the results demonstrate that film lamination—particularly with PET—can significantly enhance the tensile strength of both PP and WP specimens, with improvements strongly influenced by the film's mechanical properties, bonding effectiveness, and surface coverage. Notably, PP film, despite its lower intrinsic strength, offered modest benefits for WP specimens by mitigating surface flaws that act as stress concentrators.

2.3.5 Fracture Surface Analysis of WP Specimens

Figure 2.18 presents the fracture morphology of 25 wt% WP after tensile testing. Based on the SEM micrographs, there was no observable evidence of macro-scale fiber pull-out or inter-facial debonding on the fracture surfaces, suggesting relatively strong inter-facial adhesion between the wood fibers and the polypropylene matrix. Visual inspection of

the fractured surfaces revealed two distinct regions that could be differentiated only by color: a smaller, whitened area and a larger, brown region. However, differences in surface texture were not detectable by the naked eye. Upon examination with a stereoscopic microscope, the larger brown region appeared rougher and more topographically irregular, whereas the smaller white region appeared comparatively smoother. These morphological differences were further confirmed by SEM imaging, which—despite not capturing color—clearly revealed two distinct fracture surface textures: a rough, bumpy region occupying a larger portion of the surface, and a smoother region covering a smaller area. To facilitate interpretation, the boundaries between these regions have been clearly demarcated and labeled in the SEM micro-graphs shown in Figure 2.18**a–c**.

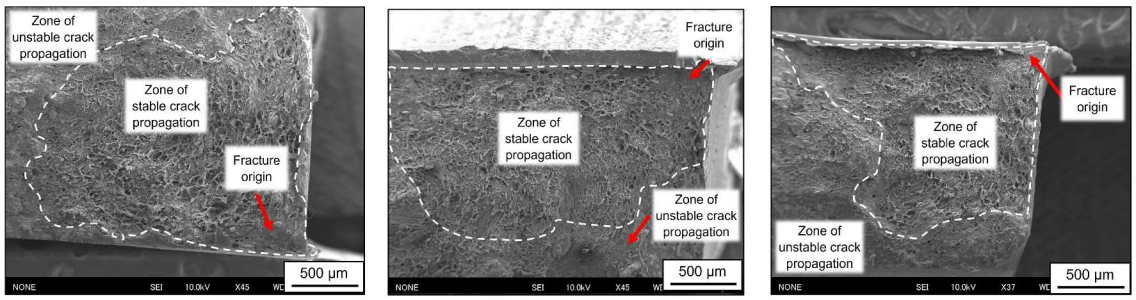

(a) Unlaminated specimen **(b)** PP-laminated specimen **(c)** PET-laminated specimen

Figure 2.18: Scanning electron micrographs of the fracture surfaces of 25 wt% WP specimens after tensile testing. Panels **(a)**, **(b)**, and **(c)** correspond to unlaminated, PP-laminated, and PET-laminated specimens, respectively. The fractured cross-section reveals two distinct areas: a rough, bumpy region and a smoother, whitened region.

This fracture pattern—comprising a larger rough, brown region and a smaller, smoother, whitened region—is consistent with the findings of Nordin et al.[142], who observed the reverse morphology under fatigue loading conditions. The whitened zone is indicative of polypropylene fibrillation, as suggested by its characteristic appearance and previously confirmed by Nordin et al.[142] through high-magnification SEM imaging. In addition, a distinct flat region was consistently observed near the corner edges of the fracture surface, located exclusively within the whitened area across all specimen configurations—unlaminated, PP-laminated, and PET-laminated—as illustrated in Figure 2.18.

In the context of fracture mechanics, crack propagation is broadly classified into two regimes: stable and unstable. In stable crack growth, the crack advances gradually under increasing load, while in unstable crack growth, rapid and catastrophic failure occurs once a critical crack length is reached [141, 143]. Based on the morphology and location of the distinct regions, it is inferred that the whitened area corresponds to the zone of stable crack growth, and the brown, rough region represents the zone of unstable crack propagation. The flat feature within the whitened region is considered the likely site of crack initiation, from which the fracture subsequently propagated across the cross-section of the specimen. As previously noted, Nordin et al. [142] reported a dominant white fibrillated region and a relatively smaller brown area in fatigue-tested specimens. This discrepancy is attributed to the nature of loading: fatigue failure occurs at lower stress amplitudes but over longer durations, allowing cracks to propagate extensively before final failure. In contrast, tensile failure, as in the present study, occurs under higher stress levels where the critical crack length is reached more rapidly, resulting in a comparatively smaller stable fracture zone and a more extensive unstable region.

To assess the effect of film lamination on the suppression of fracture initiation, it is essential to consider the proportion of the specimen's surface area covered by the laminate. Given that all specimens share an identical gauge length, the analysis can be normalized by considering a unit gauge length and focusing on the cross-sectional perimeter. For a specimen measuring 5 mm in width and 2 mm in thickness, the cross-sectional perimeter is 14 mm. The lamination film, also 5 mm wide, is applied to the broader (5 mm) surfaces of the specimen. Based on this configuration, the fraction of the perimeter covered by the laminate corresponds to approximately 10/14 for double-sided full-length lamination (2S-F), 5/14 for single-sided full-length lamination (1S-F), and 2.5/14 for single-sided half-length lamination (1S-H).

Among these configurations, 2S-F provides the most extensive surface coverage and correspondingly yielded the greatest improvement in tensile strength. This trend indicates a clear correlation between the fraction of laminated surface and the degree of mechanical reinforcement. While this enhancement is partly attributable to the inherent stiffness and strength of the laminate, scanning electron microscopy (SEM) images of the fracture surfaces suggest a complementary mechanism: surface shielding. Lamination appears to mitigate fracture initiation by covering surface irregularities and defects—particularly at or near the corners—that typically serve as sites for crack initiation under tensile loading.

As the laminated area increases, a larger number of these critical surface features are shielded, thereby reducing the likelihood of premature failure. Although the 2 mm side faces remain unlaminated in all configurations, the 2S-F specimens still exhibit notable resistance to fracture, underscoring the effectiveness of shielding the broader 5 mm faces. This observation implies that further gains in mechanical performance could potentially be achieved by extending the film to wrap around or encapsulate the side faces. Future studies should therefore explore full-surface encapsulation strategies, including coverage of the narrow sidewalls, to assess their influence on crack suppression and overall mechanical reliability.

In summary, the SEM analyses reinforce the conclusion that surface lamination enhances fracture resistance by improving surface smoothness, uniformity, and morphological integrity. By effectively sealing topographical defects and reducing the number of accessible fracture initiation sites, lamination contributes to the observed improvements in tensile strength for both neat PP and WP specimens. These findings underscore the significance of surface engineering as a viable strategy for enhancing the mechanical reliability of polymer-based composites.

2.3.6 Rule of Mixtures Prediction and Experimental Comparison

To quantitatively evaluate the influence of 0.1 mm PP and PET surface laminates on the tensile properties of neat PP and 25 wt% WP specimens, theoretical predictions were made using the classical rule of mixtures. This established analytical model estimates the effective macroscopic mechanical properties of a composite system by assuming a linear relationship between the properties of its individual constituents and their respective volume fractions. In this analysis, the laminated specimens were idealized as two-phase composite systems consisting of a surface film bonded to a polymeric substrate—either neat PP or 25 wt% WP.

To enable a consistent comparison of theoretical and experimental tensile properties, the effective volume fractions of the substrate and laminating film were estimated for each configuration—1S-H, 1S-F, and 2S-F. Given the uniform film thickness of 0.1 mm,

the average contributing thicknesses were considered as 0.05 mm for 1S-H (single-side half-coverage), 0.1 mm for 1S-F (single-side full-coverage), and 0.2 mm for 2S-F (double-side full-coverage). Because all specimens shared the same width and gauge length, volume fractions (V_f for the film and V_s for the substrate) were calculated using thickness as the sole variable. This approach provided a physically grounded basis for comparing predictions based on the rule of mixtures with experimental results, as summarized in Table 2.5.

Table 2.5: Volume fractions of substrate and laminating films for neat PP and 25 wt% WP specimens

Specimen Type	Laminating Film	Lamination Type	Substrate Volume Fraction (V_s)	Film Volume Fraction (V_f)
Neat PP	None	0S	1.00	0.00
	PET	1S-H	0.98	0.02
	PP/PET	1S-F	0.95	0.05
	PP/PET	2S-F	0.91	0.09
25 wt% WP	None	0S	1.00	0.00
	PET	1S-H	0.98	0.02
	PP/PET	1S-F	0.95	0.05
	PP/PET	2S-F	0.91	0.09

Notes: The volume fractions V_s and V_f represent the substrate and surface-laminated film, respectively, in each composite specimen.
Lamination types: **0S** = unlaminated; **1S-H** = half coverage on one surface; **1S-F** = full coverage on one surface; **2S-F** = full coverage on both surfaces.

As shown in Table 2.5, the calculated volume fractions for the laminated 25 wt% WP specimens are identical to those of the neat PP counterparts. This consistency reflects the high dimensional precision achieved during injection molding, which yielded specimens with closely matched cross-sectional geometries across both material systems. Although slight variations in cross-sectional area were observed among individual specimens, these deviations were statistically negligible and did not warrant the differentiation of volume fraction values between the two material types. The application of uniform volume fraction assumptions is therefore justified and appropriate for the comparative analysis of tensile behavior.

The theoretical tensile strength of the laminated specimen, denoted as σ_c, was estimated using the classical rule of mixtures:

$$\sigma_c = V_s\sigma_s + V_f\sigma_f \tag{2.3}$$

where σ_s and σ_f represent the tensile strengths of the unlaminated substrate and the laminating film, respectively, and V_s and V_f denote their corresponding volume fractions.

As reported in Section 2.3.4, the measured tensile strengths of the 0.1 mm PP and PET films were 29.5 MPa and 113.2 MPa, respectively. However, since all laminated specimens failed within the substrate—either neat PP or 25 wt% WP—without evidence of rupture or delamination in the bonded films, it was deemed inappropriate to use the films' ultimate tensile strengths in the predictive model. Instead, a more representative approach was adopted by determining the stress sustained by each film at the strain corresponding

to the maximum tensile stress of the respective unlaminated substrate. To implement this correction, the strain values at which the unlaminated substrates reached their tensile strength maxima were first identified from their stress–strain curves. These critical strain values were determined to be 8.2% for neat PP and 6.7% for 25 wt% WP. Given the negligible deviation in deformation behavior between laminated and unlaminated specimens—as illustrated in Figure 2.17—these strain values were considered applicable to the laminated configurations as well. This refinement ensured a more accurate representation of the stress contribution of the film under actual loading conditions.

The tensile stresses corresponding to the critical strain values were then extracted directly from the stress–strain curves of the respective PP and PET films. At 8.2% strain—corresponding to the tensile strength of neat PP—the PET film sustained a stress of 80.0 MPa, while the PP film reached 26.9 MPa. Similarly, at 6.7% strain—corresponding to the tensile strength of the 25 wt% WP substrate—the PET and PP films exhibited tensile stresses of 80.0 MPa and 27.0 MPa, respectively. These nearly identical values across the two substrate types reflect the comparable deformation levels and validate the use of these adjusted film stress values in the predictive model. The refined stress values were substituted into Equation 3.1 to generate more realistic theoretical estimates of the tensile strength for each lamination configuration. These predictions were then systematically compared with the experimentally obtained tensile strengths reported earlier in Section 2.3.4.

Table 2.6 summarizes the theoretically predicted and experimentally measured tensile strengths for all configurations. To quantify the degree of enhancement achieved through surface lamination beyond what is anticipated by simple mechanical blending, the **Model Strength Ratio (MSR)** was calculated. The MSR is defined as the ratio of the experimentally observed tensile strength (σ_E) to the theoretically predicted strength (σ_T), i.e., MSR = σ_E/σ_T. Values greater than unity indicate a strengthening effect beyond rule-of-mixtures expectations, potentially attributable to interfacial effects, load redistribution, or morphological improvements induced by lamination.

For the PP film-laminated neat PP specimens, the Model Strength Ratios (MSRs) were consistently less than 1 across all lamination configurations, indicating that the experimentally measured tensile strengths fell below the values predicted by the rule of mixtures. This deviation suggests that additional factors, beyond the relatively lower tensile strength of the PP film compared to the PP substrate, may have contributed to the reduced mechanical performance. One plausible explanation involves the behavior of the adhesive layer. Although the adhesive for plastics provided a robust bond between the PP film and the PP substrate—owing to the chemical compatibility of identical materials—it may also have introduced mechanical vulnerabilities. Specifically, its inherent brittleness could have facilitated the early onset and propagation of cracks. Given the strong interfacial bonding, delamination was unlikely; instead, once the adhesive fractured, the crack may have quickly advanced through both the film and substrate, precipitating premature failure.

Another contributing factor may lie in the relatively low stiffness of the PP film. Its compliant nature makes it more susceptible to conforming to minor topographical undulations in the adhesive layer. These long-wavelength surface fluctuations, though subtle, can act as loci for stress concentration. Even without visible defects, such mechanical heterogeneity can lower the effective strength of the composite laminate. While this hypothesis remains to be experimentally validated, it presents a credible mechanism for the systematic underperformance of the PP-laminated neat PP specimens relative to theoretical predictions. Future investigations employing techniques such as digital image

Table 2.6: Comparison between theoretically predicted and experimentally measured tensile strengths for various lamination configurations

Specimen	Laminating Film	Lamination Type	Theoretical Strength σ_T [MPa]	Experimental Strength σ_E [MPa]	MSR[a] σ_E/σ_T
Neat PP	PP	1S-H	37.0	—	—
	PP	1S-F	36.8	35.8	0.97
	PP	2S-F	36.4	34.9	0.96
	PET	1S-H	38.3	38.0	0.99
	PET	1S-F	39.3	38.4	0.98
	PET	2S-F	41.1	41.9	1.02
25 wt% WP	PP	1S-H	39.0	—	—
	PP	1S-F	38.7	39.3	1.02
	PP	2S-F	38.1	41.3	1.08
	PET	1S-H	40.4	40.7	1.01
	PET	1S-F	41.3	41.6	1.01
	PET	2S-F	43.1	47.6	1.10

[a] Model Strength Ratio (MSR) is defined as σ_E/σ_T, where σ_E is the experimentally measured tensile strength and σ_T is the theoretical value estimated using the rule of mixtures. Values above 1.00 indicate that the experimental strength exceeds the theoretical prediction.
[b] Lamination types: 1S-H = half coverage on one surface; 1S-F = full coverage on one surface; 2S-F = full coverage on both surfaces.
— indicates that experimental testing was not conducted for the given configuration.

correlation (DIC), finite element analysis (FEA), or fracture surface microscopy could help elucidate the precise mechanisms at play and determine whether microstructural features at the interface contribute significantly to early failure.

For the PET film-laminated neat PP specimens, the MSR values for the 1S-H and 1S-F configurations were slightly below unity, at 0.99 and 0.98, respectively. These results indicate that the experimentally measured tensile strengths were marginally lower than the theoretical values predicted by the rule of mixtures. However, the deviations are minimal and fall within a range that may be considered practically consistent with theoretical expectations. In contrast, the 2S-F configuration yielded an MSR of 1.02, slightly exceeding unity but still very close to the theoretical value. Collectively, these results suggest that the tensile strength of PET-laminated neat PP specimens is largely in agreement with the rule of mixtures.

The relatively good agreement can be attributed to the high stiffness of the PET film, which likely suppresses surface undulations arising from the adhesive layer, thereby minimizing stress concentrations at the film-substrate interface. In the 1S-H and 1S-F configurations, however, part of the PP substrate remains unlaminated. Consequently, surface irregularities or defects on the exposed substrate may act as local stress concentrators, slightly reducing the overall tensile strength. This effect is expected to be minor, but it could account for the small deviations observed. In the 2S-F configuration, full lamination on both surfaces may contribute to a more uniform stress distribution, explaining the slightly higher experimental strength. On the whole, the PET film-laminated

PP specimens exhibit behavior that is consistent with theoretical predictions.

For the PP film-laminated 25 wt% WP specimens, the MSR values exceeded unity across both configurations, indicating that the experimentally measured tensile strengths were higher than the theoretical values predicted by the rule of mixtures. Given the inherently low tensile strength of the PP film relative to the WP substrate, this enhancement cannot be ascribed to direct reinforcement by the film. Instead, it is more plausibly attributed to surface homogenization effects, wherein the laminated PP film may have sealed microvoids, masked surface flaws, and mitigated stress concentrations, thereby improving the overall stress distribution. This interpretation aligns with the mechanisms discussed earlier in Section 2.3.4.

A closer look at the 1S-F configuration shows that while the rule of mixtures predicts a 2% increase in tensile strength relative to the unlaminated specimen, the experimental results show no significant enhancement—yielding an MSR close to 1. This suggests general agreement with the rule of mixtures, with only minor influence from the laminated film. The modest improvement can be attributed to the limited surface coverage provided by single-sided lamination, which restricts the extent of surface homogenization. In contrast, the 2S-F configuration demonstrated a 5% strength gain, compared to a theoretical prediction of 8%. This shortfall reflects the limited mechanical contribution of the PP film, which, despite improving surface integrity, lacks sufficient strength to fully realize the potential reinforcement suggested by the model.

For the PET film-laminated 25 wt% WP specimens, the MSR values consistently exceeded unity, with the highest enhancement in tensile strength observed in the 2S-F configuration—mirroring the trend seen in the PP film-laminated counterparts. This outcome suggests that surface homogenization induced by the PET film contributed to mechanical improvements beyond the predictions of the rule of mixtures, particularly when both surfaces were fully laminated. In contrast, the MSR values for the 1S-H and 1S-F configurations remained close to one, indicating a more limited effect likely due to the smaller proportion of laminated surface area and consequently reduced surface modification.

As detailed in Table 2.4, a comparison of MSR and LSR values reinforces this interpretation. In the 2S-F configuration, the LSR reached 1.21, indicating a 21% experimental increase in strength over the unlaminated specimen, whereas the MSR was 1.10, reflecting a theoretical increase of only 10%. This 11% discrepancy is attributed entirely to surface homogenization effects—specifically, the PET film's ability to seal voids, blunt surface defects, and suppress crack initiation, thereby facilitating more uniform stress transfer during loading. These beneficial surface-related contributions, which are not captured by the rule of mixtures, underscore the importance of interfacial and morphological considerations in laminated composite performance.

Chapter 3

Influence of Surface Treatment on the Mechanical Properties of Wood Plastic Composites

3.1 Introduction

In Chapter 1, it was noted that although surface treatments for wood–plastic composites (WPCs) are well established, they have traditionally focused on enhancing surface aesthetics—such as increasing gloss—and protecting against environmental degradation, including UV exposure, moisture ingress, and microbial attack. In addition, some treatments improve functional properties like electrical and thermal conductivity, wear resistance, and adhesion to other materials. However, limited attention has been given to their potential for improving the mechanical performance of WPCs. This chapter investigates the effect of various surface treatments—namely plasma irradiation, UV irradiation, and CNF coating—on the mechanical properties of WPCs. The results demonstrate that surface treatments can indeed enhance mechanical performance. Further optimization through careful selection of coating methods, materials, and application parameters may yield even greater improvements, warranting continued investigation.

3.2 Materials and Methods

3.2.1 Raw Materials

Wood fiber (Cerbrid N; Toklas Co., Ltd., Tokyo, Japan), pre-compounded with polypropylene into a masterbatch, was used as the reinforcing material. The composition of the WP masterbatch is presented in Table 3.1. Polypropylene (PP-J106 and PP-J108; Prime Polymer Co., Ltd., Tokyo, Japan) was used as the matrix resin. Maleic anhydride-grafted polypropylene (MAPP; Kayaku Akzo Co., Ltd., Tokyo, Japan) was added as a compatibilizer at 2 wt% of the total composite weight. An acrylic paint (SHP470-FT2050; Momentive Co., Ltd., Tokyo, Japan) containing nanodispersed PEGylated cellulose nanofibers (CNFs; Renias Corporation, Tokyo, Japan) was used as a coating agent. CNFs were applied at concentrations of 0%, 1 wt%, and 4 wt%, with fiber diameters of 0.2–0.3 μm (short fibers) and 0.7 μm (long fibers). The raw materials are shown in Figures 3.1 and 3.2.

Table 3.1: Composition of WF/PP Masterbatch

Wood Fiber (WF)	Polypropylene (PP)	MAPP
68.1 wt%	29.2 wt%	2.7 wt%

Figure 3.1: Acrylic paint coating agent (SHP470-FT2050, Momentive Co., Ltd.) with varying CNF content: 0 wt%, 1 wt%, and 4 wt%.

(a) Wood/PP masterbatch

(b) PP-J108

(c) PP-J106

(d) MAPP compatibilizer

Figure 3.2: Constituent materials: (**a**) Wood/PP masterbatch, Celbrid-N (Toklas Co., Ltd.); (**b**) PP-J108 (Prime Polymer Co., Ltd.); (**c**) PP-J106 (Prime Polymer Co., Ltd.); (**d**) MAPP compatibilizer (Kayaku Akzo Co., Ltd.).

3.2.2 Fabrication of Neat PP and WP Specimens

Wood/PP composite pellets were developed by mixing PP-J106 or PP-J108 pellets with wood fiber masterbatch and MAPP. The mixture was then poured into a bi-axial kneading machine (DS0.5-3MHB-E, Satake Chemical Machinery Industry Co., Ltd., Tokyo, Japan) and kneaded at 210 °C for 15 minutes at a rotational speed of 36 rpm to improve fiber dispersion. After kneading, the compounded elements were allowed to cool and solidify for 20 minutes. The solidified material was then pulverized in a pulverizing machine (U-280, ZI-420 type, Horai Co., Ltd., Tokyo, Japan) into pellets approximately 5 mm in length. The resulting WF/PP pellets contained 15 wt%, 25 wt%, and 50 wt% wood fiber. Subsequently, both the WF/PP pellets and neat PP pellets were molded in an injection molding machine (Babyplast 6/10P, Rambaldi & Co.) [144], after applying silicone spray (Kure Industry Co., Ltd., Tokyo, Japan) as a mold release agent, at a molding temperature of 200 °C to form standard dumbbell and strip-shaped WP and neat PP specimens.

The standard dumbbell specimens for tensile testing were fabricated with gauge length, width, and thickness dimensions of 30 mm, 5 mm, and 2 mm, respectively. For impact testing, two variants of strip-shaped specimens were developed: one having a 2 mm deep notch with dimensions of $L \times W \times t = 63 \times 10 \times 4$ mm, and the other without a notch, with dimensions of $L \times W \times t = 70 \times 10 \times 4$ mm. The shapes and dimensions of the fabricated specimens complied with JIS standards. The dimensioned CAD drawings of the specimens are shown in Figure 3.3. After fabrication, a degreaser (silicone remover, Musashi Holt Co., Ltd., Tokyo, Japan) was used to remove any residual silicone spray from the specimen surfaces prior to further processing.

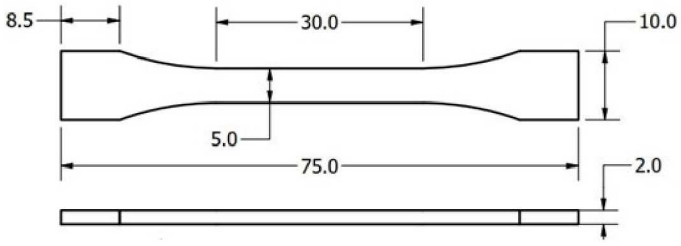

(a) Dumbbell tensile test specimen

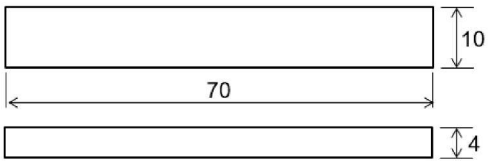

(b) Unnotched Izod-Charpy impact test specimen

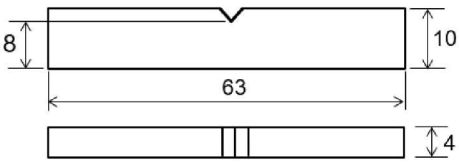

(c) Notched Izod-Charpy impact test specimen

Figure 3.3: CAD models illustrating the geometry and dimensions of tensile and impact test specimens. Panels **(a)**, **(b)**, and **(c)** correspond to dumbbell tensile test specimens, unnotched Izod-Charpy impact test specimens, and notched Izod-Charpy impact test specimens, respectively.

3.2.3 Surface Treatment of Neat PP and WP Specimens

UV and Plasma Surface Treatments

To enhance surface adhesion, the gauge sections of both neat PP and WP specimens were initially roughened using 600-grit sandpaper. Two surface modification techniques—UV irradiation and plasma treatment—were then applied. For UV treatment, both sides of

each specimen were chemically activated by exposure to ultraviolet light at a wavelength of 254 nm for 5 minutes using a handheld UV lamp (SLUV-6, AS ONE Co., Ltd.). For plasma treatment, optimal processing conditions were established through a systematic evaluation of surface polarity and wettability across a range of operational parameters. This approach was informed by prior findings that emphasized the risk of surface degradation and hydrophobic recovery under extended plasma exposure [94], thereby underscoring the necessity of empirically determining appropriate treatment settings. A processing speed of 50 $mm \cdot s^{-1}$ and a nozzle-to-surface distance of 5 mm produced the highest surface polarity of 70.12 $mN \cdot m^{-1}$—a substantial increase from the pre-treatment value of 24.78 $mN \cdot m^{-1}$—without causing visible surface damage. Additionally, the water contact angle decreased markedly from 107.9° to 24.48°, confirming a significant improvement in surface wettability. These optimized parameters were subsequently employed for plasma irradiation, which was applied to both sides of the specimens using a plasma treatment system (Japan Plasma Treat Co., Ltd., Tokyo, Japan).

Figure 3.4 illustrates the surface treatment apparatus described above, comprising a handheld UV lamp for ultraviolet irradiation and a plasma system for plasma treatment.

(a) UV lamp (SLUV-6, AS ONE Co., Ltd.)

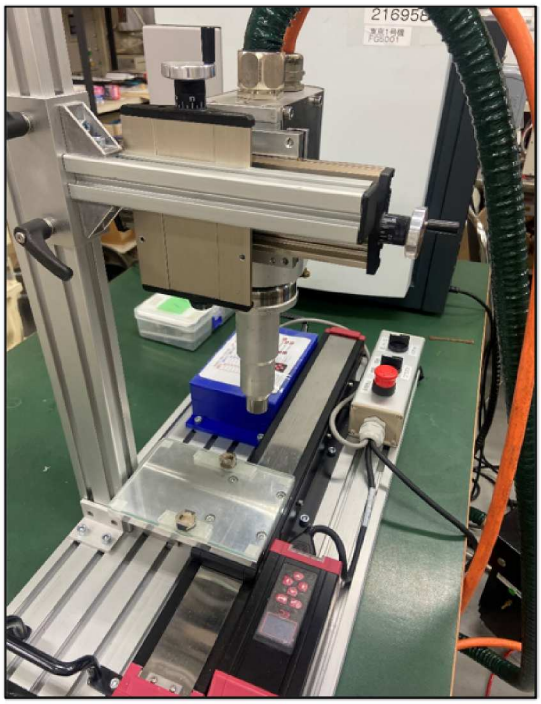

(b) Plasma treatment machine (Plasmatreat Co., Ltd.)

Figure 3.4: Surface treatment equipment used in this study: (**a**) handheld UV lamp used for ultraviolet irradiation at 254 nm, and (**b**) plasma treatment system employed under optimized conditions of 50 $mm \cdot s^{-1}$ and a 5 mm nozzle-substrate distance.

Surface Coating with CNF-Dispersed Acrylic Resin

The UV- and plasma-treated specimens were subsequently coated with an acrylic resin containing cellulose nanofiber (CNF) dispersions. An acrylic resin (SHP470-FT2050, MOMENTIVE Inc., Renias Co., Ltd., Tokyo, Japan) was dispensed into reagent bottles, to which PEGylated TEMPO-oxidized CNFs were added at concentrations of 0%, 1%, and 4%. Two types of CNF dispersions were prepared to distinguish between fiber lengths: one containing long CNFs (approximately 0.7 μm in diameter), and the other containing short CNFs (approximately 0.2–0.3 μm in diameter). Each specimen was immersed in its respective dispersion for 30 seconds to ensure uniform coating, followed by air-drying at room temperature (25 °C) until no visible liquid remained. Final drying was performed in a hot-air oven (Sanyo Electric Co., Ltd., Tokyo, Japan) at 80 °C for 30 minutes. The thickness of the coating layer—defined as the dried acrylic resin layer on the specimen surface, with or without CNF—was determined by measuring the specimen dimensions before and after coating using a micrometer. Measurements were taken at three different positions along the gauge length, and the average values were used to calculate the coating thickness as half the difference between the thicknesses before and after coating. The resulting coating thicknesses ranged from 2.4–6.0 μm for neat PP, 1.9–7.4 μm for 25wt% WP, and 2.9–7.5μm for 50 wt% WP specimens.

3.2.4 Surface Roughness and SEM Morphology

The surfaces of treated and untreated neat PP and WP specimens were examined using a field emission scanning electron microscope (FE-SEM; JSM-7000F, Japan Electron Optics Laboratory Co., Ltd.), an instrument previously presented in Chapter 2. Surface roughness measurements were conducted with a color laser microscope (KEYENCE Co., Ltd., Model VK9700/VK9710SP2214; Tokyo, Japan). A photograph of the color laser microscope utilized in this study is shown in Figure 3.5.

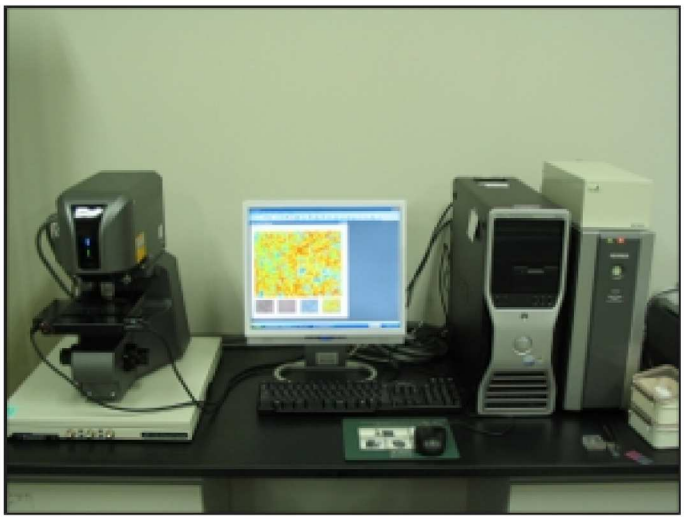

Figure 3.5: Color laser microscope (KEYENCE VK9700/VK9710SP2214) used for surface roughness measurements.

3.2.5 Tensile Test

Tensile tests were performed using a bench-top testing machine (LSC-1/30D, JT Tosi., Tokyo, Japan). The width and thickness of the dumbbell-shaped specimens were precisely measured with a micrometer, and the cross-sectional area of each specimen was subsequently calculated. Each specimen was tested at room temperature (25 °C) and a crosshead speed of 10 mm/min. A memory recorder (Memory HiCorder 8807, Hioki Electric Co., Ltd.), an amplifier (DPM, Kyowa Electric Co., Ltd.), and a strain gauge (KGFS-5-120-C1-11, Kyowa Electric Co., Ltd.) were used to capture the test time, load, and strain for each run. Five specimens were tested per experimental condition, and the mean values were calculated.

3.2.6 Impact Test

Impact tests were conducted using an Izod-Charpy impact test machine, model CIT-25JCI. The length, width, and thickness of both notched and un-notched specimens were measured using a digital vernier caliper, and the cross-sectional area of each specimen was calculated. The tests were performed at room temperature (25 °C) using a 2 J hammer weighing 0.857 kg. The center of rotation axis and center of gravity distance were set to 12.8 cm, and the distance between fulcrums was fixed at 40 mm. The Izod-Charpy impact tester is shown in Fig. 3.6.

Figure 3.6: Izod-Charpy impact test machine (CIT-25JCI) for evaluating the impact resistance of test specimens.

3.2.7 Specimen Nomenclature

The specimen codes were systematically defined to reflect three key variables: (i) the type and content of reinforcement in the polypropylene (PP) matrix, (ii) the surface treatment applied to the specimen, and (iii) the coating characteristics, including the CNF concentration and morphology.

Each specimen designation follows the format:

`[Base]-[Treatment]-[Coating]`

where:

- **[Base]**: Specifies the reinforcement type and its content in the PP matrix:
  - `PP`: Neat polypropylene
  - `WP25`, `WP50`: Wood flour at 25 wt% and 50 wt%, respectively
  - `KP20`: Cordenka fiber at 20 wt%
  - `RP15`: Ramie fiber at 15 wt%
- **[Treatment]**: Indicates the surface treatment method (if applied):
  - `UT`: Untreated
  - `P`: Plasma-irradiated
  - `UV`: UV-irradiated
- **[Coating]**: Describes the CNF-containing acrylic coating:
  - `c0`: Coated with acrylic resin, 0 wt% CNF
  - `c1S`: Coated with 1 wt% short CNF
  - `c1L`: Coated with 1 wt% long CNF
  - `c4S`: Coated with 4 wt% short CNF
  - `c4L`: Coated with 4 wt% long CNF

Example Specimen Codes:

- `WP50-UV-c4L`: Wood/PP composite (50 wt% wood), UV-treated, coated with acrylic resin containing 4 wt% long CNF.
- `KP20-P-c1S`: Cordenka/PP composite (20 wt%), plasma-treated, coated with 1 wt% short CNF.
- `PP-UT-c0`: Neat PP, untreated, coated with resin containing no CNF.

3.3 Results & Discussion

3.3.1 Surface Roughness Results of Neat PP and WP Specimens

Surface roughness (Sa) measurements of neat PP, WP25, and WP50 specimens, obtained using a color laser microscope, are presented in Figures 3.7–3.9. For each specimen category, the relative changes in Sa between treated and untreated specimens are expressed as ratios (in parentheses), while the corresponding root mean square roughness (Sq) values are indicated by the error bars. As shown in Figures 3.7 and 3.8, the Sq values for both neat PP and WP25 specimens were consistently higher in the uncoated condition compared to the coated condition. A similar trend was observed in WP50 specimens (Figure 3.9), with the exception of the Pc4S sample, which exhibited a slight increase in Sq following surface coating. Generally, the Sq data indicate that surface coating has a smoothing effect on the specimen surfaces.

The arithmetical mean height (Sa) was also analyzed in detail. A clear reduction in surface roughness was observed following the application of the resin coating. As shown in Figure 3.7, the uncoated neat PP exhibited an average arithmetical mean height (Sa) of 1.40 μm, which decreased to 0.79 μm in the coated specimens. Similarly, the Sa value for uncoated WP25 was 2.20 μm, and this was reduced to 1.09 μm after coating, as presented in Figure 3.8. A comparable trend was observed for WP50 (Figure 3.9), where the Sa value decreased from 3.90 μm in the uncoated specimens to 2.05 μm in the coated ones.

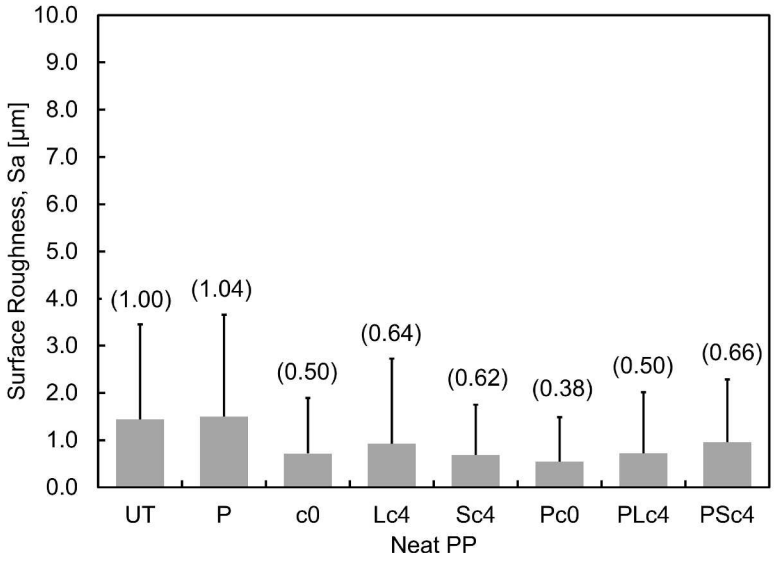

Figure 3.7: Surface roughness results for neat PP specimens.

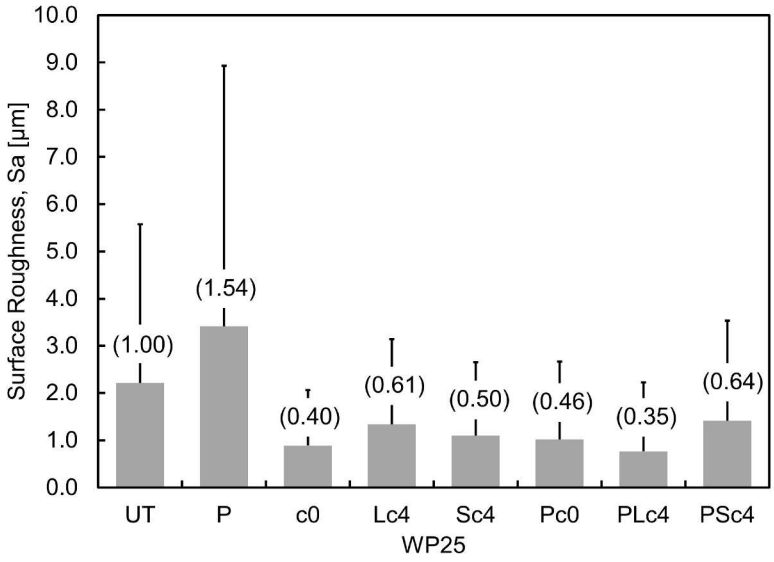

Figure 3.8: Surface roughness results for WP25 specimens.

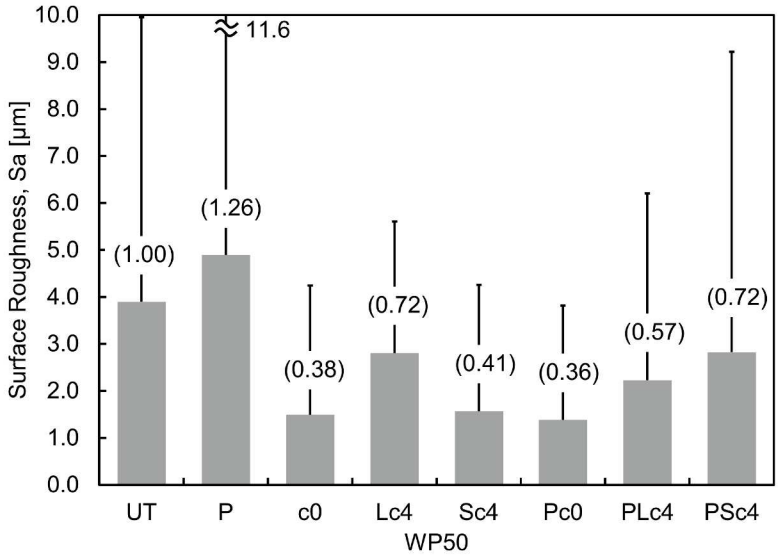

Figure 3.9: Surface roughness results for WP50 specimens.

In all cases, surface roughness was effectively reduced by approximately half through the application of the coating. This reduction in Sa is attributed to the filling and leveling effect of the resin coating, which infiltrates and smoothens surface asperities, resulting in a more uniform topography. Moreover, prior to coating, all plasma-treated specimens—PP, WP25, and WP50—exhibited relatively higher Sa values, indicating that plasma irradiation contributed to increased surface roughness.

Based on the results presented, it can be concluded that acrylic resin coating effectively reduces surface roughness across all specimen types, including both untreated and plasma-treated surfaces. This indicates that the coating serves to uniformly smooth the specimen surfaces regardless of prior surface modification. These surface topographical changes are likely to influence subsequent interfacial interactions and mechanical performance, which are examined in the following sections.

3.3.2 SEM Analysis of Surface-Treated Neat PP and WP Specimens

Figure 3.10 presents SEM micrographs illustrating the surface morphology of neat PP and WP specimens. As observed, the surface of the neat PP exhibited a comparatively smoother and more homogeneous texture relative to the wood fiber (WF)-reinforced composites. The incorporation of WF into the PP matrix led to a marked increase in surface irregularities, with roughness becoming progressively more pronounced as the WF content increased from 25 wt% (Figure 3.10**b**) to 50 wt% (Figure 3.10**c**). This trend is characterized by a higher concentration of voids, fiber pull-outs, and topographical discontinuities associated with fiber-matrix interfacial mismatches.

A comparison between uncoated and acrylic resin-coated specimens—particularly Figures 3.10**c** and **f**—demonstrates that the application of the coating significantly improved surface uniformity. The coated surfaces appeared markedly smoother, with fewer visible defects and reduced exposure of wood fibers. This smoothing effect is attributed to the filling and sealing action of the acrylic resin, which penetrates surface voids and encapsulates exposed fibers, thereby contributing to a more continuous and homogeneous surface layer. These morphological observations are in strong agreement with the surface roughness measurements discussed earlier and further substantiate the efficacy

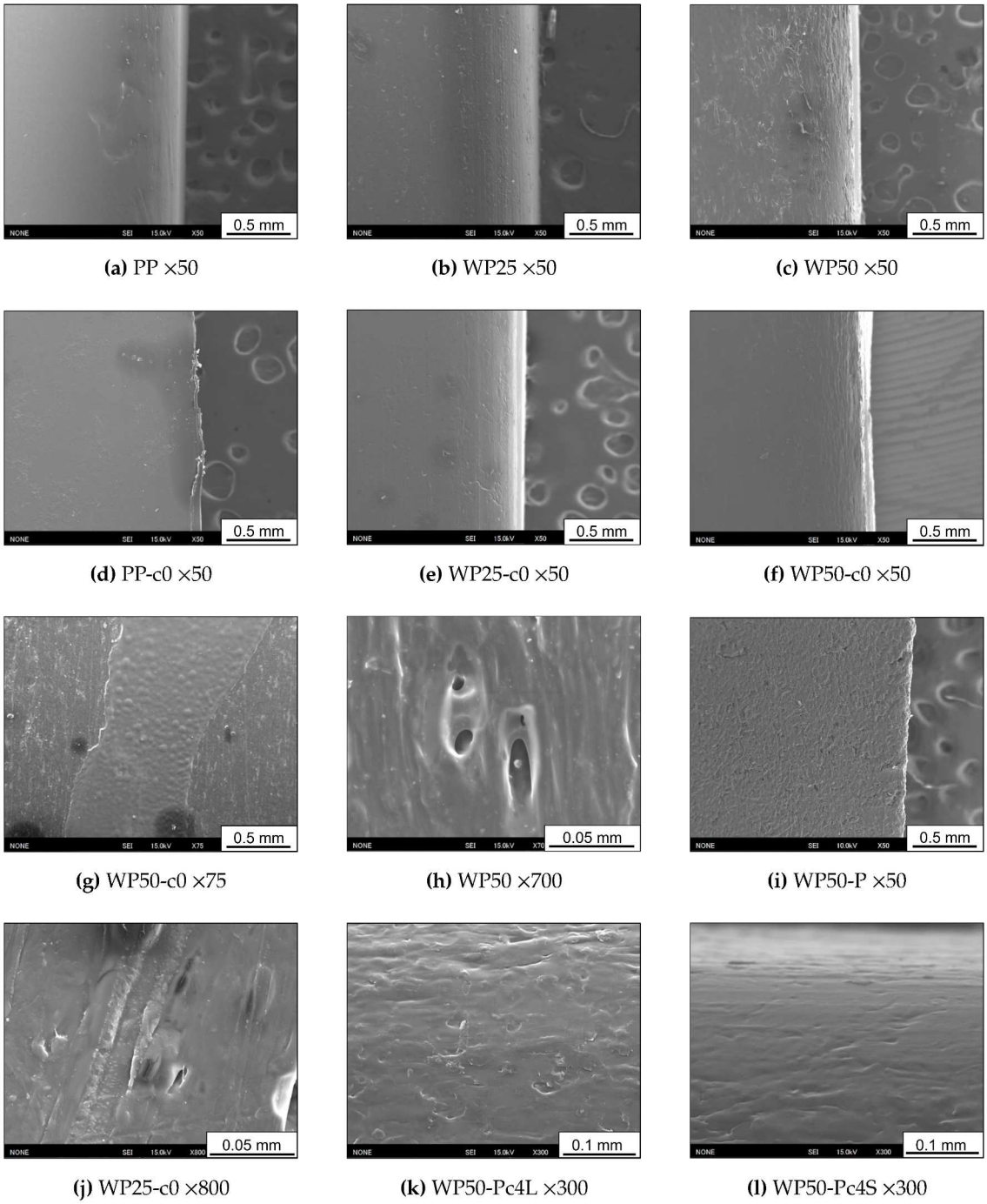

(a) PP ×50 **(b)** WP25 ×50 **(c)** WP50 ×50

(d) PP-c0 ×50 **(e)** WP25-c0 ×50 **(f)** WP50-c0 ×50

(g) WP50-c0 ×75 **(h)** WP50 ×700 **(i)** WP50-P ×50

(j) WP25-c0 ×800 **(k)** WP50-Pc4L ×300 **(l)** WP50-Pc4S ×300

Figure 3.10: Representative SEM surface micrographs of neat PP and WP specimens at varying magnifications, treated with acrylic resin containing different concentrations and types of CNF.

of the resin coating in mitigating surface heterogeneity.

In the WP50-c0 specimen (Figure 3.10**g**), regions where the acrylic resin film adhered versus where it did not are distinctly discernible, underscoring the inherently hydrophobic character of polypropylene. This lack of uniform adhesion is indicative of inadequate interfacial compatibility between the untreated PP surface and the resin layer. In contrast, the surface morphology of plasma-treated specimens prior to coating (Figure 3.10**i**) revealed a noticeably rougher and more textured profile relative to their un-

treated counterparts. This increase in surface roughness is attributed to plasma-induced surface modification, which not only alters the chemical composition but also introduces microscale topographical features that facilitate improved mechanical interlocking and adhesion of the subsequent resin layer.

Comparable findings have been reported in the literature. Yáñez-Pacios et al.[145] showed that UV/ozone treatment of WPCs improved both surface roughness and coating compatibility. Similarly, Wolkenhauer et al.[146] reported increased surface roughness in plasma-treated WPCs, attributing it to enhanced bonding performance. Their subsequent tensile and shear bond strength tests confirmed that plasma-treated WP specimens exhibited significantly stronger adhesion to solvent-borne, waterborne, and oil-based coatings compared to untreated controls.

Morphological modifications induced by the acrylic resin coating were also clearly evident. At higher magnification, the as-received WP50 specimen (Figure 3.10**h**) exhibited a heterogeneous surface marked by voids and irregular features. In contrast, the coated WP50 specimen (Figure 3.10**j**) displayed a more uniform and continuous topography, with the resin effectively filling surface voids and concealing processing-induced scratches. This smoothing effect contributed to the observed reduction in surface roughness. Furthermore, the effect of CNF length was clearly distinguishable: the surface coated with long CNFs (Figure 3.10**k**) retained more irregularities, whereas the short CNF-coated surface (Figure 3.10**l**) appeared smoother and more homogeneous. These findings suggest that short CNFs are more effective in achieving surface leveling and uniformity than long CNFs.

3.3.3 Tensile Properties of Neat PP and WP Specimens under Plasma-Based Surface Treatments

Neat PP-J108 Specimens

Table 3.2 presents a summary of the tensile properties of PP-J108 specimens subjected to various plasma-based surface treatments and coatings. Representative stress–strain curves are provided in Figure 3.11. Both untreated specimens (UT) and those coated solely with acrylic resin (c0) exhibited pronounced plastic deformation without fracture, achieving elongations exceeding 200% of the initial gauge length. This behavior highlights the intrinsic ductility of PP-J108 and its strong strain-hardening tendency. The material's ability to sustain extensive plastic deformation before failure is attributed to its high energy absorption capacity, which effectively delays crack initiation and propagation. A comparable deformation response was observed in film-laminated PP-J108 specimens, as discussed in Chapter 2.

Conversely, unlike the untreated PP-J108 specimens, fracture occurred in the CNF-coated PP-J108 specimens, which exhibited a markedly reduced elongation at break. Plasma treatment, in combination with CNF coating, further exacerbated this reduction, particularly in the Pc4L and Pc4S categories. This behavior is attributed to the intrinsic brittleness of the CNF coating film, which likely ruptured before the underlying substrate, creating localized stress concentrations at the interface. These interfacial stresses facilitated crack initiation and propagation into the substrate, ultimately resulting in premature failure. The reduction in fracture strain was most pronounced in plasma-treated specimens, owing to the improved adhesion between the CNF coating and the modified surface. This stronger interfacial bonding accelerated crack propagation, thereby promoting earlier fracture. In contrast, in specimens that were coated with CNF but not plasma-treated, the relatively weaker adhesion between the coating and the substrate

impeded crack growth, delaying failure and resulting in a less significant reduction in fracture strain. Furthermore, the inherent ductility of PP—characterized by its capacity for substantial plastic deformation prior to failure—may have further contributed to the delayed fracture observed in these specimens.

Table 3.2: Tensile properties of PP-J108 specimens under surface treatments

Code	Strength [MPa]	Fracture Strain [%]
UT	35.0 (0.3)	NF
c0	35.7 (2.0)	NF
c4L	35.8 (1.9)	88.3 (14.3)
c4S	35.8 (2.0)	138.0 (73.9)
Pc0	37.1 (0.6)	83.8 (58.7)
Pc4L	37.5 (1.0)	55.0 (88.9)
Pc4S	36.9 (1.8)	73.0 (35.0)

Note: Values in parentheses represent the coefficient of variation (CV%). "NF" indicates specimens that did not fracture within the test range (>200% strain).

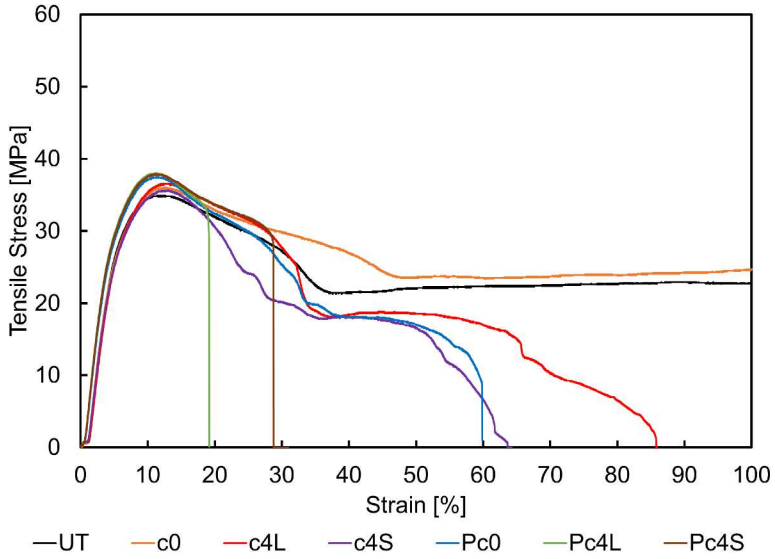

Figure 3.11: Tensile stress-strain curves for neat PP-J108 specimens treated with plasma irradiation, acrylic resin, and CNF coating.

The application of the coating agent led to an increase in tensile strength ranging from 2.0–2.3 % in non-plasma-treated specimens to 5.4–7.1 % in plasma-treated specimens. This enhancement confirms that the coating effectively filled surface voids and masked micro-defects, thereby improving surface uniformity and enabling more homogeneous stress distribution under tensile loading. The more pronounced improvement in plasma-treated specimens highlights the synergistic effect of plasma irradiation in enhancing tensile properties beyond the contribution of resin coating alone.

Plasma treatment is widely recognized for its dual role in modifying substrate surfaces through physical etching and chemical activation. The bombardment by energetic ions increases microscale surface roughness, thereby enhancing mechanical interlocking at the

interface. Simultaneously, the introduction of polar functional groups (e.g., –OH, –C=O, –COOH) elevates the surface energy and improves wettability. These physicochemical modifications facilitate superior resin wetting and promote the formation of covalent or hydrogen bonds at the interface, resulting in more efficient load transfer under tensile stress. Consequently, the improved interfacial adhesion is directly associated with the observed enhancement in the composite's mechanical performance [147, 148].

These findings demonstrate that both resin coating and plasma treatment independently improve tensile strength, and their combined application yields even greater benefits. Notably, the fact that a significant increase in strength was achieved through a simple post-treatment—immersion of plasma-treated specimens in acrylic resin—underscores the potential of this approach as an efficient and scalable strategy for surface reinforcement and quality control in polymer materials.

WP Specimens

The effects of plasma treatment, acrylic resin coating, and CNF coating on the tensile strength of WP25 and WP50 specimens are summarized in Table 3.3, with corresponding stress–strain curves presented in Figure 3.12. Among the untreated specimens, WP50-UT exhibited the highest tensile strength, surpassing that of both PP-UT and WP25-UT. This enhancement is primarily attributed to the reinforcing effect of wood fibers, which becomes increasingly pronounced with higher fiber loadings. In particular, the WP50-UT specimens achieved a maximum tensile strength of 50.7 MPa, compared to 42.6 MPa for WP25-UT, representing a 19.0 % increase associated with increasing the fiber content from 25 wt% to 50 wt%. The improvement reflects the enhanced load-carrying capacity imparted by the higher concentration of wood fibers, which contributes to more effective stress transfer within the composite matrix.

As shown in Table 3.3, the application of the acrylic resin coating led to improved tensile strength in both WP25 and WP50 specimens. For WP25, non–plasma-treated samples exhibited a tensile strength increase of 1.5% to 2.7%, while plasma-treated samples showed a greater improvement of 3.5% to 3.7%. In WP50 specimens, the increase ranged from 2.4% to 3.5% for non–plasma-treated samples and from 3.0% to 3.6% for plasma-treated ones. These improvements are attributed to the acrylic resin's ability to fill surface voids and micro-defects introduced during fiber incorporation into the polypropylene matrix. Prior to coating, these imperfections acted as stress concentrators and facilitated crack initiation, resulting in brittle fracture. The coating reduced these flaws, thereby enhancing crack resistance. It also improved surface uniformity and roughness, enabling more consistent stress distribution and reducing local stress concentrations. Together, these effects contributed to the observed increase in tensile strength.

These findings are consistent with previous studies that have reported similar effects of plasma treatment on mechanical performance and interfacial properties. Demirkir et al.[149] observed improvements in both elastic modulus and bending strength in beech and plywood following oxygen plasma treatment. Wolkenhauer et al.[150] reported enhanced adhesion across various wood species treated with plasma. Likewise, Seki et al. [151] demonstrated improved interfacial bonding in jute fiber–reinforced polyethylene composites after plasma surface modification. These studies support the present results, confirming that plasma treatment promotes stronger interfacial adhesion and contributes to enhanced mechanical properties in wood–plastic composites.

As shown in Table 3.3, the fracture strain decreased following the application of the acrylic resin coating, consistent with the trend observed in neat PP. This reduction

became more pronounced after plasma treatment. The decline in ductility is attributed to improved interfacial adhesion between the coating and the specimen surface induced by plasma irradiation. Stronger interfacial bonding promotes more efficient stress transfer from the coating to the underlying substrate, which accelerates crack initiation and propagation, thereby reducing the material's ability to undergo plastic deformation.

A comparison between neat PP and WP composites reveals that the relative improvement in tensile strength due to plasma treatment was more significant in neat PP. Specifically, plasma-treated neat PP exhibited a tensile strength increase ranging from 5.4 % to 7.1 %, whereas the WP composites showed a comparatively lower average increase of approximately 3.5 %. Moreover, as the wood fiber content increased—thereby reducing the proportion of the PP matrix—the effectiveness of plasma treatment diminished. This trend suggests that plasma-induced surface modification is more impactful in matrix-dominated systems, where the treated surface area plays a greater role in governing interfacial interactions and stress transfer. Accordingly, plasma treatment appears to be more effective in enhancing the tensile strength of neat PP than that of fiber-reinforced composites.

Table 3.3: Tensile properties of W25 and WP50 specimens under plasma treatment, resin coating, and CNF modification

Code	Tensile Strength [MPa]		Fracture Strain [%]	
	W25	**WP50**	**W25**	**WP50**
UT	40.5 (0.4)	50.7 (1.2)	10.6 (3.8)	7.29 (4.2)
c0	41.1 (1.6)	52.4 (0.8)	9.88 (7.4)	6.78 (4.9)
Lc4	41.4 (1.0)	51.9 (0.8)	9.80 (3.1)	6.54 (3.5)
Sc4	41.6 (1.5)	51.9 (1.7)	9.56 (5.7)	6.41 (6.4)
Pc0	41.9 (0.9)	52.2 (1.0)	9.14 (3.0)	6.55 (2.1)
PLc4	41.9 (0.7)	52.2 (1.4)	9.04 (6.2)	6.69 (2.1)
PSc4	42.0 (1.6)	52.5 (2.0)	9.36 (0.2)	6.62 (4.2)

Note: Values in parentheses indicate the coefficient of variation (CV%) based on replicate tests.

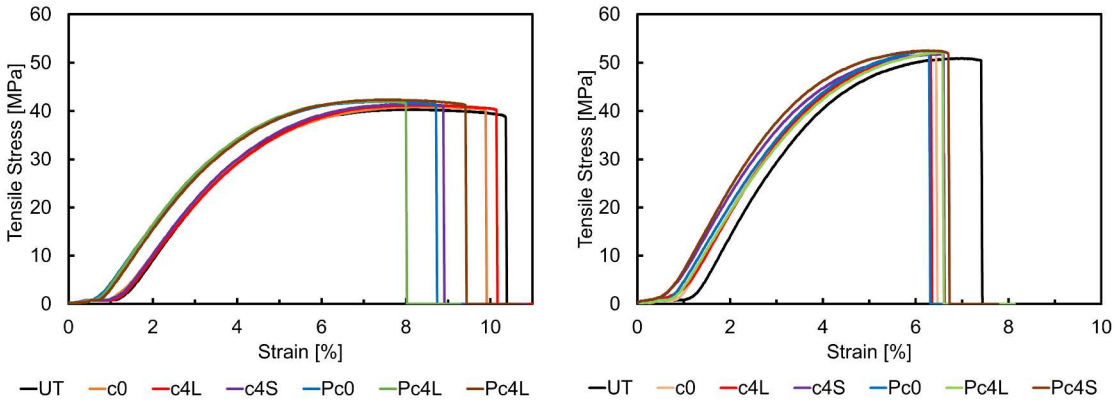

(a) WP25 specimens.

(b) WP50 specimens.

Figure 3.12: Comparison of tensile stress-strain curves for WP25 and WP50 specimens treated with plasma irradiation, acrylic resin, and CNF coating.

3.3.4 Tensile Properties of Neat PP and WP Specimens under UV-Based Surface Treatments

Neat PP-J106 Specimens

The effects of UV irradiation, acrylic resin coating, and CNF coating on the tensile behavior of PP-J106 specimens are summarized in Table 3.4, with representative stress–strain curves presented in Figure 3.13. In contrast to PP-J108, the PP-J106 specimens exhibited fundamentally different mechanical behavior, characterized by brittle fracture and low fracture strain. This stark difference highlights the influence of resin formulation on fracture mechanisms and overall ductility. Although PP-J106 and PP-J108 demonstrated comparable tensile strength values, their failure modes diverged significantly. PP-J106 fractured abruptly with minimal plastic deformation, indicative of brittle failure, whereas PP-J108 exhibited substantial ductility, undergoing extensive strain hardening and large plastic deformation prior to failure. These observations point to inherent differences in molecular structure, crystallinity, or processing history between the two polypropylene grades, which critically affect their fracture responses. Understanding such distinctions is essential when selecting PP grades for applications requiring tailored mechanical performance under specific surface modifications or loading conditions.

A modest increase in tensile strength was observed across all UV-irradiated PP-J106 specimens, with the highest improvement—5.1 %—recorded for the UVc1 condition. This enhancement is attributed to surface crosslinking and oxidative modification induced by UV exposure, which are known to elevate surface energy and introduce polar functional groups. These changes likely improved interfacial compatibility between the substrate and the coating resin, facilitating more efficient stress transfer and contributing to the observed strengthening effect. In contrast, the variation in CNF concentration within the acrylic resin did not produce a notable difference in tensile strength, with values remaining relatively consistent across the c0, c1, and c4 levels. The underlying reason for this insensitivity to CNF content remains unclear and may be influenced by complex interfacial phenomena. This observation warrants further investigation to elucidate the potential role of CNF in reinforcing UV-treated systems under the present conditions. A slight increase in fracture strain was also observed in all UV-irradiated specimens relative to the untreated control. While CNF content had minimal effect on tensile strength, a gradual—albeit limited—improvement in fracture strain was noted as the CNF concentration increased from c0 to c4. This may reflect localized energy dissipation mechanisms such as micro-fibrillation or crack deflection, which could marginally delay fracture and enhance deformability.

Compared to plasma treatment of PP-J108 specimens, which resulted in a more pronounced increase in tensile strength (up to 7.1 %), the effect of UV irradiation on PP-J106 was relatively modest. This difference may be attributed to variations in the intensity and nature of surface activation induced by each method. Plasma treatment generally produces a higher density of surface functional groups and induces greater surface roughness, both of which are known to enhance interfacial adhesion more effectively than UV treatment under comparable conditions.

Table 3.4: Tensile properties of PP-J106 specimens under UV irradiation, resin coating, and CNF modification

Code	Tensile Strength [MPa]	Fracture Strain [%]
UT	37.0 (0.4)	10.3 (7.1)
UVc0	38.7 (0.4)	11.2 (3.9)
UVc1	38.9 (1.0)	11.2 (1.9)
UVc4	38.7 (0.5)	11.4 (2.6)

Note: Values in parentheses indicate the coefficient of variation (CV%) based on replicate tests.

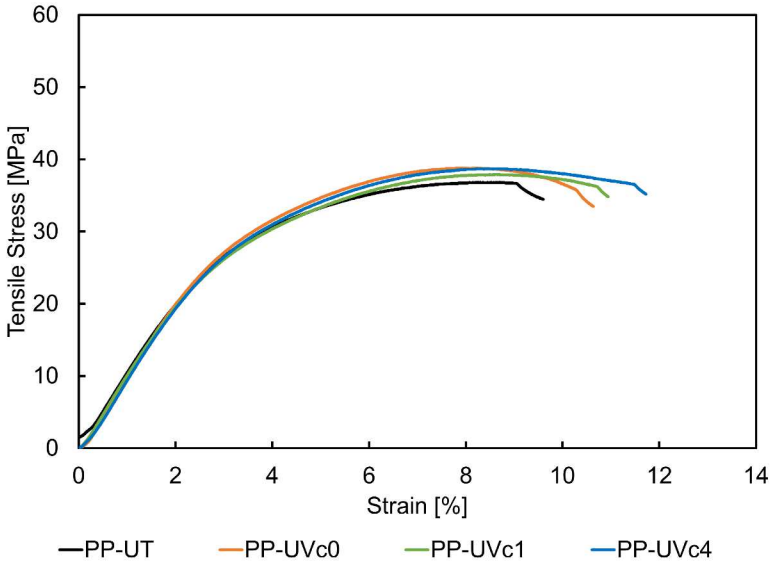

Figure 3.13: Tensile stress-strain curves for UV-irradiated, acrylic resin, and CNF-coated neat PP-J106 specimens.

WP Specimens

The tensile properties of WP25 and WP50 specimens subjected to UV irradiation, acrylic resin, and CNF coating are summarized in Table 3.5, with representative stress–strain curves provided in Figure 3.14. For the WP25 series, a consistent improvement in tensile strength was observed following surface treatment. UV irradiation enhanced surface characteristics, and subsequent coating with CNF-containing acrylic resin further increased tensile strength. Notably, strength gains correlated with rising CNF concentration, culminating in a maximum improvement of 5.1 % in the UVc4 condition compared to the untreated specimen. This enhancement is attributed to the synergistic effects of UV-induced surface oxidation and the mechanical reinforcement offered by the CNF-reinforced coating. UV irradiation likely introduced polar functional groups and mild surface roughening, promoting better adhesion between the wood–plastic substrate and the coating layer. The CNF component, in turn, may have contributed to stress transfer through local stiffening of the coating matrix.

In contrast, the WP50 series exhibited a different trend. Here, tensile strength decreased with increasing CNF concentration, with the most pronounced reduction (4.5 %) also occurring in the UVc4 condition. This inverse effect is likely due to the inherently

higher stiffness and lower ductility of the WP50 substrate, which contains a greater volume fraction of wood fibers. In such systems, the addition of a brittle CNF-containing coating, particularly one strongly bonded due to UV-induced surface activation, may lead to stress concentration at the interface, promoting premature crack initiation and propagation. The mismatch in stiffness and fracture toughness between the rigid coating and the less compliant fiber-rich substrate could therefore undermine the overall mechanical performance.

Table 3.5: Tensile properties of WP25 and WP50 specimens under UV irradiation, resin coating, and CNF modification.

Code	Tensile Strength [MPa]		Fracture Strain [%]	
	WP25	**WP50**	**WP25**	**WP50**
UT	42.6 (0.5)	50.6 (1.0)	7.50 (6.9)	5.48 (3.9)
UVc0	43.4 (0.5)	50.5 (4.0)	6.75 (0.3)	5.48 (4.6)
UVc1	44.0 (1.4)	49.2 (2.6)	6.24 (1.8)	5.29 (11.2)
UVc4	44.8 (0.5)	48.4 (4.1)	6.31 (3.8)	5.91 (1.5)

Note: Values in parentheses represent the coefficient of variation (CV%).

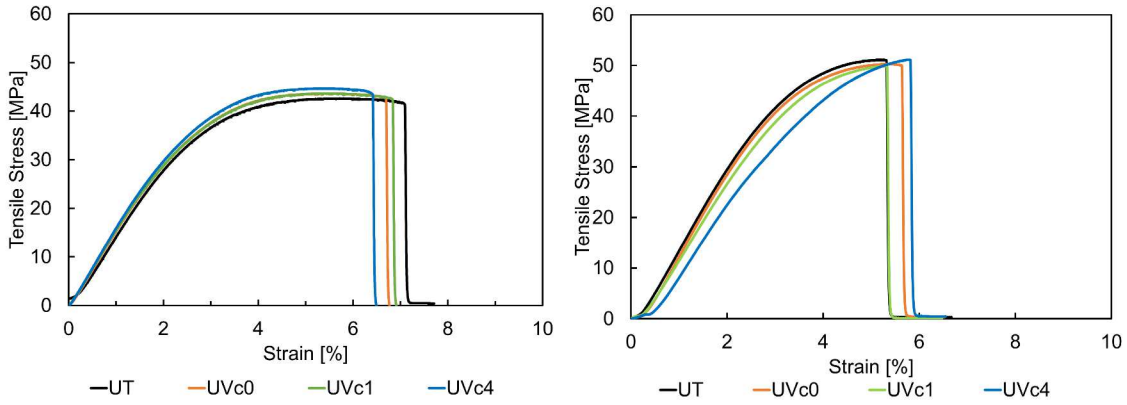

(a) WP25 specimens.

(b) WP50 specimens.

Figure 3.14: Comparison of tensile stress-strain curves for WP25 and WP50 specimens treated with uv irradiation, acrylic resin, and CNF coating.

Regarding fracture behavior, WP25 and WP50 specimens incorporating the PP-J106 matrix exhibited lower fracture strains than those with the PP-J108 matrix, consistent with the more brittle nature of the PP-J106 grade, as previously discussed. Among the UV-irradiated WP specimens, fracture strain decreased further in WP50 relative to WP25, reflecting the reduced matrix content and greater brittleness associated with the higher fiber loading. In WP25, the higher proportion of ductile PP matrix provided greater deformation capacity, which mitigated early failure and allowed more strain accommodation prior to fracture.

When compared to plasma-treated WP specimens, the strengthening effect of UV irradiation appears slightly less pronounced. Plasma-treated WP25 specimens showed strength improvements up to approximately 6.0 %, compared to a maximum of 5.1 % under UV treatment. This difference can be attributed to the higher surface activation

energy associated with plasma processes, which more effectively enhance coating adhesion and interfacial bonding as explained in the case of PP-j106. Nonetheless, UV treatment remains advantageous as a less aggressive, more accessible alternative for surface functionalization, especially when used in conjunction with an optimized coating system.

KP Specimens

Table 3.6 summarizes the tensile test results for UV-irradiated KP15 specimens, with coefficients of variation provided in parentheses. Representative stress–strain curves are shown in Figure 3.15. Among all tested materials—including neat PP and WP composites—the KP specimens demonstrated the highest tensile strength, with the KP15-c1 condition achieving a peak value of 58.8 MPa. This superior performance is particularly noteworthy given the relatively low fiber content of 15 wt%, compared to the 25 wt% and 50 wt% wood fiber content in the WP25 and WP50 specimens, respectively. The results strongly highlight the reinforcing efficiency of Cordenka fibers, a regenerated cellulose fiber with higher tensile strength and stiffness than conventional natural fibers.

Despite the clear mechanical superiority of KP specimens, the effect of UV irradiation and CNF incorporation within the resin coating was less definitive. Across all categories—including untreated (UT), CNF-free coating (c0), and CNF-loaded coatings (c1 and c4)—tensile strength values remained largely comparable, suggesting a limited influence of these surface treatments on the already-optimized KP15 composites. This may be attributed to the inherently high interfacial bonding achieved during fiber processing via the M-PaRI (Multi-Pin Assisted Resin Impregnation) method, which pre-impregnates Cordenka fibers with PP resin, thereby promoting excellent fiber–matrix compatibility. As a result, any additional surface treatment, including UV-induced functionalization or CNF reinforcement, may exert only marginal effects on tensile performance due to the already strong internal structure.

The outstanding performance of KP15 underscores two critical insights. First, it confirms the superior reinforcing capability of regenerated cellulose fibers like Cordenka compared to conventional wood fibers. Second, it highlights the effectiveness of the M-PaRI process in tailoring fiber surfaces for enhanced matrix adhesion and mechanical performance, even at lower fiber loadings. The relatively muted response to UV irradiation contrasts with the more noticeable strength improvements observed in PP and WP specimens, likely because KP specimens were already optimized structurally and interfacially prior to coating. Nonetheless, this stability across treatments may be viewed positively from a processing standpoint, indicating robustness and reliability of the composite under varying surface conditions.

Table 3.6: Tensile properties of KP15 specimens with resin coating and CNF modification

Code	Tensile Strength [MPa]	Fracture Strain [%]
UT	57.7 (1.8)	18.2 (1.5)
c0	57.7 (0.4)	16.3 (2.8)
c1	58.8 (1.2)	16.3 (3.1)
c4	57.2 (1.0)	17.1 (1.0)

Note: Values in parentheses indicate the coefficient of variation (CV%) based on replicate tests.

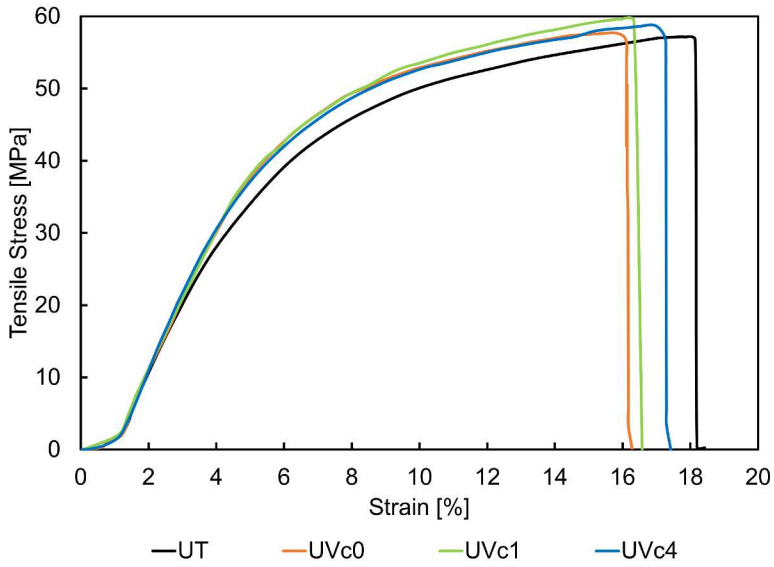

Figure 3.15: Tensile stress-strain curves for UV-irradiated, acrylic resin, and CNF-coated KP15 specimens.

3.3.5 Influence of Acrylic Resin Coating Thickness on Tensile Strength

Following the preceding analyses, the investigation was extended to examine the effect of acrylic resin coating thickness on the tensile strength of the acrylic resin and CNF coated specimens. This analysis focused on determining the tensile stress attributed to the acrylic resin coating, denoted as σ_f, under maximum specimen stress. The calculation was based on the rule of mixtures, which assumes a uniform coating thickness and quantifies the contribution of each component to the overall tensile response. The relationship between the tensile strengths of the coated and non-coated specimens was defined by the following equation:

$$\sigma_c A_c = \sigma_{nc} A_{nc} + \sigma_f A_f \tag{3.1}$$

In this equation, σ_c is the tensile strength of the coated specimen, while σ_{nc} represents the tensile strength of the non-coated specimen. The terms A_c and A_{nc} denote the cross-sectional areas of the coated and non-coated specimens, respectively, whereas A_f refers to the cross-sectional area of the acrylic resin film. The variable σ_f corresponds to the tensile stress exerted by the acrylic resin coating.

Results derived from this approach are summarized in Table 3.7, with σ_f values rounded to the nearest integer. The values show large, random variations among the neat PP, WP25, and WP50 specimens, with no clear trend or significant difference observed between coated and uncoated categories. Specifically, neither the presence of acrylic resin or CNF coating nor the type of coating showed a consistent impact on σ_f, suggesting that the values are independent of coating type or fiber content. Notably, the lowest σ_f value exceeded 144 MPa, indicating that the calculated film stress at maximum specimen stress substantially surpassed the inherent tensile strength of acrylic resin, which is unrealistic.

These findings indicate that the coating film stress did not contribute to the observed improvement in tensile strength. Instead, this enhancement was attributed to surface homogenization by the resin coating, which effectively sealed voids and improved surface smoothness, as previously discussed. Further investigations are recommended to clarify

the relationship between coating film thickness and tensile strength in WPCs and to determine the optimal coating thickness for achieving the observed improvements.

Table 3.7: Stress in acrylic resin coating layer at maximum tensile stress for PP and WP specimens

Code	PP [σ_f, MPa]	WP25 [σ_f, MPa]	WP50 [σ_f, MPa]
c0	155	206	395
c4L	144	173	241
c4S	163	394	213
Pc0	286	290	233
Pc4L	308	185	184
Pc4S	218	207	252

Note: σ_f represents the calculated stress in the resin coating layer at the point of maximum tensile load.

3.3.6 Analysis of Tensile Strength Variation with Type of CNF Coating

The tensile strength results for specimens coated with 4% CNF-S and 4% CNF-L indicate that nanofiber length did not significantly affect tensile strength under the investigated parameters. However, comparing the tensile strength of specimens coated with acrylic resin containing 4% CNF against those coated with plain acrylic resin (0% CNF) reveals that the former generally exhibited superior tensile properties. The only exception to this trend was observed in the WP50 non-plasma-treated specimens, where no improvement in tensile strength was detected.

Table 3.8 presents detailed data for both non-plasma-treated and plasma-treated specimens. For each case, the tensile strength for the specimens coated with acrylic resin containing 4% CNF was determined by averaging the tensile strength values of the 4% CNF-S and 4% CNF-L specimens within the same fiber weight fraction classification. Although the incorporation of 4% CNF into the acrylic paint matrix resulted in a measurable improvement in tensile strength, the magnitude of this enhancement was relatively minor. These findings underscore the necessity for further investigation into optimizing CNF coatings to achieve more substantial improvements in the mechanical performance of WPCs.

Table 3.8: Tensile strength of WP specimens coated with 0% and 4% CNF-modified acrylic resin under non-plasma and plasma-irradiated conditions

Fiber Content [wt%]	Non-Plasma Irradiated		Plasma Irradiated	
	0% CNF	4% CNF	0% CNF	4% CNF
0	35.7	35.8	37.1	37.2
25	41.1	41.5	41.9	42.0
50	52.4	51.9	52.2	52.4

Note: Tensile strength values are given in MPa. CNF content refers to weight percentage in the acrylic resin coating layer.

3.3.7 Impact Properties of PP J-106, WP and KP Specimens

PP-J106 Specimens

The impact resistance of PP-J106, WP, and KP specimens was evaluated using Charpy impact testing, with a standardized fiber content of 15 wt% in both WP and KP specimens to facilitate direct comparison. Figure 3.16 presents the impact strength results of unnotched neat PP-J106 specimens, while representative fracture morphologies following impact loading are shown in Figure 3.17.

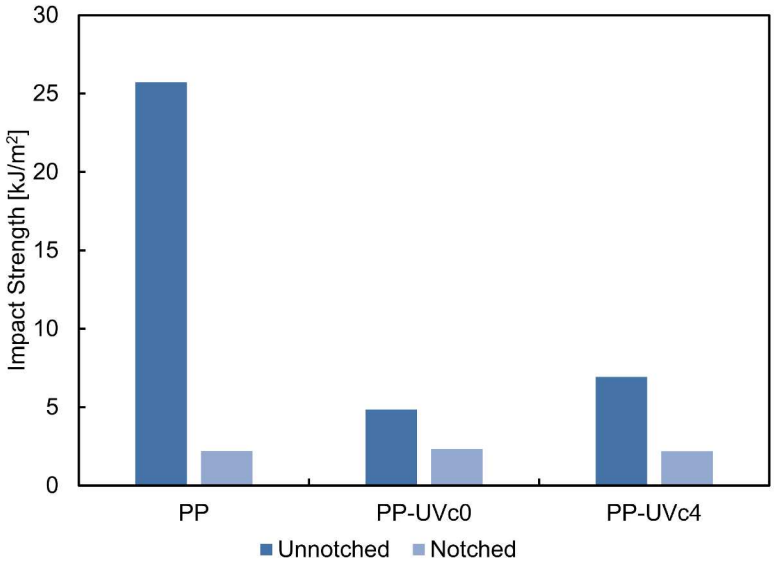

Figure 3.16: Charpy impact test results of four categories of notched and unnotched neat PP specimens.

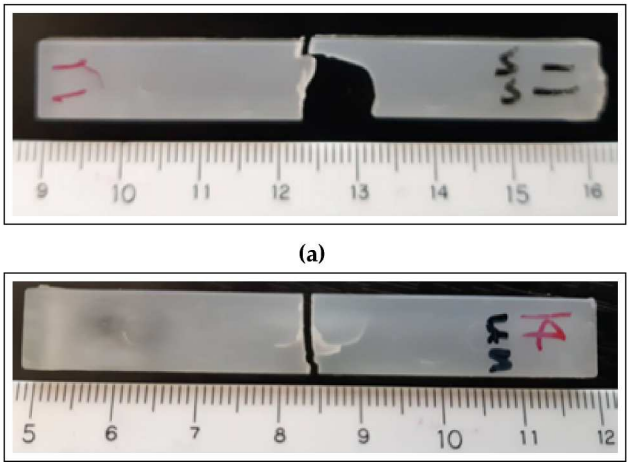

Figure 3.17: Comparison of the appearance of (**a**) non-coated and (**b**) coated PP specimens after impact testing.

As evident from Figure 3.16, the application of the acrylic resin coating led to a pronounced decrease in the impact strength of neat PP specimens—an outcome that contrasts sharply with the enhancement observed in tensile strength following the same

surface treatment. Specifically, the impact strength of the coated unnotched specimens was reduced by as much as 81 % relative to the untreated counterparts. This significant decline underscores a fundamental difference in the effect of surface coatings under different loading conditions. It is also worth noting that polypropylene is inherently more susceptible to brittle failure under impact loading than under quasi-static tensile loading. This characteristic contributes to the relatively low impact strengths observed in PP-based materials, particularly when surface modifications reduce energy dissipation capacity or introduce stress concentrators.

Further insight is provided by the Kayo Corporation materials datasheet [1], which summarizes the physical and mechanical properties of thermoplastics. As shown in Table 3.9, the intrinsic impact strength of acrylic resin (PMMA) is markedly lower than that of polypropylene. Therefore, the observed reduction in impact resistance can be reasonably attributed to the presence of the brittle acrylic coating layer on the specimen surface. Upon impact, this low-toughness coating likely acted as a weak zone, compromising the energy absorption capability of the specimen and promoting premature failure. These findings highlight the sensitivity of impact behavior to surface modifications and emphasize the importance of considering both the mechanical properties of the coating material and its interfacial characteristics with the substrate.

Table 3.9: Reported mechanical properties of polypropylene (PP) and acrylic resin (PMMA) [1].

Type of Resin	**Tensile Strength** [kg/cm^2]	**Fracture Strain** [%]	**Young's Modulus** [$10^4 kg/cm^2$]	**Impact Strength** [$kg \cdot cm/cm$]
PP	300–390	200–700	1.1–1.4	3.3–33
PMMA	560–770	2–7	2.5–3.5	2.2–2.7

Additionally, the notched PP-J106 specimens consistently exhibited lower impact strength than their unnotched counterparts across all treatment categories. This outcome aligns with the expected behavior, as notches act as stress concentrators that significantly reduce the energy required to initiate and propagate cracks under impact loading. While a modest increase in impact strength was observed in the unnotched specimens upon incorporation of 4 wt% CNF into the acrylic resin coating, no clear or consistent trend emerged regarding the effect of acrylic resin or CNF concentration on the impact resistance of notched specimens.

Fractographic observations, presented in Figures 3.17a and 3.17b, further elucidate the influence of surface coating on fracture behavior. The uncoated specimen (Figure 3.17a) exhibited multiple crack branches and secondary fracture paths, indicative of a more tortuous failure process that absorbs greater energy. In contrast, the coated specimen (Figure 3.17b) displayed a dominant linear fracture path, suggesting a more brittle failure mode with minimal energy dissipation. This behavior closely resembles that observed in notched specimens, where constrained crack propagation leads to reduced fracture energy and thus lower impact strength. The suppression of crack branching by the brittle acrylic coating likely constrained plastic deformation and promoted the formation of a single fracture plane. As a result, the energy absorbed during impact was substantially diminished. This phenomenon helps explain the reduced impact strength observed in coated and notched specimens alike. In this study, four out of six coated PP specimens exhibited linear fracture paths, and all of these recorded markedly low impact strength values. This variation in fracture behavior contributed to the relatively high scatter

observed in the impact strength measurements for coated specimens.

These findings emphasize the significant influence of surface modifications not only on the mechanical properties but also on the fracture dynamics of polymer specimens. They also underscore the need for careful consideration of crack initiation and propagation mechanisms when evaluating impact resistance, particularly in materials with surface coatings of lower toughness than the substrate.

WP15 and KP15 Specimens

The impact strength results of WP15 and KP15 specimens are presented in Figure 3.18. In contrast to the neat PP-J106 specimens, where acrylic resin coating substantially reduced impact strength, a significant enhancement was observed in the unnotched WP15 specimens following the application of the plain acrylic resin coating agent (-c0). Specifically, the impact strength increased by 40.2%, from 13.2 kJ/m^2 in the untreated specimen to 18.5 kJ/m^2 after coating. This enhancement is likely attributable to the relatively low intrinsic impact strength of the WP substrate, which is a wood fiber-reinforced polypropylene composite. In such a substrate, even a brittle coating can act beneficially by mitigating surface defects, delaying crack initiation, or suppressing localized deformation.

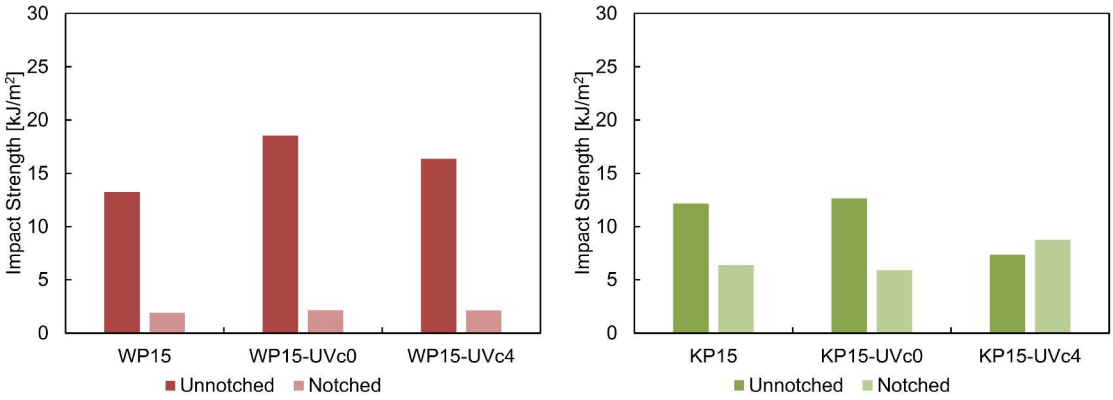

(a) WP15 specimens

(b) KP15 specimens

Figure 3.18: Charpy impact test results for notched and unnotched WP15 and KP15 specimens.

Unlike neat PP, which undergoes rapid, brittle failure when coated with a lower-toughness material, the WP composite—with its fiber–matrix heterogeneity—permits more complex interactions at the interface. The coating likely serves to bridge microcracks, reduce stress concentration near the surface, and redistribute local stresses more uniformly across the composite structure. Moreover, the natural roughness of the WP surface and the porous wood-fiber network may have facilitated mechanical interlocking with the coating layer, enhancing adhesion and contributing to improved impact resistance. When 4 wt% CNF was incorporated into the acrylic coating, the unnotched WP15 specimens still exhibited a 23.0% improvement in impact strength over the uncoated specimens. Although this increase was lower than that observed with the plain resin, it suggests that the more viscous CNF-containing coating may have influenced the fracture behavior by altering interfacial stress distribution or adding minor energy absorption capacity, albeit less effectively than the resin alone. The difference may also stem from increased coating stiffness or decreased coating ductility with CNF addition.

In contrast, the notched WP15 specimens consistently exhibited significantly lower impact strengths than their unnotched counterparts across all coating categories (WP15,

WP15-UVc0, WP15-UVc4). Furthermore, the acrylic resin and CNF coatings showed negligible influence on the notched impact performance, as the measured impact strength values remained nearly constant regardless of coating type. This behavior reflects the strong stress concentration induced by the notch, which governs the fracture process and overshadows the potential contributions of the surface layer. A broadly similar trend was observed in the KP15 specimens. The unnotched specimens coated with plain acrylic resin (-c0) showed a modest 5.9% increase in impact strength compared to the uncoated KP15 specimens. However, coating with the CNF-containing resin (-c4) resulted in a 30.0% reduction in impact strength. This deterioration may be associated with the increased stiffness and brittleness of the CNF-infused coating layer, which could act as a stress concentrator or impair crack arrest capabilities under dynamic loading.

For the notched KP15 specimens, the overall trend was consistent with that of WP15: impact strength values were lower than in unnotched specimens across most categories. An exception was observed in the KP15-c4 specimens, which unexpectedly exhibited a higher impact strength than their uncoated counterparts. However, this observation should be interpreted with caution due to the considerable scatter in the results. Indeed, large variations were noted in the impact strengths of individual WP15 and KP15 specimens across both notched and unnotched categories. This variability may stem from inherent heterogeneities in fiber distribution, interfacial bonding quality, and surface coating uniformity. Future work will therefore aim to investigate these sources of scatter in greater depth to clarify the observed trends.

Chapter 4

Mechanical Properties of Cordenka and Ramie Fiber-Reinforced Polypropylene Composites

4.1 Introduction

The literature reviewed in Chapter 1 highlights that the reinforcement of thermoplastic and thermosetting matrices, such as polypropylene (PP), polylactic acid (PLA), and epoxy (EP), with Cordenka fibers—a regenerated cellulose fiber—has led to significant improvements in the mechanical performance of these composites. Despite these advancements, there remains a need for further research to refine processing and manufacturing techniques aimed at enhancing fiber-matrix interfacial adhesion. This chapter provides a comparative analysis of the mechanical properties of Cordenka fiber-reinforced polypropylene composites and ramie fiber-reinforced polypropylene composites. To improve the interfacial bonding between the hydrophilic fibers and the hydrophobic PP matrix, the Multi-Pin-assisted Resin Infiltration (M-PaRI) method was employed. This innovative method involves pre-impregnating the fibers, both Cordenka and ramie, with PP resin to form strands, which are then compounded with the PP matrix. The approach enhances the hydrophobicity of the fibers, improving their compatibility with the PP matrix. The results indicate a notable improvement in fiber-matrix bonding due to the M-PaRI process. Furthermore, Cordenka fibers exhibited superior mechanical properties compared to ramie fibers, along with better retention of fiber length within the matrix after composite fabrication. These findings demonstrate that the regeneration process of cellulose-based fibers offers a viable strategy for significantly enhancing the mechanical performance of their composites.

4.2 Materials and Methods

Cordenka single yarn regenerated fiber (Cordenka 700, 1840 dtex, f 1000; supplied by GmbH & Co. KG, Obernburg, Germany) was utilized as the reinforcement material in this study. On the other hand, ramie single twisted yarn (No. 16; a typical natural cellulosic fiber manufactured by TOSCO Co., Ltd., Tokyo, Japan) served as the comparative material. Figure 4.1 shows the two reinforcement materials, and Table 4.1 outlines their physical properties [152, 153]. Additionally, polypropylene (PP J-900GP, $M_W = 35 \times 10^4$, $T_m = 180$ °C, Idemitsu Petrochemical Co., Ltd., Tokuyama, Japan) was used as the base

material [154, 155], while maleic anhydride-grafted polypropylene (MAPP, Kayaku Akzo Co., Ltd., Tokyo, Japan) was added as a compatibilizer at approximately 2 wt% relative to the base material. MAPP was preferred for its excellent compatibility not only with natural cellulose such as wood fiber, but also with regenerated cellulose like Cordenka [156].

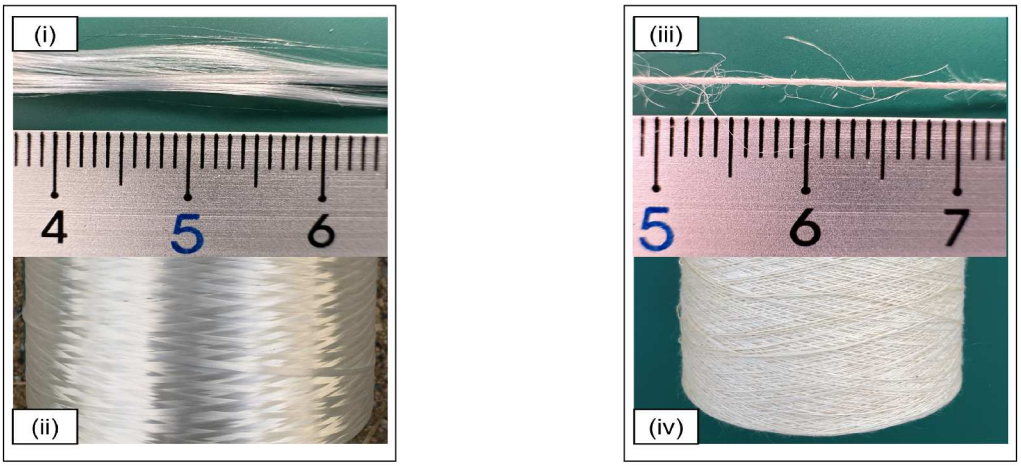

Figure 4.1: Reinforcement raw materials: (**a**) Cordenka single yarn, showing (i) the yarn itself and (ii) its spool, and (**b**) Ramie single twisted yarn, showing (iii) the yarn itself and (iv) its spool. The scale applies exclusively to the yarns.

Table 4.1: Physical properties of Cordenka and ramie fibers.

Fiber Type	Density [g/cm^3]	Width§/ Diameter [μm]	Length [mm]	Moisture Content [%]
Ramie†	1.5	40	150*	8
Cordenka‡	1.5	12.5	Continuous	13

§ The ramie fiber cross-section is non-circular, so the lateral dimension is termed width.
* The value shown represents the approximate average length of ramie fibers.
† Data for ramie fibers from Kim et al. [152].
‡ Data for Cordenka fibers from the Cordenka Technical Data Sheet [153].

4.2.1 Tensile Testing of Single Cordenka and Ramie Fiber Specimens

Tensile testing of single Cordenka and ramie fibers was conducted in accordance with JIS R7606:2000, the standard method for evaluating the tensile properties of individual fibers. Test specimens were prepared by mounting single fibers on specially cut gripper paper tabs, as illustrated in Figure 4.2. Each fiber was aligned along a predefined axis and secured using cellophane tape and instant adhesive. The gauge length was set to 10mm. To accurately determine the fiber cross-sectional area, diameters were measured in two orthogonal directions using a video microscope (KH-1300, HIROX Co., Ltd., Tokyo, Japan), designating the larger and smaller diameters as the major and minor axes, respectively. The cross-section was approximated as an ellipse, and the area was calculated from measurements taken at 50 points per specimen. The mean of these values

was adopted as the representative cross-sectional area, following the procedure outlined by Tanabe et al.[157].

Tensile tests were performed using a micro-load cell tensile and compression testing machine developed at Yamaguchi University (load cell capacity: 20N), as shown in Figure4.3. Special attention was given to ensure accurate axial alignment and to avoid preloading or shock during specimen preparation. Both ends of the tabbing paper were carefully cut without applying load to prevent premature damage. Testing commenced immediately after isolating the central gauge section. Experiments were conducted at room temperature with a crosshead speed of 1.0 mm/min, and the tensile load–elongation response was recorded until fracture. Load signals were converted to voltage via the load cell and captured using a strain measurement amplifier (DPM-911, Kyowa Electronic Instruments Co., Ltd.) in conjunction with a digital oscilloscope (Memory HiCorder MR8870, HIOKI E.E. Corporation). To ensure statistical robustness and account for inherent variability in fiber strength, at least 20 specimens were tested for each fiber type under identical conditions.

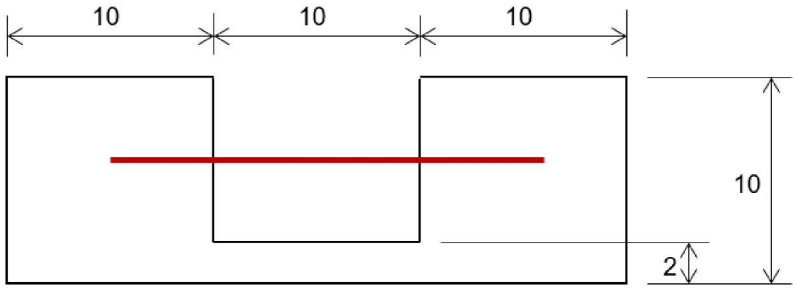

Figure 4.2: Schematic illustration of the setup showing the gripper paper (with grid pattern) used to secure the ends of Cordenka and ramie monofilaments (depicted by the bold red line) during tensile testing. The gripper paper ensures accurate alignment and fixation of the monofilaments, facilitating precise measurement of their tensile properties.

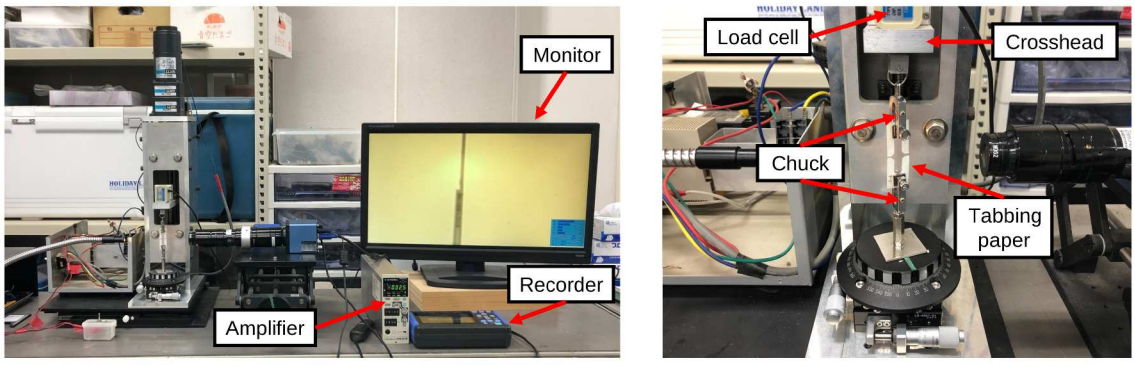

Figure 4.3: Micro load cell tensile and compression testing apparatus used for evaluating the tensile properties of single Cordenka and ramie fibers. The system provides high-resolution force measurements suitable for micro-scale specimens.

4.2.2 Fabrication of KP and RP Composite Strands

Cordenka and ramie composite strands were developed using the Multi-Pin-Assisted Resin Infiltration (M-PaRI) technique [76]. This method utilized a single-axis extruder which combined the coating and resin impregnation processes. The distinctive feature

of this method is its ability to develop composite strands without pre-cutting individual strands. Generally, the mechanical properties of short fiber-reinforced composites depend on the fiber length, and cutting individual strands typically leads to decreased mechanical performance. In conventional processing techniques, achieving optimal fiber dispersion while maintaining fiber length during the kneading process is inherently difficult, often resulting in the prioritization of dispersion for quality control purposes. However, the method utilized in this study offers a distinct advantage, enabling the production of GC materials without severing individual fibers. This approach ensures uniform fiber dispersion while preserving their original lengths, thereby enhancing the overall material properties.

The single-axis extruder, equipped with a 15 mm spinning device, was used in this study (Musashino Kikai Co., Ltd., Tokyo, Japan). Using this system, PP blended with MAPP was kneaded at a barrel zone temperature of 180°C and a screw speed of 5.0 r.p.m. This extruder offers key advantages, such as precise and consistent control over melt temperature and pressure at the coating die section, along with uniform kneading of the PP. A schematic of the strand continuous forming method, M-PaRI, utilized in this study is shown in Figure 4.4.

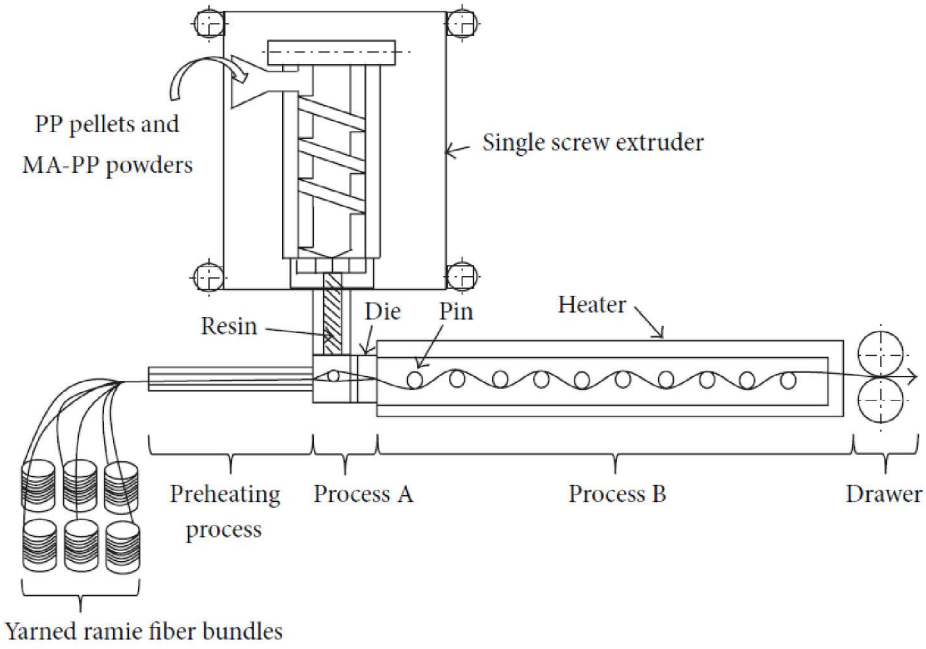

Figure 4.4: Schematic illustration of the Multi-pin-assisted resin infiltration (M-PaRI) technique.

The kneaded PP resin was coated onto preheated ramie spun yarn (single yarn) as it passed through the die in Process A. Subsequently, in Process B, the yarn was pulled through multiple pins (37 pins) placed inside a heater, alternately coming into contact with the pins, which allowed the resin to impregnate the fibers within the single yarn. The molded ramie and Cordenka yarn composite strands shown in Figure 4.5 were then drawn out through the die at a speed of 800 rpm.

4.2.3 Fabrication of KP and RP Composite Specimens

In order to further improve fiber dispersion, the fabricated ramie and Cordenka strands were cut into pellets approximately 15 mm in length and kneaded using a biaxial com-

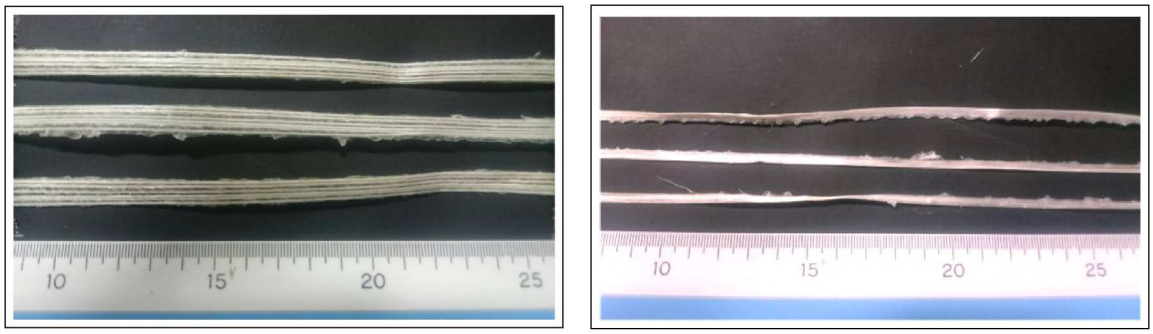

(a) Ramie yarn composite strand **(b)** Cordenka yarn composite strand

Figure 4.5: (**a**) Ramie and (**b**) Cordenka yarn composite strands prepared by M-PaRI technique.

pounding machine (No.655 Laboplast Mill). The fiber content was determined to be 30 wt% by comparing the prepared pellets with individual yarns. To adjust the fiber content to 20 wt% and 15 wt%, PP and MAPP were added to the pellets in ratios of 0.67:1 and 1:1, respectively. The cut pellets, along with the added materials, were then kneaded at a cylinder temperature of 190 °C, with a screw rotation speed of 30 rpm, and for a mixing time of 10 minutes. Subsequently, the compounded materials were ground into pellets approximately 5 mm in length using a grinder (P-1314, Horai Co., Ltd., Osaka, Japan). The pellets were then molded into dumbbell-shaped specimens for tensile tests and strip-shaped specimens for impact tests using a Babyplast (6/10P) injection molding machine (Rambaldi + Co. srl, San Giovanni in Persiceto, Italy) at a molding temperature of 200°C.

The dumbbell-shaped specimens were designed with dimensions of 15 mm gauge length, 3 mm width, and 2 mm thickness, in accordance with ASTM D638 standards. The strip-shaped specimens measured 10 mm in width, 4 mm in thickness, and 80 mm in length, following JIS 7111 standards. Additionally, for the strip-shaped specimens, variants were created with no notches, notches on one side, and notches on both sides. The notch dimensions were specified as a depth of 2 mm, a radius of 0.25 mm, and an angle of 45°. Figure 4.6 illustrates the geometric models and dimensions (in mm) of the specimens used in this study.

4.2.4 Tensile Test

Tensile tests were performed on both dumbbell-shaped and strip-shaped specimens using a compact tabletop tensile testing machine (LSC-1/30D, 1 kN capacity, manufactured by JT Tosi). Prior to testing, the thickness and width of each specimen were measured with a caliper, and the corresponding cross-sectional areas were calculated. Subsequently, tensile tests were conducted at room temperature and crosshead speed of 10 mm/min. Five specimens were tested in each experimental run, and data on test duration, applied load, and strain were recorded using a data logger, amplifier, and strain gauges (KGF-5-120-C1-11, Kyowa Electronic Instruments Co., Ltd., Tokyo, Japan). The strain gauges were positioned at mid-span on one side of each specimen, attached with an adhesive for strain gauges at one end, while the other ends were connected to the strain amplification device.

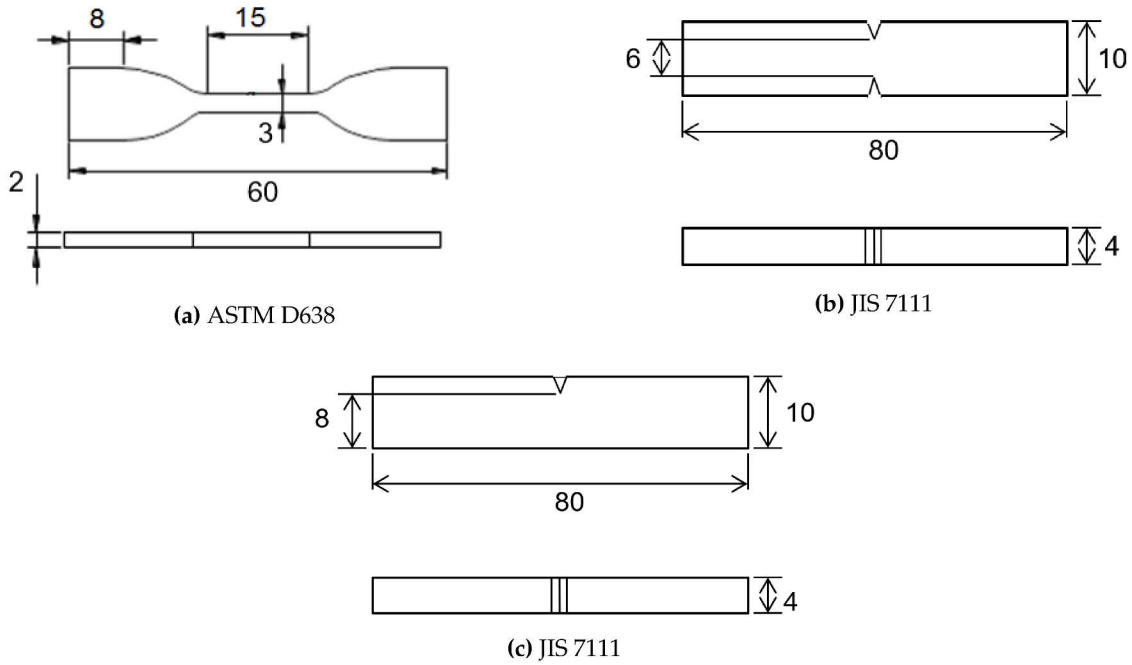

(a) ASTM D638

(b) JIS 7111

(c) JIS 7111

Figure 4.6: CAD geometric models of (**a**) ASTM D638 dumbbell-shaped tensile test specimen, (**b**) JIS 7111 tensile test specimen with a notch on either side, and (**c**) JIS 7111 impact test specimen with a notch on one side.

4.2.5 Impact Test

Charpy impact testing was carried out using an Izod–Charpy impact testing machine (CIT-25JCI). The specimens tested included rectangular specimens both with and without notches. Prior to testing, the thickness, width, and length of each specimen were measured using calipers to determine the cross-sectional area. The impact tests were performed using a 2J hammer weighing 0.857 kg, with a 12.80 cm distance between the centers. Each experimental run consisted of testing five specimens, and all tests were conducted at room temperature.

4.2.6 Fractographic Analysis

Fractured specimen surfaces were observed using a field emission scanning electron microscope (JSM-7500F, JEOL Ltd., Akishima, Tokyo, Japan) to examine their microstructural features. The observations were conducted at a distance of 15 mm from each fracture location on the specimens. For this study, one dumbbell-shaped specimen and two rectangular specimens were selected from each composition used in the tensile and impact tests: RP15, RP20, KP15, and KP20. Great care was taken to ensure that the selected fracture surfaces were oriented horizontally during the selection process.

4.2.7 Measurement of Fiber Lengths Extracted from PP-Based Composites Reinforced with Cordenka and Ramie Fibers

The lengths of fibers in the fabricated KP and RP specimens were measured using a Soxhlet extractor (Water Bath BS600, Yamato Scientific Co., Ltd., Tokyo, Japan). This apparatus was employed to dissolve the polymer (PP) matrix with an appropriate solvent, thereby isolating the insoluble components: Cordenka and ramie fibers. The extracted

fibers were then dispersed on slide glass and examined for length using a video microscope. Soxhlet extraction tests were performed on one dumbbell-shaped specimen each for RP15, RP20, KP15, and KP20. The lengths of 500 fibers were observed and recorded as test results.

4.3 Results and Discussion

4.3.1 SEM Fractographic Analysis of KP and RP Specimens

Figure 4.7 shows representative SEM images of fracture surfaces of 20 wt% KP and 20 wt% RP specimens. Looking at the fracture surface of the KP specimen in Figure 4.7 **a**, there is clear evidence of weak fiber–matrix adhesion, indicated by extensive fiber pull-out. The SEM images also reveal fiber breakage accompanied with clear gaps in the PP matrix, with some loose fibers visibly protruding from the fracture surface. These gaps and the presence of pulled-out fibers suggest a lack of effective stress transfer between the matrix and the reinforcing fibers, likely due to insufficient interfacial bonding. These findings contrast with those of Chen et al. [158], who, through SEM and Polarized Optical Microscopy (POM) analysis of the fractured surface of AF/PP composites, confirmed strong fiber–matrix interfacial adhesion.

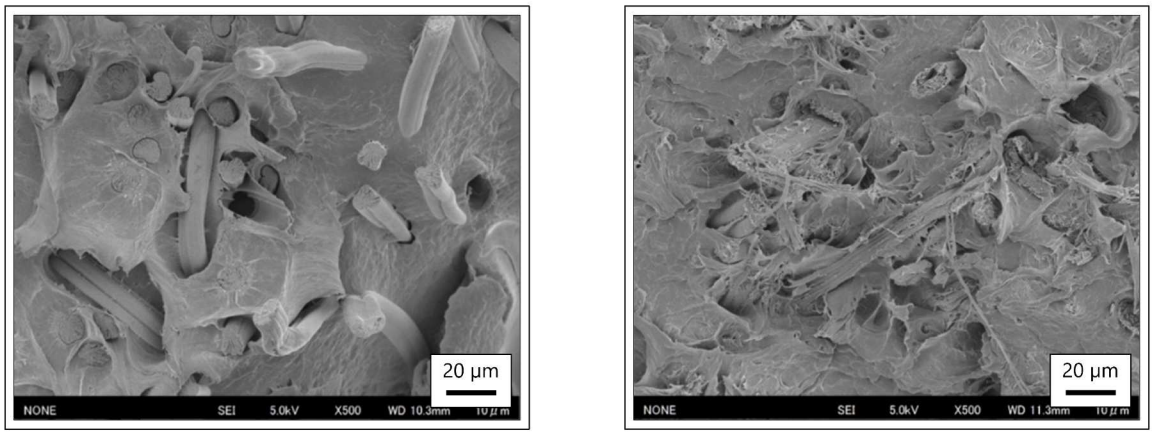

(a) 20 wt% KP **(b)** 20 wt% RP

Figure 4.7: SEM fracture surface images of (**a**) 20 wt% KP and (**b**) 20 wt% RP specimens.

The observed combination of fiber pull-out and breakage points to a mixed-mode failure, where adhesion between the fibers and the matrix is insufficient to prevent debonding under load, while the fibers themselves are unable to sustain higher stress levels. This highlights the need for enhanced surface treatment of fibers or optimized matrix–fiber interactions to improve the overall mechanical performance of KP composites. Thus, to achieve better adhesion, further investigation into suitable coupling agents is necessary. However, based on the results of Soxhlet tests discussed later, Cordenka fibers remained longer in the matrix compared to ramie fibers. This retention of fibers in the matrix prevented crack propagation during the pull-out process, hence the observed exhibition of high fracture energy [159].

Conversely, a careful examination of the scanning electron microscope image of the fracture surface of the RP composite reveals minimal fiber pull-out and few gaps between the fibers and the resin, indicating good adhesive strength (see Figure 4.7**b**). The adhesion between natural fibers, recycled cellulose fibers, and the PP/MAPP matrix is influenced

by the surface roughness of the fibers. Smooth surfaces, such as those of Cordenka fibers, are at a disadvantage in this regard [160]. Based on these observations, it can be inferred that RP composites exhibit superior adhesion compared to KP composites under the MAPP to PP ratio utilized in this study.

4.3.2 Tensile Properties of Single Cordenka and Ramie Fibers

Table 4.2 shows the results of the single fiber tensile tests for Cordenka and ramie fibers. The coefficients of variation are indicated in parentheses, and the corresponding representative stress–strain curves are shown in Figure 4.8. Strains were calculated based on the applied crosshead speeds and the specimen gauge length shown in Figure 4.6. The results indicate that although Cordenka fibers had a lower Young's modulus than ramie fibers, they exhibited superior tensile strength and fracture strain. The tensile strengths of some cellulosic natural fibers, such as flax [161] and curaua [162], have been reported to compare favorably with Cordenka. However, their fracture strain is significantly lower than that of Cordenka, typically ranging from 2 to 4% [163, 164]. Thus, despite the similarity in tensile strength, Cordenka retains the advantage of higher fracture strain. In terms of fracture energy, or toughness, Cordenka fibers exhibited values more than three times higher. Furthermore, it is worth noting that Cordenka fibers consistently showed lower coefficients of variation compared to ramie fibers, corroborating more stable properties.

Table 4.2: Tensile properties of single ramie and Cordenka fibers obtained in the current study.

Fiber Type	No. of Specimens	Tensile Strength [MPa]	Young's Modulus [GPa]	Fracture Strain [%]	Fracture Energy [MJ/m^3]
Cordenka	23	888 [0.19]	7.5 [0.29]	12.0 [0.21]	1.07 [0.34]
Ramie	22	571 [0.31]	20.5 [0.56]	3.30 [0.36]	0.30 [0.51]

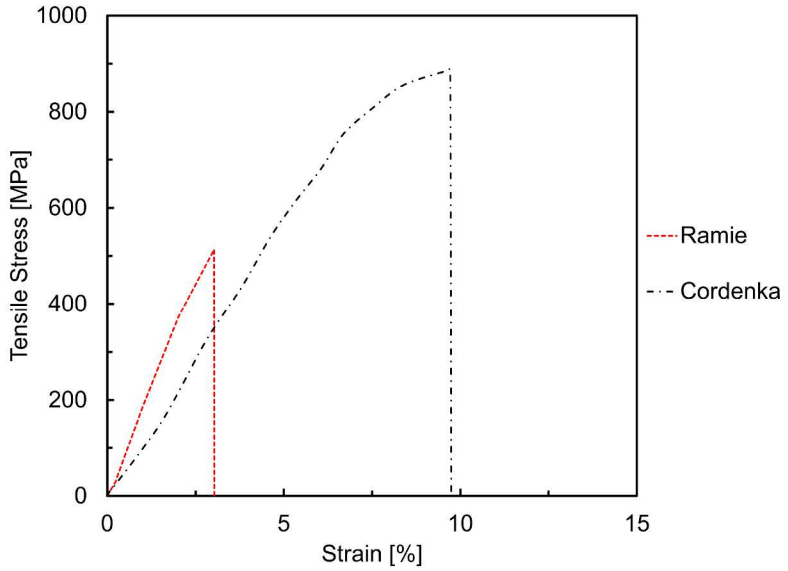

Figure 4.8: Typical stress–strain curves of Cordenka and ramie monofilaments.

4.3.3 Tensile Properties of Dumbbell-Shaped PP, KP, and RP Specimens

Tensile test results of neat PP, KP and RP specimens are presented in Table 4.3, with the representative stress–strain diagrams shown in Figure 4.9. The stress–strain curves clearly indicate that both KP and RP specimens exhibited higher tensile strengths than the neat PP specimen, with the 20 wt% KP specimen yielding the highest tensile strength of 68.7 MPa. Additionally, tensile strength further increased with increase in fiber content. Specifically, at 20 wt% fiber content, the tensile strength of RP and KP specimens increased by 22.6% and 105%, respectively, compared to neat PP specimens. In a similar study involving synthetic fibers, Chen et al. [158] reinforced neat PP with aramid fiber (AF) and reported a maximum tensile strength of 67.8 MPa at 20 wt% AF, representing a 111.8% improvement over neat PP.

Table 4.3: Tensile test results of dumbbell-shaped neat PP, RP, and KP specimens.

Specimen Type	Number of Samples	Tensile Strength [MPa]	Young's Modulus[1] [GPa]	Fracture Energy [MJ/m^3]
Neat PP	5	33.7	1.84	–
15 wt% KP	5	62.6	3.16	6.68
20 wt% KP	5	68.7	3.24	5.85
15 wt% RP	5	40.3	2.74	2.64
20 wt% RP	5	41.4	2.90	2.82

[1] Calculated from strains measured by strain gauge.

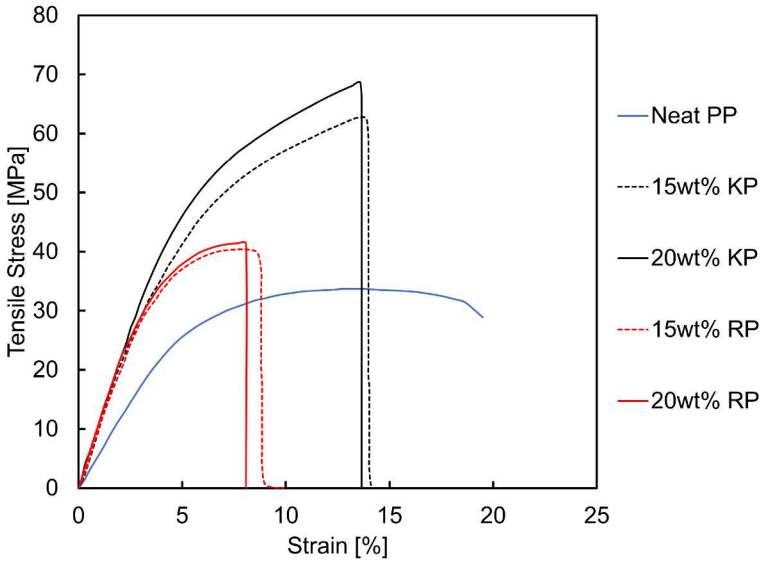

Figure 4.9: Typical tensile stress–strain curves of dumbbell-shaped PP, KP, and RP specimens.

Fernandez et al. [165] also reinforced the PP matrix with recycled carbon fiber (rCF) and achieved maximum tensile strength exceeding 60 MPa with 30 wt% rCF. Both authors reported a decrease in fracture strain with an increase in fiber content. Ari et al. [166] analyzed the mechanical performance of PP composites reinforced with chopped glass

fiber (GF), carbon fiber (CF), and aramid fiber (AF). They found that the most significant tensile strength improvements occurred at 30 vol.% fiber content for each material. GF reinforcement increased the tensile strength from 38.0 MPa to 78.5 MPa, CF increased it to 74.2 MPa, and AF raised it to 72.2 MPa. From the above comparative studies, it may be infered that the tensile properties of KP composites achieved in this current study show comparable performance to traditional synthetic fiber-reinforced PP composites.

In absolute terms, both the 15 wt% and 20 wt% KP composites showed approximately 1.6 times higher tensile strength than the RP composites. This finding aligns with the properties of the single Cordenka and ramie fibers used in this study, illustrated earlier in Figure 4.8, where a single Cordenka fiber exhibited about 1.5 times higher tensile strength than a single ramie fiber. Also, as described in Section 4.3.2, the Young's modulus of Cordenka monofilament was observed to be lower than that of ramie monofilament. However, in the reinforced composites, this situation is reversed, with the Young's modulus of KP composites reported to be slightly higher than that of RP composites.

Furthermore, to assess the magnitude of strength improvement on PP matrix achieved by the Cordenka fibers used in this study, findings from previous literature on the strength increase observed with CNF fiber-reinforced PP matrices—referred to in the introduction as 'processed' fibers—are summarized and compared with the current results. For instance, Kahavita et al. [57] reported a maximum tensile strength of 27.8 MPa in silane surface-modified CNF/PP composites at 3.5 wt% CNF, representing a 12.6% increase over neat PP. Similarly, Norrrahim et al. [167] observed a tensile strength increase of at least 31% in neat PP after incorporating 3 wt% CNF filler. In another study, they found that the optimal tensile strength was achieved with CNF concentrations of 1% to 3% [168]. Based on this comparison, it is evident that the performance of the KP composites developed in this study exceeded that of CNF-reinforced PP composites reported in previous studies.

In addition to the PP matrix, polylactic acid (PLA) has also been extensively studied, with many researchers attempting to utilize the impressive strength properties of CNF reinforcement in a PLA matrix. This focus has been driven by the fact that PLA is a biodegradable resin, hence CNF/PLA is a fully green composite, i.e., more environmentally friendly compared to composites with natural fiber reinforcements compounded with recyclable PP matrix. For example, Jonoobi et al. [169] obtained maximum tensile strength of 71 MPa, and reported a 22.4% and 24.1% increase in the tensile and flexural strengths, respectively, of PLA upon reinforcement with 5 wt% CNF. Senkum et al. [170] melt-compounded poly(methyl methacrylate)-functionalized CNFs in PLA matrix and achieved a tensile strength of 79 MPa, an improvement of nearly 30% over neat PLA at 20 wt% reinforcement loading. Other researchers pointed out that this strength increase is due to the nucleation effect of CNFs on the matrix [171, 172]. In cellulose nanowhisker (CNW)- and cellulose nanocrystal (CNC)-reinforced PLA nanocomposites, it has also been reported that CNW and CNC induce crystal nucleation of PLA and increase its crystallinity [173, 174, 175]. It has further been confirmed that such functioning as a crystal nucleus can also occur through nanofibrils formed by fibrillation of ramie fibers, although the resin is polyamide [176]. Since PP is also a semi-crystalline thermoplastic, the reinforcing effect of CNFs described above is considered to be crystallization strengthening of the matrix material rather than fiber reinforcement.

On the other hand, other researchers have reported a decline in tensile strength of thermoplastic polymer materials as a result of adding CNF, even though in some cases other mechanical properties were enhanced. For instance, Yang et al. [56] reported a maximum tensile strength of 21.3 MPa with 2 wt% CNF filler in a PP matrix, which was actually a 3.0% decrease from the original strength of neat PP. Although Young's

modulus consistently improved with increasing CNF content from 0 wt% to 10 wt%, the tensile strength results were less favorable. Similarly, Jung et al. [55] found that CNF/PP composites developed from N_2 plasma-treated PP and alkaline CNF achieved a maximum tensile strength of 24.5 MPa at 1 wt% CNF, reflecting a 27.9% decline from the tensile strength of neat PP. Zhang et al. [177] also experimented with 0.5 wt% CNF in the PLA matrix and noticed an 18.4% increase in tensile modulus, whereas the tensile strength dropped by 7.4%, from 47.5 to 44 MPa. They attributed this drop in tensile strength to poor interfacial adhesion between CNF and PLA.

Thus, from the sampled literature discussed above, it may be pointed out that the mechanical properties of thermoplastic composites reinforced with Cordenka and ramie fibers compare favorably with those of CNF fiber-reinforced thermoplastic composites. However, higher concentrations of Cordenka and ramie fibers than CNF fibers are necessary for the realization of these comparable properties. This is because the optimum fiber content for the fiber-reinforcing effect is much larger than that of crystallization strengthening, enabling it to far exceed the maximum possible strength that can be achieved by the matrix. On the other hand, the reported decline in mechanical properties of CNF/PP composites resulting from an increase in CNF content beyond optimum values, typically between 1 wt% and 5 wt%, is due to agglomeration of CNF, which is a well-known and widely reported defect in CNF-based polymer composites [99, 178, 179, 180, 181, 182, 183]. To solve this problem, research on chemical modification of CNF is currently being conducted with intent to improve nanodispersibility of CNF in polymer matrices [184, 185, 186, 187, 188]. In any case, high fiber content can be achieved in Cordenka and ramie fiber-reinforced polymer composites due to low fiber-to-fiber cohesion. This is because macroscale fibers have a significantly smaller specific surface area compared to nanoscale CNFs.

In the fracture strain results presented in Figure 4.8, the tensile tests for the neat PP specimens were terminated at 20% strain, as the material exhibited continued elongation without attaining fracture. On the other hand, the fracture strains of the KP specimens were found to be greater than those of the RP specimens. While both composites showed similar initial slopes in the elastic region, the KP specimens exhibited significant strain hardening in the nonlinear region, indicating a larger area under the stress–strain curve, which implies higher fracture energy. Looking at the fracture energy data shown in Table 4.3 obtained by numerical approximation of the area under each corresponding stress–strain curve, it can be seen that KP composites showed fracture energy values approximately 2.1 to 2.5 times higher than those of RP composites. Furthermore, as evidenced by Figure 4.8, the nonlinear region of both composite materials tended to align with the strain level where the PP matrix entered its nonlinear region, suggesting that the onset of nonlinearity was influenced by the deformation behavior of the matrix material. This behavior contrasted markedly with that observed in the Cordenka and ramie monofilament tensile stress–strain curves, where Cordenka fibers exhibited significant deformation resistance before failure, unlike ramie fibers. Therefore, the high strain hardening observed in the nonlinear region of the monofilament test results was likely dependent on fiber behavior. As discussed later, ramie fibers did not reach a critical fiber length within the matrix material, resulting in RP composites exhibiting behavior dominated by the deformation of the PP matrix even in the nonlinear region.

4.3.4 Tensile Properties of Strip-Shaped Neat PP, KP, and RP Specimens

The resistance of KP composites to notches was evaluated by comparing the properties of notched specimens to unnotched ones. Table 4.4 presents the tensile test results of strip specimens with notches on both sides and their ratios compared to dumbbell-shaped (unnotched) specimens, and Figure 4.10 illustrates the stress–strain curves for the notched test specimens. The results indicate that even with the presence of notches, the tensile strength of KP specimens still exceeded that of both RP and neat PP specimens. Furthermore, the KP specimens exhibited higher fracture energy compared to RP specimens and achieved levels comparable to neat PP. Notably, the 15 wt% KP composite displayed the highest tensile strength and fracture energy among all the tested specimens.

Table 4.4: Tensile test results of strip specimens with notches in comparison to dumbbell specimens.

Specimen Type	Tensile Strength [MPa]	Strength Ratio to Unnotched	Fracture Energy [MJ/m^3]	Energy Ratio to Unnotched
Neat PP	28.40	0.84	1.28	–
15 wt% RP	30.28	0.75	0.83	0.314
20 wt% RP	31.38	0.75	0.72	0.255
15 wt% KP	40.15	0.64	1.52	0.228
20 wt% KP	38.50	0.56	1.10	0.188

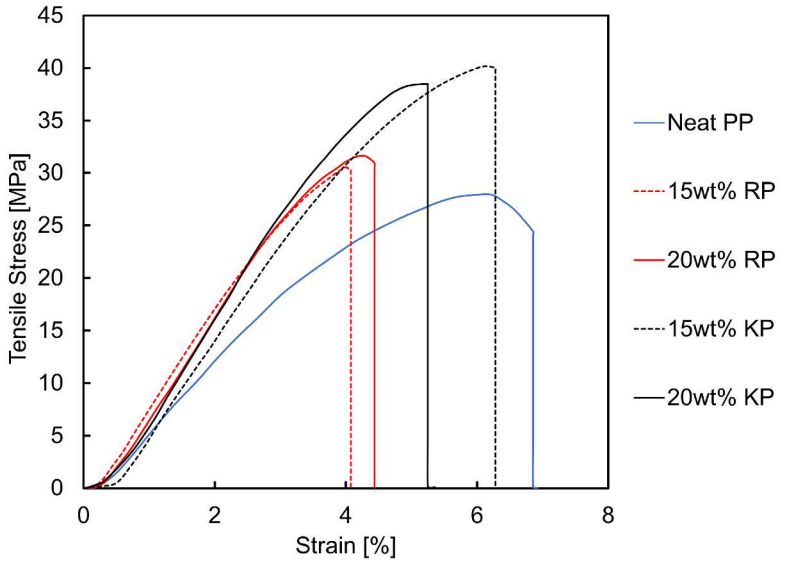

Figure 4.10: Typical tensile stress–strain curves for strip-shaped notched specimens.

Focusing on the tensile strength and fracture energy ratio to the unnotched dumbbell-shaped specimens, it is evident that KP specimens exhibited greater reduction compared to other specimens, indicating that they do not exhibit very good resistance to notches. Comparing Figure 4.10, which illustrates the stress–strain curves of notched specimens, with Figure 4.9, which shows the stress–strain curve of the dumbbell-shaped specimen, it

is evident that a significant portion of the nonlinear region disappeared. In other words, for KP specimens, stress concentration due to the notches hinders strain hardening in the nonlinear region, causing the Cordenka fibers to break prematurely, significantly reducing tensile strength and fracture energy. RP specimens showed a comparable loss in the nonlinear region due to their poor strain-hardening properties. Therefore, it can be inferred that RP composites do not undergo as substantial a reduction in tensile strength and fracture energy as KP composites.

4.3.5 Impact Properties of PP J-900GP, KP, and RP Specimens

Table 4.5 presents the results of the Charpy impact test for notched and unnotched neat PP, KP, and RP specimens. For the unnotched neat PP specimens, an initial impact test was conducted using a 2.0 J hammer as a trial, under the same conditions as the other tests. However, it was observed that these specimens did not fracture, in contrast to the KP and RP specimens, which did fracture. Consequently, a 7.5 J hammer was used for the neat PP specimens, and the impact strength values obtained with the 7.5 J hammer were recorded.

The results showed that the KP specimens exhibited superior impact strength compared to the RP specimens, with the unnotched 15 wt% KP specimens attaining the highest impact strength of 47.7 kJ/m^2. In particular, the impact energy of the KP specimens was approximately 2 to 2.5 times greater than that of the RP specimens in both notched and unnotched categories. This multiplication factor closely aligns with the fracture energy ratio observed in the tensile test results for dumbbell-shaped specimens shown in Table 4.3, and significantly surpasses the corresponding ratios recorded in the notched tensile test results presented in Table 4.4. These findings indicate that KP composites exhibit superior impact energy absorption capabilities compared to RP composites.

Table 4.5: Charpy impact properties of PP J-900GP, KP and RP specimens.

Specimen Type	Impact Energy [kJ/m^2]		N/U Ratio
	Unnotched (U)	Notched (N)	
PP J-900GP	66.8 (7.5J)	1.8	-
15 wt% RP	19.6	3.7	0.189
20 wt% RP	19.5	3.9	0.200
15 wt% KP	47.7	8.7	0.182
20 wt% KP	40.5	10.0	0.247

In the study by Chen et al. [158], the Izod notched impact strength of AF-reinforced PP composites peaked at 40.1 kJ/m^2 with 40 wt% AF loading. Similarly, Fernandez et al. [165] reported a maximum impact strength of over 35 kJ/m^2 for rCF/PP composites at 20 wt% rCF. Both studies on non-biodegradable fibers reported impact strength values lower than those observed for KP composites in the current study, supporting the hypothesis that KP composites can competitively match the mechanical performance of traditional synthetic fiber-reinforced plastic composites.

Additionally, in the case of KP composites, it has been reported that adding non-compatibilizing agents [189] or omitting compatibilizers entirely [156] slightly reduces

static strength but significantly enhances impact strength. Generally, in composite materials with low interfacial strength, crack propagation tends to be dispersed through interfacial debonding, which allows for greater energy absorption. However, low interfacial strength also results in slower stress recovery from the fiber ends, which is detrimental to achieving high static strength. Consequently, KP composites exhibit a higher impact energy ratio compared to the tensile strength ratio of RP composites.

As for the neat PP specimens, large variations in impact strength values were observed in the notched specimens, indicating that PP material is highly susceptible to the effects of notches. Focusing on the specimens without notches, it can be seen that as the fiber content decreased, the impact strength of both KP and RP specimens increased. On the other hand, for specimens with notches, an increase in fiber content led to an increase in impact strength. These trends are likely due to the inherent weakness of neat PP against notches. The elongation of the fibers and their pullout from the matrix are believed to effectively absorb impact energy and mitigate crack propagation originating from the notch.

4.4 Cordenka and Ramie Fiber Length Measurement Results

Figure 4.11 shows the images of the Cordenka and ramie fibers after the Soxhlet test.

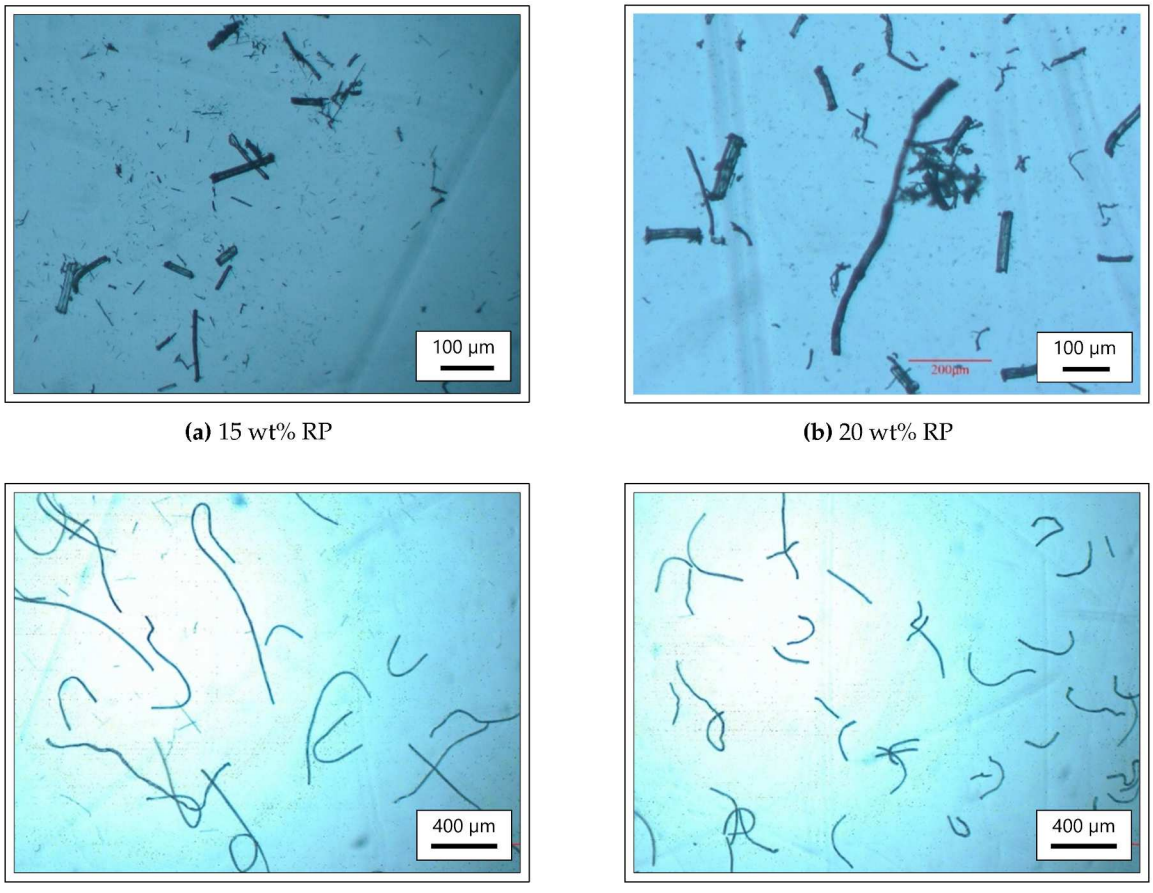

(a) 15 wt% RP

(b) 20 wt% RP

(c) 15 wt% KP

(d) 20 wt% KP

Figure 4.11: Soxhlet test images showing the state of fiber dispersion on the surfaces of KP and RP composites.

It is evident from the images that the extracted Cordenka fibers from the KP composite, especially from the 15 wt% sample, appear to have still retained significantly longer lengths compared to the extracted ramie fibers from the RP composite. Also, from the fiber length measurement results presented in Table 4.6, it is clearly seen that in the 20 wt% KP sample, the fiber lengths decreased to about half their initial lengths. This suggests that as the fiber content increases, fibers are more likely to entangle and break during the kneading process. On the other hand, for the RP samples, many relatively short fibers were observed in both the 15 wt% and 20 wt% samples. The aspect ratio of these fibers was found to be between six and eight, indicating that the fiber reinforcing effect was insufficient to significantly enhance the mechanical properties of the composite.

Table 4.6: Average fiber length, aspect ratio, critical fiber length, and fiber diameter of Soxhlet-extracted fibers for RP and KP specimens.

Specimen Type	Avg. Fiber Length [μm]	Aspect Ratio	Critical Fiber Length [μm]	Fiber Diameter [μm]
15 wt% RP	158	6	369	25
20 wt% RP	210	8		
15 wt% KP	650	52	298	13
20 wt% KP	330	26		

To quantitatively evaluate this effect, the critical fiber length (l_c) was determined using the Kelly–Tyson model [190], expressed as follows:

$$l_c = \frac{d_f}{2\tau_{my}} \cdot \sigma_f^* \tag{4.1}$$

In this equation, l_c denotes the critical fiber length, d_f represents the fiber diameter or width, σ_f^* is the fiber strength, and τ_{my} indicates the shear yield stress of the matrix resin. The shear yield stress of the PP matrix resin (τ_{my}) was calculated using the fracture strain levels observed during the tensile testing of the composites, which closely approached the tensile strength of PP. This value was further refined according to the Mises criterion, being divided by $\sqrt{3}$. The analysis revealed that the average length of the extracted Cordenka fibers exceeded the calculated l_c, while the ramie fibers consistently remained below l_c.

Additionally, from the frequency distribution graph of the measured fiber lengths shown in Figure 4.12, it can be observed that many of the Cordenka fibers in the 15 wt% KP composite and about half of those in the 20 wt% KP composite exceeded l_c. On the other hand, many of the ramie fibers in the RP composites fell below l_c. Although the Young's modulus of ramie fiber is higher than that of Cordenka fiber, this difference in length likely caused the reversal of Young's modulus between the two composites, as shown in Table 4.3. However, the observed variations in fiber length do not appear to have a significant effect on the increase in tensile strength. This is evident when comparing the tensile strength ratio of Cordenka fibers to ramie fibers (C/r), calculated from Table 4.2 (1.56), with the tensile strength ratios of the corresponding composites in Table 4.3, which are 1.55 for 15%C/r and 1.66 for 20%C/r.

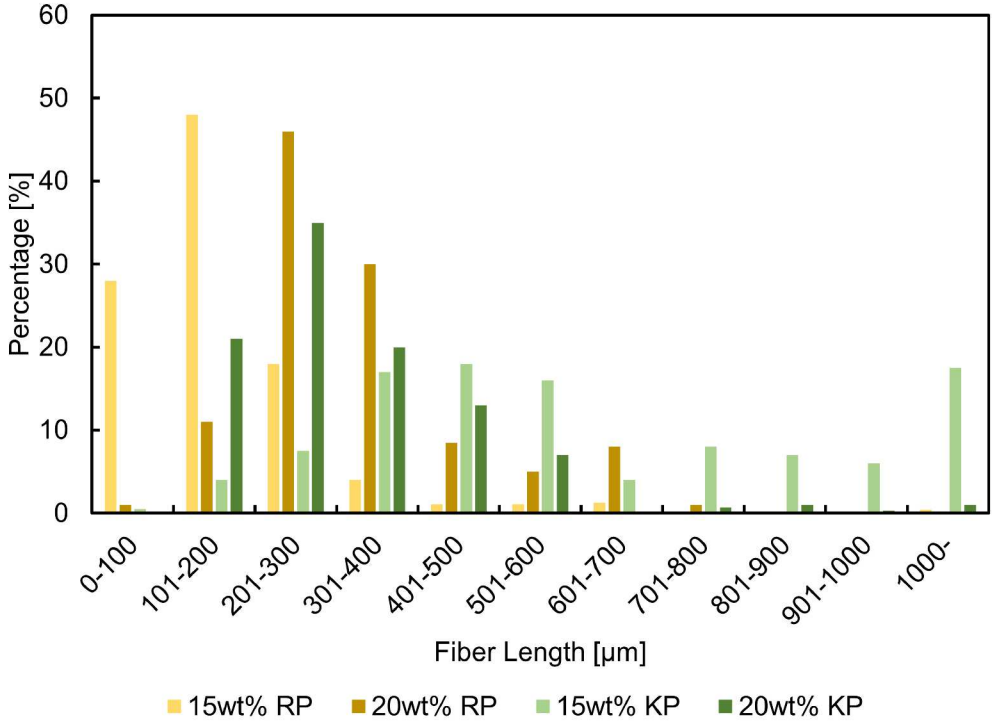

Figure 4.12: Fiber length distribution graph.

Chapter 5

Conclusions and Recommendations

This study investigated the mechanical and morphological properties of polypropylene composites reinforced with wood fibers, the artificial biodegradable cellulosic fiber Cordenka, and ramie fibers at various fiber-matrix ratios. The WP, KP, and RP composites were fabricated using the injection molding technique. For the KP and RP specimens, fiber pre-treatment was performed via the M-PaRI process prior to injection molding. Surface functionalization of the fabricated specimens involved plasma irradiation, UV irradiation, the application of acrylic resin and CNF coating, as well as PP and PET film lamination. The influence of several parameters—including fiber type, fiber-matrix ratio, CNF type and content, and film laminate type—on the mechanical properties of the developed composites was extensively analyzed and documented.

A summary of the key findings, conclusions, and recommendations for future research is presented below.

5.1 Conclusions

Tensile strength of WP composites increased with fiber content, from 25 to 50wt%, accompanied by a reduction in fracture strain. This behavior reflects the reinforcing effect of wood fibers, which enhanced stiffness and strength while reducing ductility. KP composites demonstrated superior tensile performance, achieving a maximum strength of 68.7MPa at 20wt% fiber content, compared to 52.5MPa for WP at 50 wt%. The superior performance of Cordenka-reinforced composites was primarily attributed to the greater fiber length, higher intrinsic tensile strength, and improved fiber–matrix interfacial bonding, the latter enhanced by the multi-pin assisted resin impregnation (M-PaRI) method. The more uniform structure and higher aspect ratio of Cordenka fibers also facilitated more effective stress transfer, contributing to improved reinforcement compared to wood fibers.

Surface treatment of both PP and WP specimens—using methods such as plasma irradiation, ultraviolet irradiation, PEGylated cellulose nanofiber–acrylic resin coating, and surface lamination—led to significant improvements in tensile strength. Among the lamination configurations examined, double-sided lamination, in which film was bonded to both the upper and lower surfaces of the specimen, produced the greatest increase in tensile strength. This effect was consistent across both film types—polypropylene and polyethylene terephthalate—and both substrate materials. These results indicate that the primary benefit of lamination arises from its ability to homogenize the specimen struc-

ture, rather than from the intrinsic mechanical strength of the films. In contrast, at lower lamination levels such as single-sided half lamination, polypropylene films tended to reduce the tensile strength of neat polypropylene specimens, likely due to their relatively lower stiffness and strength compared to polyethylene terephthalate films.

Plasma treatment of the specimens resulted in a measurable decrease in fracture strain relative to untreated controls. This reduction was attributed to the increased surface roughness and enhanced stiffness imparted by plasma irradiation, which was believed to diminish the material's capacity for plastic deformation. Consequently, plasma exposure promoted a more brittle fracture mode, leading to premature failure. Furthermore, specimens fabricated from the PP-J108 resin and their corresponding wood-plastic composites exhibited significantly greater fracture strain compared to those derived from PP-J106 and its composites. This disparity reflected the intrinsic mechanical differences between the two polypropylene grades: PP-J106 displayed brittle fracture behavior characterized by limited elongation at break, whereas PP-J108 demonstrated pronounced ductility with substantial plastic deformation prior to failure. Collectively, these findings indicate that both surface treatment effects and the inherent ductility of the PP matrix are critical determinants of the fracture response in these composite systems.

Scanning electron microscopy (SEM) and surface roughness analysis revealed that the incorporation of WF into the PP matrix introduced surface voids and irregularities, leading to increased surface roughness. Application of an acrylic resin coating effectively filled these voids, resulting in a reduction in surface roughness by approximately 50%. SEM images also showed that specimens coated with CNF-S had smoother surfaces than those coated with CNF-L, indicating that the type of CNF suspension plays a significant role in determining surface morphology. For film-laminated specimens, both PP and PET films substantially reduced surface roughness and improved surface uniformity by covering surface imperfections and sealing voids. Among the surface treatment methods evaluated, PP and PET lamination proved more effective in enhancing surface texture and homogeneity than acrylic resin or CNF coatings, likely due to their continuous film structure and superior ability to conform to and mask the underlying substrate irregularities.

Fractographic analysis of the WP specimens revealed that fracture consistently initiated at the corners of the specimen cross-sections. Film lamination appeared to delay crack initiation by effectively sealing these vulnerable sites. Among the laminated configurations, double-sided PET film specimens—whether with PP or WF/PP substrates—exhibited the greatest enhancement in tensile strength. This finding suggests that increased PET film coverage effectively reduces the number of exposed fracture origins, thereby improving mechanical performance. However, as previously discussed, this trend did not apply to specimens laminated with PP film. Despite comparable surface coverage, increased lamination with PP film resulted in lower tensile strength, likely due to the film's relatively poor mechanical properties, which may have introduced local weaknesses or reduced the stiffness of the surface layer. With regard to fracture mechanisms observed in KP and RP specimens, the two composites demonstrated distinctly different behaviors: KP specimens exhibited a combination of fiber pull-out, interfacial debonding, and fiber breakage, indicating a mixed-mode fracture mechanism. This was likely due to the relatively smoother surface morphology and lower interfacial adhesion of the regenerated cellulose fibers. In contrast, RP specimens showed minimal fiber pull-out and fewer interfacial voids, reflecting stronger fiber–matrix bonding—possibly due to the rougher

surface texture and higher stiffness of the ramie fibers, which promote better mechanical interlocking and stress transfer at the interface.

A comparison of the KP and RP composites revealed that KP composites possessed significantly higher tensile strength and toughness. For instance, the 20 wt% KP specimens achieved a maximum tensile strength of 68.7 MPa, while the corresponding RP specimens exhibited a maximum tensile strength of 41.4 MPa. Furthermore, the fracture energy values of the KP composites were approximately 2.1 to 2.5 times greater than those of the RP composites. Notched specimen tensile tests demonstrated that stress concentration at the notch inhibited strain hardening, leading to premature fiber breakage and a substantial reduction in tensile strength and fracture energy.

In the Charpy impact test, unnotched KP and RP specimens showed that the 15 wt% KP specimens exhibited the highest impact energy, measuring 47.7 kJ/m^2, which was significantly greater than the 19.6 kJ/m^2 observed for the RP specimens. This result suggests that composites with low interfacial strength tend to exhibit crack propagation primarily through interfacial debonding, a mechanism that facilitates higher energy absorption. However, this low interfacial strength also impedes effective stress recovery at the fiber ends, negatively impacting the attainment of high static strength. Consequently, KP composites demonstrated a higher impact energy ratio compared to the tensile strength ratio observed in RP composites.

A comparison of the impact strengths of PP, WP15, and KP15 specimens showed contrasting effects of acrylic resin surface treatment. In neat PP specimens, immersion coating with acrylic resin—regardless of CNF content—resulted in a notable reduction in impact strength relative to untreated PP, suggesting that the brittle nature of the cured coating impeded energy absorption during impact. In contrast, the WP15 and KP15 composites exhibited increases in impact strength by 30% and 5.9%, respectively, compared to their untreated counterparts. This enhancement may be attributed to improved surface densification and partial crack deflection at the coated interface, which could mitigate localized stress concentrations during impact loading. Fractographic analysis of the impact-tested PP specimens further indicated that the acrylic resin layer restricted longitudinal crack propagation, supporting the inference that the coating altered the fracture path and failure dynamics.

Fiber length analysis based on the Kelly–Tyson model confirmed that Cordenka fibers in the KP composites maintained lengths exceeding the critical threshold required for effective stress transfer within the polypropylene matrix. Frequency distribution data revealed that a majority of fibers in the 15 wt% KP composite, and approximately half in the 20 wt% KP composite, surpassed the calculated critical length, while most ramie fibers in the RP composites fell below this threshold. Although ramie fibers possess a higher intrinsic modulus than Cordenka fibers, their shorter lengths likely limited their reinforcing efficiency. This difference in length distribution is consistent with the observed reversal in composite stiffness, where KP composites exhibited higher Young's modulus than RP composites. However, this variation in fiber length appeared to have minimal impact on tensile strength, as the composite strength ratios between KP and RP closely matched the corresponding ratios of the raw fiber strengths.

This study comprehensively demonstrated that surface modification techniques—such as plasma irradiation, UV treatment, acrylic resin coatings incorporating cellulose

nanofibers, and film lamination—are not only effective in enhancing surface uniformity but also contribute meaningfully to the mechanical performance of polypropylene-based composites. Among these, double-sided PET film lamination proved particularly effective in improving tensile properties by mitigating surface defects that act as fracture initiation sites. Additionally, the use of regenerated cellulose fibers, specifically Cordenka, offered superior reinforcement compared to wood and ramie fibers, owing to their favorable length retention and compatibility with the polypropylene matrix. The application of the multi-pin assisted resin impregnation (M-PaRI) method prior to injection molding further enhanced interfacial bonding, supporting efficient stress transfer and improved mechanical behavior. Collectively, these findings underscore the importance of both surface engineering and fiber-matrix design in advancing the performance of natural and regenerated fiber-reinforced polymer composites, while also reinforcing the potential of sustainable alternatives to conventional synthetic reinforcements.

5.2 Recommendations for Future Research

Further investigation into the effects of CNF fiber length on tensile strength, particularly by employing a broader range of fiber lengths to enable a more comprehensive evaluation. Additionally, exploring the influence of acrylic resin and CNF coating layer thickness on the tensile strength of WPCs will provide a deeper understanding of their impact on mechanical performance.

Research should focus on optimizing the composite manufacturing processes utilized in this study, including injection molding parameters and M-PaRI conditions, to achieve superior mechanical properties compared to those obtained in the present work.

To address the inherent notch sensitivity of neat polypropylene, which contributed to the reduced toughness of KP specimens relative to Cordenka fibers, future research should explore the development of Cordenka fiber-reinforced toughened polypropylene or alternative thermoplastic matrices to enhance the toughness of notched composite specimens.

Exploring novel CNF surface coating techniques is recommended to further improve the mechanical properties of both WP and KP composites.

X-ray diffraction (XRD) analysis should be performed on neat PP specimens and PP film laminates to compare their crystallinity indices and evaluate the influence of lamination on the crystalline structure.

The development and evaluation of CNF-based composite films as potential alternatives to PP films is suggested, with a focus on investigating their impact on the mechanical and morphological properties of WP and KP composites.

References

[1] Kayo Corporation, "List of Physical Properties of Plastics (Thermoplastics)," https://kayo-corp.co.jp/common/pdf/pla_propertylist01.pdf, 2024, accessed on [September 18, 2024].

[2] B. Xu, M.-Y. Wei, X.-Y. Wu, J.-G. Lei, Z.-W. Zhou, L.-Y. Fu, and L.-K. Zhu, "An injecting molding method for forming the hfrp/pa6 composite parts," *Polymers*, vol. 14, no. 23, p. 5085, 2022.

[3] A. Sayam, A. M. Rahman, M. S. Rahman, S. A. Smriti, F. Ahmed, M. F. Rabbi, M. Hossain, and M. O. Faruque, "A review on carbon fiber-reinforced hierarchical composites: Mechanical performance, manufacturing process, structural applications and allied challenges," *Carbon Letters*, vol. 32, no. 5, pp. 1173–1205, 2022.

[4] S. M. Rangappa, S. Siengchin, J. Parameswaranpillai, M. Jawaid, and T. Ozbakkaloglu, "Lignocellulosic fiber reinforced composites: Progress, performance, properties, applications, and future perspectives," *Polymer Composites*, vol. 43, no. 2, pp. 645–691, 2022.

[5] W. O. Ondiek, H. Ngetha, J. N. Keraita, and J. B. Byiringiro, "Investigating the effect of fiber concentration and fiber size on mechanical properties of rice husk fiber reinforced polyester composites," *International Journal of Composite Materials*, vol. 8, no. 5, pp. 105–115, 2018.

[6] J. Andrzejewski, M. Barczewski, and M. Szostak, "Injection molding of highly filled polypropylene-based biocomposites. buckwheat husk and wood flour filler: A comparison of agricultural and wood industry waste utilization," *Polymers*, vol. 11, no. 11, p. 1881, 2019.

[7] M. M.-U. Haque, K. Goda, S. Ogoe, and Y. Sunaga, "Fatigue analysis and fatigue reliability of polypropylene/wood flour composites," *Advanced Industrial and Engineering Polymer Research*, vol. 2, no. 3, pp. 136–142, 2019.

[8] K. Mokobia, E. M. Jonathan, G. Oyiborhoro, M. Maliki, and I. H. Ifijen, "Environmental degradation of polymer-based composite materials: challenges and mitigation strategies," in *TMS Annual Meeting & Exhibition*. Springer, 2024, pp. 1218–1236.

[9] M. Megha, M. Kamaraj, T. G. Nithya, S. GokilaLakshmi, P. Santhosh, and B. Balavaishnavi, "Biodegradable polymers–research and applications," *Physical Sciences Reviews*, vol. 9, no. 2, pp. 949–972, 2024.

[10] B. A. Makinde-Isola, A. S. Taiwo, I. O. Oladele, A. D. Akinwekomi, S. O. Adelani, and L. N. Onuh, "Development of sustainable and biodegradable materials: a review on banana and sisal fibre based polymer composites," *Journal of Thermoplastic Composite Materials*, vol. 37, no. 4, pp. 1519–1539, 2024.

[11] J. Qureshi, "A review of recycling methods for fibre reinforced polymer composites," *Sustainability*, vol. 14, no. 24, p. 16855, 2022.

[12] X. Xue, S.-Y. Liu, Z.-Y. Zhang, Q.-Z. Wang, and C.-Z. Xiao, "A technology review of recycling methods for fiber-reinforced thermosets," *Journal of Reinforced Plastics and Composites*, vol. 41, no. 11-12, pp. 459–480, 2022.

[13] P.-Y. Chen, R. Feng, Y. Xu, and J.-H. Zhu, "Recycling and reutilization of waste carbon fiber reinforced plastics: Current status and prospects," *Polymers*, vol. 15, no. 17, p. 3508, 2023.

[14] S. Bulińska, A. Sujak, and M. Pyzalski, "From waste to renewables: Challenges and opportunities in recycling glass fibre composite products from wind turbine blades for sustainable cement production," *Sustainability*, vol. 16, no. 12, p. 5150, 2024.

[15] M. B. MACİT and A. GÜRSEL, "An investigation on recycling of the glass fiber reinforced thermoset composite wastes," *Afyon Kocatepe Üniversitesi Uluslararası Mühendislik Teknolojileri ve Uygulamalı Bilimler Dergisi*, vol. 5, no. 2, pp. 32–39, 2022.

[16] V. Sommer and G. Walther, "Recycling and recovery infrastructures for glass and carbon fiber reinforced plastic waste from wind energy industry: A european case study," *Waste Management*, vol. 121, pp. 265–275, 2021.

[17] G.-Z. Yin and X.-M. Yang, "Biodegradable polymers: a cure for the planet, but a long way to go," *Journal of Polymer Research*, vol. 27, no. 2, p. 38, 2020.

[18] B. Kaith, H. Mittal, R. Jindal, M. Maiti, and S. Kalia, "Environment benevolent biodegradable polymers: Synthesis, biodegradability, and applications," *Cellulose Fibers: Bio-and Nano-Polymer Composites: Green Chemistry and Technology*, pp. 425–451, 2011.

[19] A. Fitzgerald, W. Proud, A. Kandemir, R. J. Murphy, D. A. Jesson, R. S. Trask, I. Hamerton, and M. L. Longana, "A life cycle engineering perspective on biocomposites as a solution for a sustainable recovery," *Sustainability*, vol. 13, no. 3, p. 1160, 2021.

[20] A. E. Krauklis, C. W. Karl, A. I. Gagani, and J. K. Jørgensen, "Composite material recycling technology—state-of-the-art and sustainable development for the 2020s," *Journal of Composites Science*, vol. 5, no. 1, p. 28, 2021.

[21] Y. Feng, H. Hao, H. Lu, C. L. Chow, and D. Lau, "Exploring the development and applications of sustainable natural fiber composites: A review from a nanoscale perspective," *Composites Part B: Engineering*, p. 111369, 2024.

[22] A. K. Maurya, F. M. de Souza, T. Dawsey, and R. K. Gupta, "Biodegradable polymers and composites: recent development and challenges," *Polymer Composites*, vol. 45, no. 4, pp. 2896–2918, 2024.

[23] B. K. Dejene and T. M. Geletaw, "Development of fully green composites utilizing thermoplastic starch and cellulosic fibers from agro-waste: a critical review," *Polymer-Plastics Technology and Materials*, vol. 63, no. 5, pp. 540–569, 2024.

[24] M. Y. Khalid, A. Al Rashid, Z. U. Arif, W. Ahmed, H. Arshad, and A. A. Zaidi, "Natural fiber reinforced composites: Sustainable materials for emerging applications," *Results in Engineering*, vol. 11, p. 100263, 2021.

[25] A. K. Mohanty, M. Misra, and L. Drzal, "Sustainable bio-composites from renewable resources: opportunities and challenges in the green materials world," *Journal of Polymers and the Environment*, vol. 10, pp. 19–26, 2002.

[26] R. Scaffaro, A. Maio, E. F. Gulino, G. Alaimo, and M. Morreale, "Green composites based on pla and agricultural or marine waste prepared by fdm," *Polymers*, vol. 13, no. 9, p. 1361, 2021.

[27] J. I. P. Singh, S. Singh, and V. Dhawan, "Effect of alkali treatment on mechanical properties of jute fiber-reinforced partially biodegradable green composites using epoxy resin matrix," *Polymers and polymer composites*, vol. 28, no. 6, pp. 388–397, 2020.

[28] V. Crupi, G. Epasto, F. Napolitano, G. Palomba, I. Papa, and P. Russo, "Green composites for maritime engineering: A review," *Journal of Marine Science and Engineering*, vol. 11, no. 3, p. 599, 2023.

[29] O. K. Cakmak, "Biodegradable polymers—a review on properties, processing, and degradation mechanism," *Circular Economy and Sustainability*, vol. 4, no. 1, pp. 339–362, 2024.

[30] S. Paul, B. Sen, S. Das, S. J. Abbas, S. N. Pradhan, K. Sen, and S. I. Ali, "Incarnation of bioplastics: recuperation of plastic pollution," *International Journal of Environmental Analytical Chemistry*, vol. 103, no. 19, pp. 8217–8240, 2023.

[31] Japan Society of Mechanical Engineers, *Mechanical Engineering Handbook*, 6th ed. Tokyo, Japan: Japan Society of Mechanical Engineers, 1977.

[32] S. Gross, G. Tarragano, R. R. MacBride, and C. O. Port, *Modern Plastics Encyclopedia, 1973-1974 Edition*. Philadelphia, Pennsylvania, USA: McGraw-Hill, 1973, vol. 50-10A.

[33] U. K. Vaidya and K. Chawla, "Processing of fibre reinforced thermoplastic composites," *International Materials Reviews*, vol. 53, no. 4, pp. 185–218, 2008.

[34] L. S. Hua, L. W. Chen, B. J. Geng, L. Kristak, P. Antov, M. Pędzik, T. Rogoziński, H. R. Taghiyari, M. A. R. Lubis, W. Fatriasari *et al.*, "Particleboard from agricultural biomass and recycled wood waste: A review," *journal of materials research and technology*, 2022.

[35] B. Jian, S. Mohrmann, H. Li, Y. Li, M. Ashraf, J. Zhou, and X. Zheng, "A review on flexural properties of wood-plastic composites," *Polymers*, vol. 14, no. 19, p. 3942, 2022.

[36] P. Lamba, D. P. Kaur, S. Raj, and J. Sorout, "Recycling/reuse of plastic waste as construction material for sustainable development: a review," *Environmental Science and Pollution Research*, vol. 29, no. 57, pp. 86 156–86 179, 2022.

[37] M. Nordin, Y. Makino, K. Goda, and H. Ito, "Fatigue fracture properties of wood plastic composites," *SEN-I GAKKAISHI*, vol. 71, no. 12, pp. 339–344, 2015.

[38] Fortune Business Insights, "Wood plastic composites market size, share & covid-19 impact analysis," 2022, accessed: 2025-06-13. [Online]. Available: https://www.fortunebusinessinsights.com/wood-plastic-composite-market-102821

[39] D. Friedrich, "Change in key mechanical properties from postprocess hot pressing of commercial wood-plastic composites with different fibre contents," *Polymer Bulletin*, vol. 80, no. 4, pp. 4263–4288, 2023.

[40] ——, "Additive manufacturing of post-process thermoformed wood-plastic composite cladding," *Automation in Construction*, vol. 139, p. 104322, 2022.

[41] N. Carter, I. Grant, M. Dewey, M. Bourque, and D. J. Neivandt, "Production and characterization of cellulose nanofiber slurries and sheets for biomedical applications," *Frontiers in Nanotechnology*, p. 86, 2021.

[42] A. Isogai, T. Saito, and H. Fukuzumi, "Tempo-oxidized cellulose nanofibers," *nanoscale*, vol. 3, no. 1, pp. 71–85, 2011.

[43] A. Yokoi, K. Yoshida, H. Koga, M. Kitagawa, Y. Nagao, M. Iida, S. Kawaguchi, M. Zhang, J. Nakayama, Y. Yamamoto *et al.*, "Spatial exosome analysis using cellulose nanofiber sheets reveals the location heterogeneity of extracellular vesicles," *Nature Communications*, vol. 14, no. 1, p. 6915, 2023.

[44] T. Kondo, "Cellulose nanofibrils pulverized from biomass resources: past, present, and future perspectives," *KONA Powder and Particle Journal*, vol. 40, pp. 109–123, 2023.

[45] T. Saito, R. Kuramae, J. Wohlert, L. A. Berglund, and A. Isogai, "An ultrastrong nanofibrillar biomaterial: the strength of single cellulose nanofibrils revealed via sonication-induced fragmentation," *Biomacromolecules*, vol. 14, no. 1, pp. 248–253, 2013.

[46] H. Takagi, A. Nakagaito, K. Nishimura, and T. Matsui, "Mechanical characterisation of nanocellulose composites after structural modification," *WIT Transactions on the Built Environment*, vol. 166, pp. 335–341, 2016.

[47] W. Tu, S. Wang, Q. Deng, D. Li, Y. Zhang, Q. Wang, and H. Jiang, "Review on nanocellulose composites and cnfs assembled microfiber toward automotive applications," *Nanotechnology Reviews*, vol. 13, no. 1, p. 20240006, 2024.

[48] L. Wang, K. Okada, Y. Hikima, M. Ohshima, T. Sekiguchi, and H. Yano, "Effect of cellulose nanofiber (cnf) surface treatment on cellular structures and mechanical properties of polypropylene/cnf nanocomposite foams via core-back foam injection molding," *Polymers*, vol. 11, no. 2, p. 249, 2019.

[49] B. N. Jung, H. W. Jung, D. Kang, G. H. Kim, and J. K. Shim, "Synergistic effect of cellulose nanofiber and nanoclay as distributed phase in a polypropylene based nanocomposite system," *Polymers*, vol. 12, no. 10, p. 2399, 2020.

[50] A. Sharma, M. Thakur, M. Bhattacharya, T. Mandal, and S. Goswami, "Commercial application of cellulose nano-composites–a review," *Biotechnology Reports*, vol. 21, p. e00316, 2019.

[51] K. Nelson, T. Retsina, M. Iakovlev, A. van Heiningen, Y. Deng, J. A. Shatkin, and A. Mulyadi, "American process: production of low cost nanocellulose for renewable, advanced materials applications," *Materials research for manufacturing: An industrial perspective of turning materials into new products*, pp. 267–302, 2016.

[52] D. MOON, K. TSUKAHARA, M. SAGISAKA, and K. TAHARA, "Effect of cellulose nanofibers composites in automotive components on greenhouse gas emissions," *Journal of the Japan Institute of Energy*, vol. 95, no. 8, pp. 648–652, 2016.

[53] M. N. F. Norrrahim, T. Yasim-Anuar, M. Jenol, N. M. Nurazzi, S. Sapuan, and R. Ilyas, "Performance evaluation of cellulose nanofiber reinforced polypropylene biocomposites for automotive applications," in *Biocomposite and synthetic composites for automotive applications*. Elsevier, 2021, pp. 199–215.

[54] D. Moon, M. Sagisaka, K. Tahara, and K. Tsukahara, "Progress towards sustainable production: environmental, economic, and social assessments of the cellulose nanofiber production process," *Sustainability*, vol. 9, no. 12, p. 2368, 2017.

[55] B. N. Jung, H. W. Jung, D. Kang, G. H. Kim, M. Lee, S. W. Hwang, and J. K. Shim, "The fabrication of affinity improved nanocomposites with plasma treated polypropylene (pp) and alkaline cellulose nanofiber (cnf) suspension," *Polymer Testing*, vol. 85, p. 106352, 2020.

[56] H.-S. Yang and D. J. Gardner, "Mechanical properties of cellulose nanofibril-filled polypropylene composites," *Wood and fiber science*, pp. 143–152, 2011.

[57] K. Kahavita, A. Samarasekara, D. Amarasinghe, and L. Karunanayake, "Influence of surface modification of cellulose nanofibers (cnf) as the reinforcement of polypropylene based composite," in *2019 Moratuwa Engineering Research Conference (MERCon)*. IEEE, 2019, pp. 99–104.

[58] K.-i. Niihara, T. Noguchi, T. Makise, W. Kashima, M. Endo, and A. Isogai, "Cellulose nanofibril/polypropylene composites prepared under elastic kneading conditions," *Cellulose*, vol. 29, no. 9, pp. 4993–5006, 2022.

[59] K. Aoki, "Development of cellulose nanofiber (cnf)/pp composites," *Oleo Science*, vol. 24, no. 5, pp. 205–210, 2024.

[60] Z. Yang, X. Li, J. Si, Z. Cui, and K. Peng, "Morphological, mechanical and thermal properties of poly (lactic acid)(pla)/cellulose nanofibrils (cnf) composites nanofiber for tissue engineering," *Journal of Wuhan University of Technology-Mater. Sci. Ed.*, vol. 34, pp. 207–215, 2019.

[61] X. Yan, Y. Shao, Z. Gao, B. Wu, C. Wang, C. Zhu, and L. Tu, "Preparation and properties of cellulose nanofiber/ti3c2tx/poly (lactic acid) composite film," *Journal of Polymer Research*, vol. 31, no. 2, p. 58, 2024.

[62] E. A. Agnes, E. Hillig, A. J. Zattera, L. R. Beltrami, J. A. Covas, L. Hilliou, J. D. Sousa, L. Calado, M. Pinto, and A. de Andrade Lucas, "Potentialities of cellulose nanofibers (cnfs) in low density polyethylene (ldpe) composites," *European Journal of Wood and Wood Products*, pp. 1–10, 2024.

[63] B. Wu, S. Wang, J. Tang, and N. Lin, "Nanocellulose in high-value applications for reported trial and commercial products," *Advanced Functional Materials from Nanopolysaccharides*, pp. 389–409, 2019.

[64] A. Behera and A. Behera, "Nanomaterials," *Advanced Materials: An Introduction to Modern Materials Science*, pp. 77–125, 2022.

[65] C. Woodings, "Cellulose fibers, regenerated," *Encyclopedia of polymer science and technology*, pp. 1–48, 2002.

[66] H.-P. Fink and J. Ganster, "Novel thermoplastic composites from commodity polymers and man-made cellulose fibers," in *Macromolecular Symposia*, vol. 244, no. 1. Wiley Online Library, 2006, pp. 107–118.

[67] T. Huber, B. Kuckhoff, T. Gries, D. Veit, S. Pang, N. Graupner, J. Müssig, and M. P. Staiger, "Three-dimensional braiding of continuous regenerated cellulose fibres," *Journal of Industrial Textiles*, vol. 45, no. 5, pp. 707–715, 2016.

[68] M. Das, "Man-made cellulose fibre reinforcements (mmcfr)," in *Biocomposites for High-Performance Applications*. Elsevier, 2017, pp. 23–55.

[69] S.-R. Shamsuddin, K.-Y. Lee, and A. Bismarck, "Ductile unidirectional continuous rayon fibre-reinforced hierarchical composites," *Composites Part A: Applied Science and Manufacturing*, vol. 90, pp. 633–641, 2016.

[70] B. Bax and J. Müssig, "Impact and tensile properties of pla/cordenka and pla/flax composites," *Composites science and technology*, vol. 68, no. 7-8, pp. 1601–1607, 2008.

[71] J. Ganster, H.-P. Fink, and M. Pinnow, "High-tenacity man-made cellulose fibre reinforced thermoplastics–injection moulding compounds with polypropylene and alternative matrices," *Composites Part A: Applied Science and Manufacturing*, vol. 37, no. 10, pp. 1796–1804, 2006.

[72] P. F. Alao, L. Marrot, M. D. Burnard, G. Lavrič, M. Saarna, and J. Kers, "Impact of alkali and silane treatment on hemp/pla composites' performance: From micro to macro scale," *Polymers*, vol. 13, no. 6, p. 851, 2021.

[73] X. Wang, Y. Cui, Q. Xu, B. Xie, and W. Li, "Effects of alkali and silane treatment on the mechanical properties of jute-fiber-reinforced recycled polypropylene composites," *Journal of Vinyl and Additive Technology*, vol. 16, no. 3, pp. 183–188, 2010.

[74] B. Mylsamy, S. K. M. Shanmugam, K. Aruchamy, S. Palanisamy, R. Nagarajan, and N. Ayrilmis, "A review on natural fiber composites: Polymer matrices, fiber surface treatments, fabrication methods, properties, and applications," *Polymer Engineering & Science*, 2024.

[75] A. Ali, K. Shaker, Y. Nawab, M. Jabbar, T. Hussain, J. Militky, and V. Baheti, "Hydrophobic treatment of natural fibers and their composites—a review," *Journal of Industrial Textiles*, vol. 47, no. 8, pp. 2153–2183, 2018.

[76] H.-B. Kim, K. Goda, J. Noda, and K. Aoki, "Developing simple production of continuous ramie single yarn reinforced composite strands," *Advances in Mechanical Engineering*, vol. 5, p. 496274, 2013.

[77] M. Rabbi, T. Islam, and G. S. Islam, "Injection-molded natural fiber-reinforced polymer composites–a review," *International Journal of Mechanical and Materials Engineering*, vol. 16, pp. 1–21, 2021.

[78] J. Rao, L. Bao, B. Wang, M. Fan, and L. Feo, "Plasma surface modification and bonding enhancement for bamboo composites," *Composites Part B: Engineering*, vol. 138, pp. 157–167, 2018.

[79] K. Shanmugam, "Cellulose nanofiber lamination of the paper substrates via spray coating—proof of concept and barrier performance," *Online Journal of Materials Science*, pp. 30–51, 2022.

[80] M. Lakovaara, J. A. Sirviö, R. Sliz, S. Wang, and H. Liimatainen, "Cellulose nanoworm coatings for enhancing the water resistance of nanocellulose film substrates in printed electronics," *Biomacromolecules*, 2024.

[81] D.-C. Wang, S.-N. Lei, S. Zhong, X. Xiao, and Q.-H. Guo, "Cellulose-based conductive materials for energy and sensing applications," *Polymers*, vol. 15, no. 20, p. 4159, 2023.

[82] G. Liang, Y. Qi, R. Gong, Y. Hu, F. Yao, Y. Liu, B. Liu, Y. Zhao, Y. Dai, and X. Dong, "Nanocellulose-reinforced polyurethane as flexible coating for cork floor," *Progress in Organic Coatings*, vol. 178, p. 107480, 2023.

[83] S. Eichhorn, C. Baillie, N. Zafeiropoulos, L. Mwaikambo, M. Ansell, A. a. Dufresne, K. Entwistle, P. Herrera-Franco, G. Escamilla, L. Groom *et al.*, "Current international research into cellulosic fibres and composites," *Journal of materials Science*, vol. 36, pp. 2107–2131, 2001.

[84] N. Yuji, "Surface modification technology: current situation and future development," *Applied Physics*, vol. 82, no. 5, pp. 376–384, 2013.

[85] K. Hämäläinen and T. Kärki, "Effects of atmospheric plasma treatment on the surface properties of wood-plastic composites," in *Advanced Materials Research*, vol. 718. Trans Tech Publ, 2013, pp. 176–185.

[86] A. J. Yáñez-Pacios and J. M. Martín-Martínez, "Comparative adhesion, ageing resistance, and surface properties of wood plastic composite treated with low pressure plasma and atmospheric pressure plasma jet," *Polymers*, vol. 10, no. 6, p. 643, 2018.

[87] M. Farsi, "Wood-plastic composites: Influence of wood flour chemical modification on the mechanical performance," *Journal of reinforced plastics and composites*, vol. 29, no. 24, pp. 3587–3592, 2010.

[88] H. Kallakas, M. Shamim, T. Olutubo, T. Poltimäe, T. Süld, A. Krumme, and J. Kers, "Effect of chemical modification of wood flour on the mechanical properties of wood-plastic composites." *Agronomy research*, vol. 13, no. 3, 2015.

[89] S. Migneault, A. Koubaa, P. Perré, and B. Riedl, "Effects of wood fiber surface chemistry on strength of wood–plastic composites," *Applied Surface Science*, vol. 343, pp. 11–18, 2015.

[90] I. Widiastuti, A. B. Panuntun, S. Eko Bayu, V. L. P. Sutrisno, G. Pramesti *et al.*, "Mechanical properties and water absorption behaviour of virgin/recycled polypropylene wood waste composites: A comparative analysis of injection and compression moulding," *Journal of the Korean Wood Science and Technology*, vol. 53, no. 2, pp. 164–176, 2025.

[91] J. Friedrich, L. Wigant, W. Unger, A. Lippitz, and H. Wittrich, "Corona, spark and combined uv and ozone modification of polymer films webp23," *Surface and coatings technology*, vol. 98, no. 1-3, pp. 879–885, 1998.

[92] A. J. Yáñez-Pacios and J. M. Martín-Martínez, "Surface modification and improved adhesion of wood-plastic composites (wpcs) made with different polymers by treatment with atmospheric pressure rotating plasma jet," *International Journal of Adhesion and Adhesives*, vol. 77, pp. 204–213, 2017.

[93] G. Scarselli, D. Quan, N. Murphy, B. Deegan, D. Dowling, and A. Ivankovic, "Adhesion improvement of thermoplastics-based composites by atmospheric plasma and uv treatments," *Applied Composite Materials*, vol. 28, pp. 71–89, 2021.

[94] B. Hünnekens, G. Avramidis, G. Ohms, A. Krause, W. Viöl, and H. Militz, "Impact of plasma treatment under atmospheric pressure on surface chemistry and surface morphology of extruded and injection-molded wood-polymer composites (wpc)," *Applied surface science*, vol. 441, pp. 564–574, 2018.

[95] M. Mortazavi and M. Nosonovsky, "A model for diffusion-driven hydrophobic recovery in plasma treated polymers," *Applied Surface Science*, vol. 258, no. 18, pp. 6876–6883, 2012.

[96] E. Bormashenko, G. Chaniel, and R. Grynyov, "Towards understanding hydrophobic recovery of plasma treated polymers: Storing in high polarity liquids suppresses hydrophobic recovery," *Applied Surface Science*, vol. 273, pp. 549–553, 2013.

[97] S. Luo, C. Lv, L. Chang, and W. Guo, "Enhancing crystallization and toughness of wood flour/polypropylene composites via matrix crystalline modification: a comparative study of two β-nucleating agents," *Polymers*, vol. 14, no. 17, p. 3561, 2022.

[98] M. Fujishita, C. Luo, K. Aoki, and Y. Uetsuji, "Fiber dispersion control and its advantages on nonlinear mechanical properties in cellulose composites," *Composites Part A: Applied Science and Manufacturing*, vol. 190, p. 108639, 2025.

[99] S. Hwang, Y. Han, and D. J. Gardner, "Morphological characteristics of spray dried cellulose nanofibers produced using various wood pulp feedstocks and their effects on polypropylene composite properties," *Composites Part B: Engineering*, vol. 268, p. 111093, 2024.

[100] M. Y. Al-Haik, S. Aldajah, W. Siddique, M. M. Kabir, and Y. Haik, "Mechanical and thermal characterization of polypropylene-reinforced nanocrystalline cellulose nanocomposites," *Journal of Thermoplastic Composite Materials*, vol. 35, no. 5, pp. 680–691, 2022.

[101] G. Pokhrel, D. J. Gardner, and Y. Han, "Properties of wood–plastic composites manufactured from two different wood feedstocks: Wood flour and wood pellets," *Polymers*, vol. 13, no. 16, p. 2769, 2021.

[102] J. Zhu, Y. Fang, R. Yang, Y. Fu, G. Li, X. Bai, W. Wang, Y. Song, and Q. Wang, "A fully bio-based intumescent flame retardant for enhancing the flame retardancy and smoke suppression properties of wood flour polypropylene composites," *Polymer Degradation and Stability*, vol. 231, p. 111072, 2025.

[103] S. Gairola, S. Sinha, and I. Singh, "Improvement of flame retardancy and anti-dripping properties of polypropylene composites via ecofriendly borax cross-linked lignocellulosic fiber," *Composite Structures*, vol. 354, p. 118822, 2025.

[104] R. Yang, Y. Fu, J. Zhu, G. Li, C. Yan, Y. Fang, X. Bai, W. Wang, Y. Song, and Q. Wang, "Fabrication of montmorillonite wrapped with layered double hydroxide synergistic app to improve the flame retardancy and mechanical properties for wood flour/polypropylene composites," *Composites Communications*, p. 102438, 2025.

[105] C. Zárate-Pérez, R. Ramírez-Aguilar, E. A. Franco-Urquiza, and C. Sánchez-Alvarado, "The role of coupling agents in the mechanical and thermal properties of polypropylene/wood flour composites," *Macromol*, vol. 3, no. 1, pp. 65–78, 2023.

[106] H. Zhang, "Effect of a novel coupling agent, alkyl ketene dimer, on the mechanical properties of wood–plastic composites," *Materials & Design*, vol. 59, pp. 130–134, 2014.

[107] D. Ndiaye and A. Tidjani, "Effects of coupling agents on thermal behavior and mechanical properties of wood flour/polypropylene composites," *Journal of composite materials*, vol. 46, no. 24, pp. 3067–3075, 2012.

[108] M. A. M. Elamin, Z. A. Osman, T. A. Otitoju *et al.*, "Preparation and characterization of wood-plastic composite by utilizing a hybrid compatibilizer system," *Industrial Crops and Products*, vol. 154, p. 112659, 2020.

[109] Y. Zhou, D. Hui, Y. Wang, and M. Fan, "Nanomechanical and dynamic mechanical properties of rubber–wood–plastic composites," *Nanotechnology Reviews*, vol. 11, no. 1, pp. 167–175, 2021.

[110] S. Khamtree, C. Srivabut, S. Khamtree, and R. Kaewmai, "Effects of natural fiber waste, content, and coupling agent on the physical and mechanical properties of wood species–plastic composites as green materials," *Fibers and Polymers*, pp. 1–12, 2024.

[111] M. Ghorbani, N. Poorzahed, and S. M. Amininasab, "Morphological, physical, and mechanical properties of silanized wood-polymer composite," *Journal of composite materials*, vol. 54, no. 11, pp. 1403–1412, 2020.

[112] S.-K. Yeh, K.-J. Kim, and R. K. Gupta, "Synergistic effect of coupling agents on polypropylene-based wood–plastic composites," *Journal of Applied Polymer Science*, vol. 127, no. 2, pp. 1047–1053, 2013.

[113] T. Y. Elrasasi, L. M. Reda, L. A. Mohamed, and D. I. Moubarak, "Effect of coupling agent ratio on the physical and mechanical properties of wood-recycled high density poly ethylene composites," Preprint, Research Square, 2024, https://doi.org/10.21203/rs.3.rs-3928312/v1, CC BY 4.0 License.

[114] M. Farsi and F. M. Sani, "Effects of multi-walled carbon nanotubes on the physical and mechanical properties of high-density polyethylene/wood flour nanocomposites," *Journal of Thermoplastic Composite Materials*, vol. 27, no. 8, pp. 1139–1154, 2014.

[115] N. L. Bhandari, S. Thomas, C. K. Das, and R. Adhikari, "Role of compatibilizer on morphological and mechanical properties of low cost polypropylene/wood flour composites," *Journal of Nepal Chemical Society*, vol. 29, pp. 113–120, 2012.

[116] A. Nourbakhsh, A. Ashori, H. Ziaei Tabari, and F. Rezaei, "Mechanical and thermochemical properties of wood-flour/polypropylene blends," *Polymer bulletin*, vol. 65, pp. 691–700, 2010.

[117] H. Ma, V. Guna, T. Raju, A. N. Murthy, and N. Reddy, "Converting flax processing waste into value added biocomposites," *Industrial Crops and Products*, vol. 195, p. 116434, 2023.

[118] H. Younesi-Kordkheili and A. Pizzi, "Nanolignin, a coupling bio-agent for woodplastic composites," *J Renew Mater*, vol. 11, pp. 2075–2083, 2023.

[119] F. Espinach, F. Vilaseca, Q. Tarrés, M. Delgado-Aguilar, R. Aguado, and P. Mutjé, "An alternative method to evaluate the micromechanics tensile strength properties of natural fiber strand reinforced polyolefin composites. the case of hemp strand-reinforced polypropylene," *Composites Part B: Engineering*, vol. 273, p. 111211, 2024.

[120] H. Younesi-Kordkheili, "Maleated nanolignin as a new coupling agent for woodplastic composites," *Journal of Composite Materials*, vol. 57, no. 30, pp. 4649–4658, 2023.

[121] J. Guillén-Mallette, I. Flores-Cerón, S. C. Pech-Cohuo, E. J. López-Naranjo, C. V. Cupul-Manzano, A. Valadez-González, and R. H. Cruz-Estrada, "Effect of moisture absorption-desorption cycles, uv irradiation and coupling agent on the mechanical performance of pinewood waste/polyethylene composites," *Clean Technologies and Recycling*, vol. 3, no. 3, pp. 193–220, 2023.

[122] R. Sahai and R. Pardeshi, "Comparative study of effect of different coupling agent on mechanical properties and water absorption on wheat straw-reinforced polystyrene composites," *Journal of Thermoplastic Composite Materials*, vol. 34, no. 4, pp. 433–450, 2021.

[123] S. K. Hosseinihashemi and F. Arwinfar, "Effect of fungal infection on physico-mechanical resistance of wpc made from thermally treated wood/pp," *Mobilya ve Ahşap Malzeme Araştırmaları Dergisi*, vol. 6, no. 1, pp. 90–103, 2023.

[124] Y. Teramoto, "Recent advances in multi-scale experimental analysis to assess the role of compatibilizers in cellulosic filler-reinforced plastic composites," *Journal of Composites Science*, vol. 5, no. 5, p. 138, 2021.

[125] C. Homkhiew, S. Rawangwong, W. Boonchouytan, and V. Suchaiya, "Morphological, mechanical, and physical properties of ground rubber tire thermoplastic elastomer/rubberwood sawdust composites: Effects of composition contents and rubber types," *Journal of Thermoplastic Composite Materials*, vol. 36, no. 5, pp. 1952–1977, 2023.

[126] I. Widiastuti, R. Prananda, J. A. Putra, D. R. Ananda, and Y. Estriyanto, "Optimizing the water absorption behaviour and natural weathering resistance of compatibilized ironwood-based recycled polypropylene composites," *Composites Part C: Open Access*, vol. 12, p. 100423, 2023.

[127] M. Ghorbani, N. Talebi, M. Amininasab, and F. Dastoorian, "The effect of acrylate modification of wood flour on the structural characteristics and physical behavior of wood flour/polypropylene composite product," *Journal of Wood and Forest Science and Technology*, vol. 30, no. 4, pp. 3–16, 2023.

[128] M. E. Vallejos, F. Vilaseca, J. A. Méndez, F. X. Espinach, R. J. Aguado, M. Delgado-Aguilar, and P. Mutjé, "Response of polypropylene composites reinforced with natural fibers: impact strength and water-uptake behaviors," *Polymers*, vol. 15, no. 4, p. 900, 2023.

[129] E. Birinci, "Determination of technological properties of wood plastic nanocomposites produced by flat press reinforced with nano mgo," *Journal of Composite Materials*, vol. 57, no. 9, pp. 1641–1651, 2023.

[130] M. Ferdinánd, M. Jerabek, R. Várdai, T. Lummerstorfer, C. Pretschuh, M. Gahleitner, G. Faludi, J. Móczó, and B. Pukánszky, "Impact modification of wood flour reinforced pp composites: Problems, analysis, solution," *Composites Part A: Applied Science and Manufacturing*, vol. 167, p. 107445, 2023.

[131] S. Wang, J. K. Muiruri, X. Y. D. Soo, S. Liu, W. Thitsartarn, B. H. Tan, A. Suwardi, Z. Li, Q. Zhu, and X. J. Loh, "Bio-polypropylene and polypropylene-based biocomposites: Solutions for a sustainable future," *Chemistry–An Asian Journal*, vol. 18, no. 2, p. e202200972, 2023.

[132] R. Wang, X. You, S. Qi, R. Tian, and H. Zhang, "Enhancing mechanical performance of high-lignin-filled polypropylene via reactive extrusion," *Polymers*, vol. 16, no. 4, p. 520, 2024.

[133] K. O. Iwuozor, T. T. Micheal, K. T. Micheal, S. S. Emmanuel, E. C. Emenike, and A. G. Adeniyi, "Plant biomass-based composites in the maritime industry: A review," *Marine Structures*, vol. 96, p. 103609, 2024.

[134] A. Kovalovs, K. Kalnins, P. Franciszczak, A. Bledzki *et al.*, "Low velocity impact response of polypropylene biocomposites reinforced with man-made cellulose and soft wood fibres," in *Proceedings of the 20th International Scientific Conference Engineering for Rural Development, Jelgava, Latvia*, 2021, pp. 26–28.

[135] J. Meredith, S. R. Coles, R. Powe, E. Collings, S. Cozien-Cazuc, B. Weager, J. Müssig, and K. Kirwan, "On the static and dynamic properties of flax and cordenka epoxy composites," *Composites Science and Technology*, vol. 80, pp. 31–38, 2013.

[136] T. Malaba and J. Wang, "Unidirectional cordenka fibre-reinforced furan resin full biocomposite: Properties and influence of high fibre mass fraction," *Journal of Composites*, vol. 2015, no. 1, p. 707151, 2015.

[137] G. Japins, P. Franciszczak, K. Kalnins, and A. Kovalovs, "Mechanical properties of polypropylene biocomposites reinforced with man-made cellulose fibres and cellulose microfibres," in *IOP Conference Series: Materials Science and Engineering*, vol. 500, no. 1. IOP Publishing, 2019, p. 012008.

[138] D. Wunderlich and B. Zimmerer, "Technical rayon: Present and future. 50th dornbirn man-made fibers congress," *Dornbirn, Austria*, 2011.

[139] W. Ondiek, M. Kondo, M. Adachi, A. Macadre, and K. Goda, "Effect of surface coating and plasma treatment on mechanical properties of wood plastic composites," *Journal of Composites Science*, vol. 7, no. 7, p. 296, 2023.

[140] N. E. Dowling, S. L. Kampe, and M. V. Kral, *Mechanical Behavior of Materials*, 5th ed. Upper Saddle River, NJ: Pearson, 2019.

[141] T. L. Anderson, *Fracture Mechanics: Fundamentals and Applications*, 4th ed. Boca Raton, FL: CRC Press, 2017.

[142] M. Nordin, Y. Makino, K. Goda, and H. Ito, "Fatigue fracture properties of wood-plastic composites," *Journal of the Society of Fiber Science and Technology, Japan*, vol. 71, no. 12, pp. 339–344, 2015.

[143] G. C. Sih, *Mechanics of Fracture Initiation and Propagation*. Dordrecht: Springer Netherlands, 1991.

[144] M. Nordin, K. Sakamoto, H. Azhari, K. Goda, M. Okamoto, H. Ito, and T. Endo, "Tensile and impact properties of pulverized oil palm fiber reinforced polypropylene composites: A comparison study with wood fiber reinforced polypropylene composites," *Journal of Mechanical Engineering and Sciences*, vol. 12, no. 4, pp. 4191–4202, 2018.

[145] A. J. Yáñez-Pacios and J. M. Martín-Martínez, "Surface modification and adhesion of wood-plastic composite (wpc) treated with uv/ozone," *Composite Interfaces*, vol. 25, no. 2, pp. 127–149, 2018.

[146] A. Wolkenhauer, G. Avramidis, E. Hauswald, H. Militz, and W. Viöl, "Plasma treatment of wood–plastic composites to enhance their adhesion properties," *Journal of Adhesion Science and Technology*, vol. 22, no. 16, pp. 2025–2037, 2008.

[147] K. L. Mittal and A. N. Netravali, *Polymer Surface Modification to Enhance Adhesion: Techniques and Applications*. John Wiley & Sons, 2024. [Online]. Available: https://www.wiley.com/en-us/Polymer+Surface+Modification+to+Enhance+Adhesion%3A+Techniques+and+Applications-p-9781394231034

[148] N. Inagaki, *Plasma Surface Modification and Plasma Polymerization*. CRC Press (Taylor & Francis), 2014. [Online]. Available: https://www.taylorfrancis.com/books/mono/10.1201/9781498710831/plasma-surface-modification-plasma-polymerization-norihiro-inagaki

[149] C. Demirkir, I. Aydin, S. Colak, and H. Ozturk, "Effects of plasma surface treatment on bending strength and modulus of elasticity of beech and poplar plywood," *Maderas. Ciencia y tecnología*, vol. 19, no. 2, pp. 195–202, 2017.

[150] A. Wolkenhauer, G. Avramidis, E. Hauswald, H. Militz, and W. Viöl, "Sanding vs. plasma treatment of aged wood: A comparison with respect to surface energy," *International Journal of Adhesion and Adhesives*, vol. 29, no. 1, pp. 18–22, 2009.

[151] Y. Seki, K. Sever, M. Sarikanat, H. A. Güleç, and I. H. Tavman, "The influence of oxygen plasma treatment of jute fibers on mechanical properties of jute fiber reinforced thermoplastic composites," in *Proceedings of the 5th international advanced technologies symposium (IATS'09)*, vol. 13, 2009.

[152] H.-B. Kim and K. Goda, "Production of a single ramie spun yarn/pp composite tape and reliability analysis in elastic modulus," *Seikei-Kakou*, vol. 28, no. 8, pp. 343–349, 2020.

[153] C. Rayon, "Technical data sheet multifilament yarn," Cordenka GmbH & Co. KG, Tech. Rep. 2, 2022, accessed: 2024-10-06. [Online]. Available: https://a.storyblok.com/f/121148/x/bdba5c0470/tds_rayon-multifilament-yarn.pdf

[154] S. Sato, K. Oka, and A. Murakami, "Heat transfer behavior of melting polymers in laminar flow field," *Polymer Engineering & Science*, vol. 44, no. 3, pp. 423–432, 2004.

[155] S. Sato, Y. Sakata, J. Aoki, and K. Kubota, "Effects of filler on heat transmission behavior of flowing melt polymer composites," *Polymer Engineering & Science*, vol. 46, no. 10, pp. 1387–1393, 2006.

[156] P. Franciszczak and A. Bledzki, "Tailoring of dual-interface in high tenacity pp composites–toughening with positive hybrid effect," *Composites Part A: Applied Science and Manufacturing*, vol. 83, pp. 185–192, 2016.

[157] K. Tanabe, T. Matsuo, K. Goda, and J. Ohki, "Strength evaluation of kurawa fibers considering cross-sectional area variation," *Materials*, vol. 57, no. 5, pp. 454–460, 2008.

[158] X. Chen, S. Zhang, G. Xu, X. Zhu, and W. Liu, "Mechanical, flammability, and crystallization behavior of polypropylene composites reinforced by aramid fibers," *Journal of applied polymer science*, vol. 125, no. 2, pp. 1166–1175, 2012.

[159] F. L. Matthews and R. D. Rawlings, *Composite materials: engineering and science*. Elsevier, 1999.

[160] N. Graupner, J. Rößler, G. Ziegmann, and J. Müssig, "Fibre/matrix adhesion of cellulose fibres in pla, pp and mapp: A critical review of pull-out test, microbond test and single fibre fragmentation test results," *Composites Part A: Applied Science and Manufacturing*, vol. 63, pp. 133–148, 2014.

[161] C. Baley, A. Bourmaud, and P. Davies, "Eighty years of composites reinforced by flax fibres: A historical review," *Composites Part A: Applied Science and Manufacturing*, vol. 144, p. 106333, 2021.

[162] A. Gomes, T. Matsuo, K. Goda, and J. Ohgi, "Development and effect of alkali treatment on tensile properties of curaua fiber green composites," *Composites Part A: Applied Science and Manufacturing*, vol. 38, no. 8, pp. 1811–1820, 2007.

[163] M. Jörg, *Industrial applications of natural fibres: structure, properties and technical applications*. John Wiley & Sons, 2010.

[164] A. K. Mohanty, M. Misra, and L. T. Drzal, *Natural Fibers, Biopolymers, and Biocomposites*. CRC Press, 2005.

[165] A. Fernández, M. Santangelo-Muro, J. P. Fernández-Blázquez, C. S. Lopes, and J. M. Molina-Aldareguia, "Processing and properties of long recycled-carbon-fibre reinforced polypropylene," *Composites Part B: Engineering*, vol. 211, p. 108653, 2021.

[166] A. Ari, A. Bayram, M. Karahan, and S. Karagöz, "Comparison of the mechanical properties of chopped glass, carbon, and aramid fiber reinforced polypropylene," *Polymers and Polymer Composites*, vol. 30, p. 09673911221098570, 2022.

[167] M. N. F. Norrrahim, H. Ariffin, T. A. T. Yasim-Anuar, M. A. Hassan, N. A. Ibrahim, W. M. Z. W. Yunus, and H. Nishida, "Performance evaluation of cellulose nanofiber with residual hemicellulose as a nanofiller in polypropylene-based nanocomposite," *Polymers*, vol. 13, no. 7, p. 1064, 2021.

[168] M. N. F. Norrrahim, T. Yasim-Anuar, M. Jenol, N. M. Nurazzi, S. Sapuan, and R. Ilyas, "Performance evaluation of cellulose nanofiber reinforced polypropylene biocomposites for automotive applications," in *Biocomposite and synthetic composites for automotive applications*. Elsevier, 2021, pp. 199–215.

[169] M. Jonoobi, J. Harun, A. P. Mathew, and K. Oksman, "Mechanical properties of cellulose nanofiber (cnf) reinforced polylactic acid (pla) prepared by twin screw extrusion," *Composites science and technology*, vol. 70, no. 12, pp. 1742–1747, 2010.

[170] H. Senkum, P. V. Kelly, A. A. Ahmad, S. S. Es-haghi, and W. M. Gramlich, "Strengthening polylactic acid (pla) composites with poly (methyl methacrylate)-functionalized cellulose nanofibrils created through grafting-through emulsion polymerization," *RSC Applied Polymers*, vol. 2, no. 2, pp. 224–237, 2024.

[171] T. Ambone, A. Torris, and K. Shanmuganathan, "Enhancing the mechanical properties of 3d printed polylactic acid using nanocellulose," *Polymer Engineering & Science*, vol. 60, no. 8, pp. 1842–1855, 2020.

[172] A. N. Frone, S. Berlioz, J.-F. Chailan, and D. M. Panaitescu, "Morphology and thermal properties of pla–cellulose nanofibers composites," *Carbohydrate polymers*, vol. 91, no. 1, pp. 377–384, 2013.

[173] E. M. Sullivan, R. J. Moon, and K. Kalaitzidou, "Processing and characterization of cellulose nanocrystals/polylactic acid nanocomposite films," *Materials*, vol. 8, no. 12, pp. 8106–8116, 2015.

[174] M. D. Sanchez-Garcia and J. M. Lagaron, "On the use of plant cellulose nanowhiskers to enhance the barrier properties of polylactic acid," *Cellulose*, vol. 17, pp. 987–1004, 2010.

[175] S. H. Sung, Y. Chang, and J. Han, "Development of polylactic acid nanocomposite films reinforced with cellulose nanocrystals derived from coffee silverskin," *Carbohydrate polymers*, vol. 169, pp. 495–503, 2017.

[176] T. Matsunaga, Y. Sato, T. Ozaki, A. Macadre, and K. Goda, "Crystallization reinforcement of biobased pa resin by fibrillation of natural fibers," *Journal of the Japan Society for Composite Materials*, vol. 47, no. 4, pp. 137–142, 2021.

[177] Z. Zhang, B. Cao, and N. Jiang, "The mechanical properties and degradation behavior of 3d-printed cellulose nanofiber/polylactic acid composites," *Materials*, vol. 16, no. 18, p. 6197, 2023.

[178] J. K. Pandey, A. N. Nakagaito, and H. Takagi, "Fabrication and applications of cellulose nanoparticle-based polymer composites," *Polymer Engineering & Science*, vol. 53, no. 1, pp. 1–8, 2013.

[179] T. A. T. Yasim-Anuar, H. Ariffin, M. N. F. Norrrahim, M. A. Hassan, T. Tsukegi, and H. Nishida, "Sustainable one-pot process for the production of cellulose nanofiber and polyethylene/cellulose nanofiber composites," *Journal of cleaner production*, vol. 207, pp. 590–599, 2019.

[180] T. A. T. Yasim-Anuar, H. Ariffin, M. N. F. Norrrahim, M. A. Hassan, Y. Andou, T. Tsukegi, and H. Nishida, "Well-dispersed cellulose nanofiber in low density polyethylene nanocomposite by liquid-assisted extrusion," *Polymers*, vol. 12, no. 4, p. 927, 2020.

[181] K. Keeratipinit, P. Wijaranakul, W. Wanmolee, and B. Hararak, "Preparation of high-toughness cellulose nanofiber/polylactic acid bionanocomposite films via gel-like cellulose nanofibers," *ACS Omega*, 2024.

[182] M. Mehdinia, M. Farajollah Pour, H. Yousefi, A. Dorieh, A. J. Lamanna, and E. Fini, "Developing bio-nano composites using cellulose-nanofiber-reinforced epoxy," *Journal of Composites Science*, vol. 8, no. 7, p. 250, 2024.

[183] K. Matsumoto, K. Takemura, R. Kitamura, H. Katogi, T. Tanaka, and H. Takagi, "Cellulose nanofiber-introduced continuous-ramie yarn-reinforced polylactic acid filament for 3d printing: novel fabrication process and mechanical properties," *Composites Part A: Applied Science and Manufacturing*, vol. 176, p. 107836, 2024.

[184] K. Yamato, Y. Yoshida, Y. Kumamoto, and A. Isogai, "Surface modification of tempo-oxidized cellulose nanofibers, and properties of their acrylate and epoxy resin composite films," *Cellulose*, vol. 29, no. 5, pp. 2839–2853, 2022.

[185] S. Liu, Z.-X. Low, Z. Xie, and H. Wang, "Tempo-oxidized cellulose nanofibers: a renewable nanomaterial for environmental and energy applications," *Advanced Materials Technologies*, vol. 6, no. 7, p. 2001180, 2021.

[186] R. Ning, Y. Ono, and A. Isogai, "Effects of uv irradiation of tempo-oxidized cellulose nanofibril/water dispersions on chemical structure, molar mass, and morphology," *Cellulose*, vol. 31, no. 4, pp. 2251–2265, 2024.

[187] Y. Goi, S. Fujisawa, T. Saito, K. Yamane, K. Kuroda, and A. Isogai, "Dual functions of tempo-oxidized cellulose nanofibers in oil-in-water emulsions: a pickering emulsifier and a unique dispersion stabilizer," *Langmuir*, vol. 35, no. 33, pp. 10 920–10 926, 2019.

[188] J. Qu, Z. Yuan, C. Wang, A. Wang, X. Liu, B. Wei, and Y. Wen, "Enhancing the redispersibility of tempo-mediated oxidized cellulose nanofibrils in n, n-dimethylformamide by modification with cetyltrimethylammonium bromide," *Cellulose*, vol. 26, pp. 7769–7780, 2019.

[189] M. Feldmann, "The effects of the injection moulding temperature on the mechanical properties and morphology of polypropylene man-made cellulose fibre composites," *Composites Part A: Applied Science and Manufacturing*, vol. 87, pp. 146–152, 2016.

[190] D. Hull, *An Introduction to Composite Materials*. Cambridge, UK: Cambridge University Press, 1981.